Original article

Development of Machine Learning Techniques for the Multiclass Semantic Segmentation of Underwater Images

D. ANITHA[1],*, C. RANI[2], K. SUGANYA DEVI[3], S.P. VALLI[4]

[1]Department of Computer Science and Engineering (CSE), University College of Engineering, Panruti, India.
[2]Department of CSE, Government College of Engineering, Bodinayakkanur, India.
[3]Department of CSE, National Institute of Technology Silchar, Assam, India.
[4]Department of CSE, B. S. Abdur Rahman Crescent Institute of Science and Technology, Chennai, India.

Abstract   The Neptune grass (NG) is an endemic plant of the Mediterranean Sea. Successive studies carried out show a significant decrease in their presence in this sea. Concern for the conservation of NG implies being able to monitor its evolution and thus be able to determine if its presence is increasing or decreasing in seabeds. Nowadays, expensive and limited methods are used to carry out this follow-up, which often also involves manual intervention. The work carried out aims to automatically determine the type of seabed from underwater images, performing semantic segmentation using deep neural networks. In this work, a deep neural network has been implemented to carry out a semantic segmentation of images of the seabed, offering improvements with respect to the techniques currently used to obtain this information. The developed neural network allows for distinguishing in the images of the seabed the areas of NG, rock, and sand. The possibility of identifying other elements present, such as dead NG, both the plant itself and its loose leaves scattered on the bottom, has also been explored in this work.

✉   *Corresponding author: D. Anitha, Department of Computer Science and Engineering (CSE), University College of Engineering, Panruti, India E-mail: anithacsephd@gmail.com

Introduction

The NG is an aquatic plant endemic to the Mediterranean and of great ecological value. It protects the coast from erosion; it is the base of the ecosystem for a multitude of marine species; it also oxygenates the water and captures CO_2, making it an element that mitigates climate change. Despite being a protected species and carrying out actions for its conservation, NG continues to decline due to trawling, boat anchors, pollution, climate change, etc. [1–4]. In order to carry out control and recovery, it is necessary to be able to monitor the evolution of NG meadows. This monitoring is currently being done by:

- Divers: So it is a very slow and expensive task.
- Satellite images: detection problems in deep water.
- SONAR: commonly used to make bathymetric maps.
- Autonomous underwater vehicle (AUV) equipped with sensors.

The work carried out identifies the type of seabed from underwater images. This identification consists of indicating in each pixel of the image what it is; in this case, it will be indicated in each pixel if it is NG, sand, rock, etc. This way of classifying images is called multiclass semantic segmentation. To achieve this semantic segmentation, artificial intelligence (AI) will be used, specifically a deep neural network. It is intended to automate the detection of NG in an AUV, which will make maps of the seabed with which to monitor NG. This work is an evolution of a work [5–8]. The improvement consists of carrying out multiclass semantic segmentation; that is, the previous work only identified in the image if there is NG or not in an area. With this work, it is possible to identify, in addition to NG, other types of elements, such as if the floor is made of sand or rock [9].

Figure 1 shows an example of monoclass semantic segmentation and another of multiclass, where the original image has been colored to identify the different types of background. Figure 1A(a) shows the monoclass classification [10–11], where the green color represents areas of NG and the rest of the uncolored image indicates that it is not NG. Figure 1A(b) is the case of multiclass semantic segmentation carried out in this work. Where, in addition to the green color for the NG, the rock is colored red, the sand is yellow, and what has not been identified has not been colored.

Being able to identify, in addition to the NG, the type of soil can help to see the evolution of the growth or regression of the NG depending on the terrain. Thus, in addition to being able to help take actions in certain areas, it also serves to monitor their results.

Literature Review

In 1989, M. Doherty proposed using a segmentation approach to object detection on sonar images [12]. He observes that the pixels associated with a target do not have the same statistical distribution (in terms of gray levels) as the pixels associated with the seabed. He then proposes to carry out an appropriate thresholding of the images to highlight the echoes. In order to validate the detection, it sets up a search for the shadows associated with these echoes using a set of smoothing and averaging operations. These premises show what will be one of the approaches most commonly used in object detection over the following decades, namely a segmentation of the image into three classes: the echo of a target, the shadow, and the bottom. In 1995, M. Bello introduced random Markov fields in this context and demonstrated that they are suitable for such segmentation [13]. These results push M. Mignotte and C. Collet to deepen this method [14–17]. However, due to the significant calculation times and current computer capacities, it was necessary to wait until 2003 and the study proposed by S. Reed and colleagues to obtain an efficient algorithm [18–19]. Using a priori spatial information (on target sizes and geometric signatures), a detection-oriented Markov field model is then developed to segment the image into these three classes. In 2014, [20] proposed to review this method by applying the graph-cuts method [21] to it to further accelerate the convergence of results. Another approach initiated by B. Calder in [22, 23] proposes to use a stochastic Bayesian model in order to classify each pixel of an image. For this, it carries out Bayesian modelling of the data and uses a Gibbs field to model the targets. The approach is considered robust but very computationally intensive. F. Maussang et al. [24] have also invested in the statistical approach to segment sonar images and, in particular, SAS images [25–26]. These methods are based on the relationship between the mean and standard deviation of the Rayleigh distribution of gray levels in sonar images. By modelling the responses of the background using a Weibull law, they observe that the mean and the standard deviation are linked by a multiplicative constant. However, for echo and shadow areas, the authors note that this relationship is no longer as strict. They then propose to take advantage of this by applying two thresholds in a plan defined by the mean and the standard deviation. These then make it possible to extract the areas of echoes and shadows. Salience detection methods are now commonly used and propose seeing an object as an anomaly in a textured region. They seek to model the differences between a given bottom zone and its vicinity. For example, in [27], L. Linett is based on the fact that background reverberations can be modelled
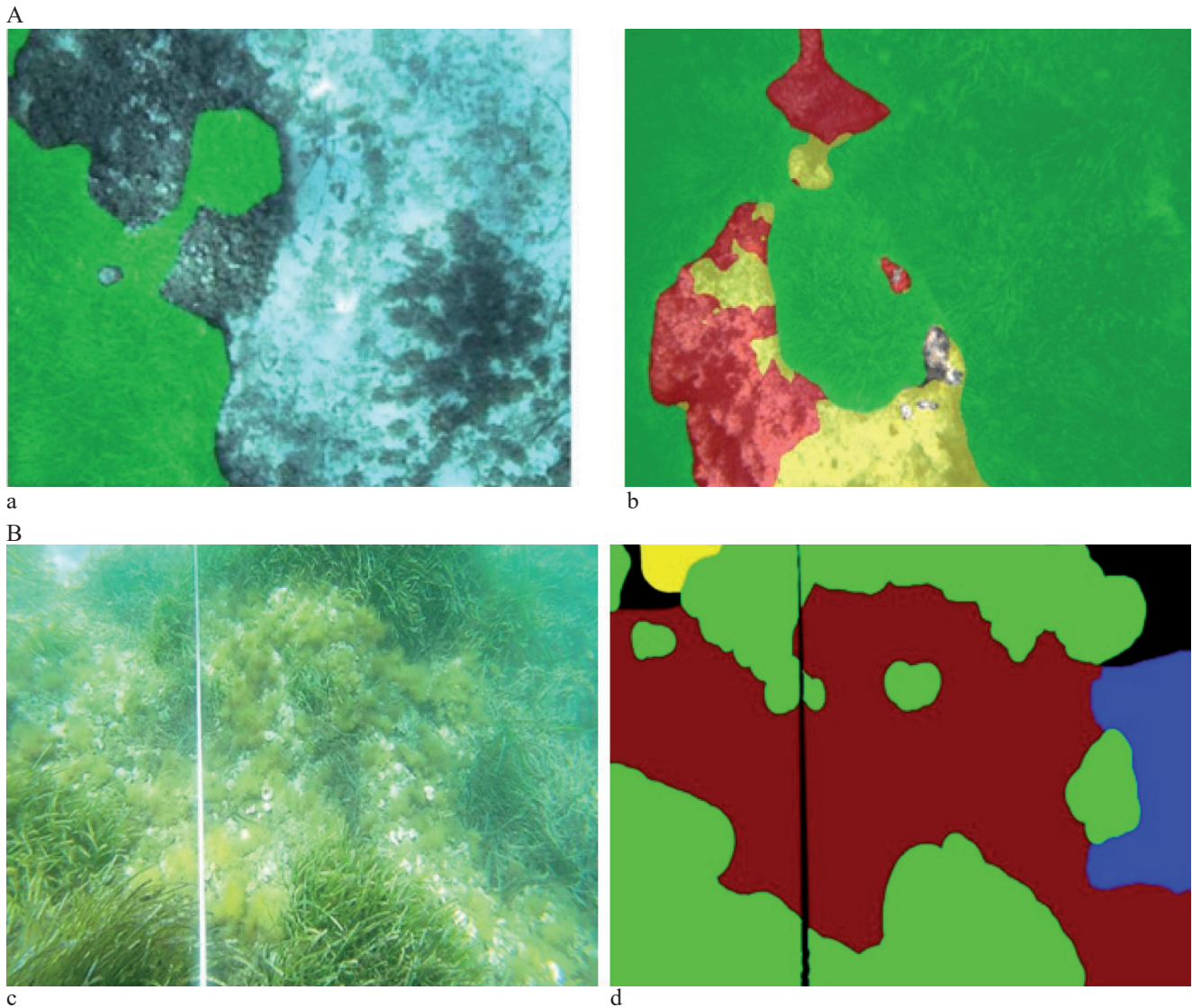
A

a

B

c   d

Fig. 1: A. Comparison of monoclass (a) and multiclass (b) semantic segmentation; B. Labeling of images.

by a fractional Brownian process [28], whose distribution is described by its fractal dimension. He then considers that a region whose fractal dimension is different from these neighbours can contain an object. In [29], L. Attalah uses Shannon entropy to detect salient regions. Indeed, he finds that regions containing shadows or echoes have a higher entropy than simple seabed areas. Thus, the author proposes to detect objects via the detection of peaks in the entropy function. In [30], the sonar image is broken down into blocks (of the typical size of an underwater mine, i.e., of the order of a meter), and the author proposes to calculate the correlation, according to the columns, between the different blocks from the same region. According to the author, underwater mines will then have a high correlation value, and a simple threshold would make it possible to detect them. In [30], we propose a salience detection algorithm whose calculations are done through the concept of integral image. The latter makes it possible to achieve detection speeds close to real-time on SAS images, despite their very large dimensions. From a set of sliding windows of varying sizes, the author proposes to estimate zones of echoes and shadows using a cascading architecture. The simplicity and speed of the algorithm are its main assets, which allow it to be one of the few that can be implemented on board AUVs. The classification based on models is entirely based on a priori knowledge that we have about the objects to be detected. This information then makes it possible to create a model for each target that one wishes to highlight. Such approaches are useful for classifying targets on which we do not have many examples (i.e., no learning is possible). In the literature on ATR, many methods have been proposed, and all rely exclusively on model matching; we can cite, for example, [31]. Only the implementations are then different, with a wide variety of algorithms. Some of these approaches propose to use contour-based matching algorithms like those of S. Reed [18]. Its algorithm allows cooperation between active contours to extract the echo and

the shadow of the targets jointly in a complex environment. Dempster Shafer's decision theory is then used to classify observed detections against known patterns.

Development of the proposed work

In this work, the necessary neural network has been implemented to achieve the semantic segmentation of the images of the seabed. To achieve this, the Tensor flow libraries have been used, and the programming has been done in Python. The present code is an evolution of a work to detect NG [2], which in turn is an adaptation of another work to detect roads [7]. In addition to the programming part of the neural network, the data for the training sessions had to be prepared and the necessary metrics defined to validate the results and verify the quality of the models obtained.

Data collection

For this work, 302 images obtained from recordings made by cameras mounted on an AUV have been used. The images are of the seabed of the Balearic Islands, especially Mallorca. These images are taken with different lighting conditions and water turbulence; this variety makes the trained network more versatile. Although the original images may have different dimensions, before carrying out the training, they are resized to 480x360, which is the size that the implemented neural network supports.

The images have been divided into two collections:
▪ 242 images for training (80%).
▪ 60 images for the tests (20%).

All the images had to be labelled as well. This labelling consists of manually performing a semantic segmentation for each image; in this way, we will have the desired results that the neural network needs to train and validate. To carry out the labelling of an image, a color must be defined for each class that is to be identified. Once the classes are defined, each pixel of the original image must be colored with its corresponding color. Figure 1B shows an example of how an original figure (c) is edited to obtain a labelled figure (d).

The colors that have been defined for each class to be identified in the underwater images are shown in Table 1.

Architecture used

To implement multiclass segmentation, I have based myself on a multilayer neural network, in which the input of the network is an RGB color image to which several transformations are applied, as shown in Figure 2, to achieve multiclass semantic segmentation [2].

Table 1. Correspondence of classes and colors

Name	Description	Color
NG-a	Living NG Kill	
NG-d	dead NG leaves	
Rock	clean rocky bottom	
rock-d	Rocky bottom with algae or other elements	
sandy	clean sand background	
Sand-d	Sandy bottom with algae or other elements	
matte-s	Dead NG clump on sand bottom	
Matte-r	Dead NG clump on rock bottom	
Background	Fund that does not correspond to any of the classes to be classified or that has not been identified	

In Figure 2, the number above the layers represents the dimensions of the feature maps that are used in that layer. The number below the layer represents the number of feature maps that layer has; in cases where an X is shown, it corresponds to the number of classes to be identified.

The layer structure is divided into two phases:

Encoder: in this first encoding phase, the characteristics of the image are extracted using convolution and pool layers.

Decoder: in the second phase of decoding, the image is reconstructed by means of transposed convolution; in this way, the classification of each pixel of the image is obtained.
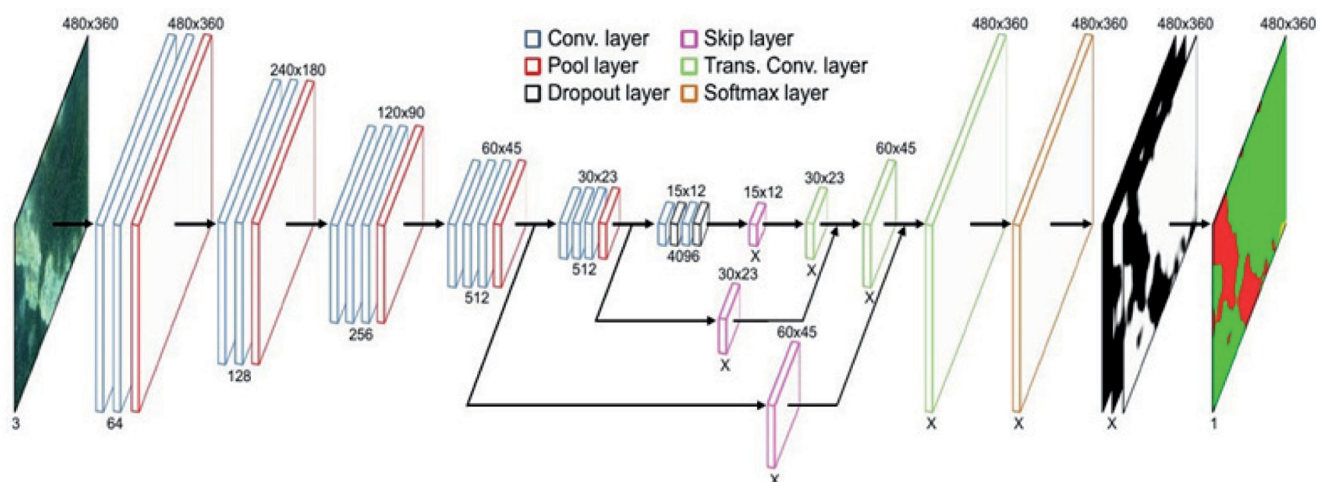

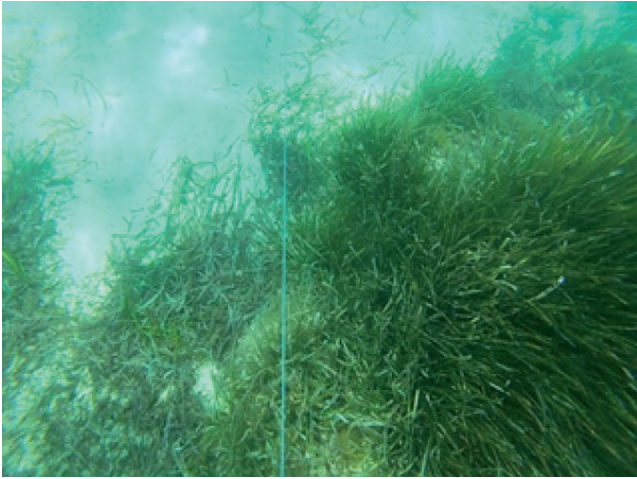Fig. 2. Layered architecture of the neural network used

Fig. 3. Image labelling for training

Encoder

The dimensions of the images to be processed will be 480x360 pixels in RGB. In the first stage, the image is received and processed by the first convolution layer. This first stage consists of 2 layers of 64 convolutions and a layer that performs the Max_Pool to reduce the size of the features by half (240x180 pixels). The second stage again consists of two convolution layers, although now the number of convolutions is doubled. When the convolutions are finished, a Max Pool is applied again to reduce the dimensions by half again (120x90 pixels).

The third and fourth stages follow the same procedure by adding a third convolution layer, doubling the number of convolutions, and halving the dimensions. In the fifth stage, the number of convolutions is maintained and the dimensions are reduced by half. In the sixth stage, in addition to the convolution layers, some dropout layers are included that are only used during training to avoid overfitting. At this stage the feature maps have been reduced to a size of 15x12.

3.2.2 Decoder

The decoder contains a map for each class to be classified. As the decoder stages progress, the size of the maps increases until they reach the size of the original image. The skip layer basically consists of a convolution of the feature map to obtain a new map per class. In the seventh stage, it consists of a skip layer, so from the sixth stage onwards, one map per class is obtained. The eighth stage consists of a transposed convolution that increases the size of the image. In the ninth stage, the transposed convolution of the sum of the layers of the previous stage and the skip layer of the fifth stage are performed, increasing the size of the image again. The tenth stage performs the transposed convolution of the sum of the layers of the previous stage and the skip layer of the fourth stage, increasing the size of the original

image. In the eleventh stage, the softmax function is applied to normalize the result obtained. Finally, in the last stage, we obtain a map by class. The value of each position on this map represents the probability that this pixel is of being in the class of the map. Therefore, to decide which class each pixel belongs to, the one with the highest value is chosen. As each class is assigned a color at the end, an image is obtained where each pixel is classified.

Training

To calculate the values of the neural network model, a supervised training phase will be carried out. This training consists of adjusting the parameters of the model from a collection of images with their corresponding labelled images. Figure 3 shows how an image (a) has been labelled (b) in order to carry out the training. Each color represents a class; the green is NG, the blue is dead NG, the yellow is sand, and the brown is sand with other elements.

The training consists of processing the images and comparing the obtained result with the desired result using a loss function. By applying the loss function, the model error is obtained, from which the model weights are adjusted. This procedure is repeated several times to progressively adjust the weights. Using an algorithm called back propagation, thanks to the gradient of the loss function, the weights of the model are calculated. To avoid overfitting and improve the result of the model obtained, dropout layers are usually added. Overfitting is a problem that can appear in neural networks. What it causes is that the model obtained after training works correctly for the images used in the training but not for the new ones. What the dropout layers do is randomly deactivate some connections in the neural network. In this way, the trained network is forced to be more versatile, thanks to the fact that the activation of more connections is forced when identifying the characteristics of the image [4] and [5]. Figure 4 shows a scheme of how the
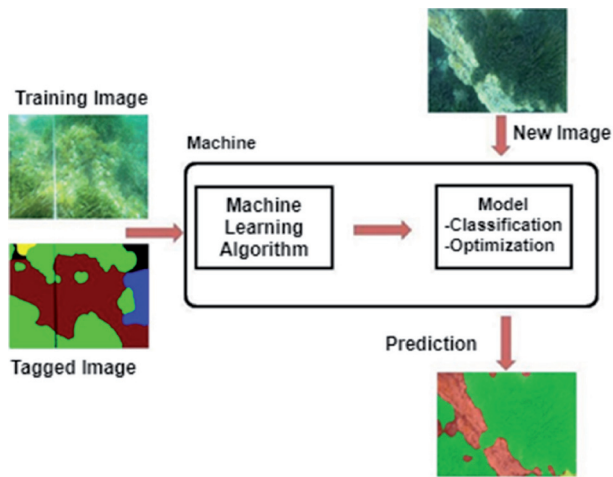
Fig. 4. Model training scheme

model is trained so that once it is trained, it can perform the inference of new images.

Hyperparameters used in training

There are a number of parameters that are used during training that directly influence the output of the trained model. Some of these parameters are:

Data augmentation consists of increasing the amount of data used during training. To do this, modifications are made to the contrast and brightness of the images used for training, thus increasing the variety of images and reducing overfitting.

Learning Rate: This affects how the model converges to the result during each step. A larger size can achieve the final result sooner, and smaller values obtain more optimal results. Therefore, it is necessary to determine an appropriate value that reaches a compromise between speed and quality of the results.

Number of iterations: defines the number of times to perform the back propagation and train again.

The suitability of these parameters depends on each problem to be solved. In this case, the same ones have been used as in work [2]. Since we are facing the same problem, the same types of images are used, and the same architecture is used simply by increasing the number of classes to be identified. During the training, data augmentation is used, with a learning rate of 1e-05 and 16000 iterations.

Models

Due to the different and varied classes present in the set of images, it is decided to carry out different training sessions, each of them grouping all the classes in a different way. In this way, since the input data for the network is different, different models will be obtained. The groupings made for the different trained models are shown in Table 2.

Because the images labelled as Sand and Sand-d are very similar and there are not enough images for the training to be effective in distinguishing them, it has been decided to group them all in the same Sand class. The same goes for the rock class and rock-d, which have been lumped together under the rock type.

Model I

When carrying out the training of model I, it has been decided to carry out a minimum classification, trying to dispense with the classes that appear less in the images, grouping them with the class that most resembles them. For this reason, the living NG (NG-a) and the dead NG leaves (NG-d) have been grouped into the same class, with all the rocky funds in the rock class and all the sand funds in the sand class. Table 3 shows the classification used for model I.

Table 2. Grouping of classes for the models used

All classes			Model III		Model II		Model I	
Name	Description	Color	Name	Color	Name	Color	Name	Color
NG-a	Living NG Kill	(green)	NG-a	(green)	NG-a	(green)	NG	(green)
NG-d	dead NG leaves	(blue)	NG-d	(blue)	NG-d	(blue)		
Rock	clean rocky bottom	(red)	Rock matte	(red)	Rock	(red)	Rock	(red)
rock-d	Rocky bottom with other elements	(dark red)						
Matte-r	Dead NG clump on rock bottom	(cyan)	sandy	(magenta)				
matte-s	Dead NG clump on sand bottom	(magenta)						
sandy	clean sand background	(yellow)	Name NG-a	(yellow)	Sand	(yellow)	Sand	(yellow)
Sand-d	Sand background with other elements	(olive)						
Background	Fund that does not correspond to any of the classes to be classified or that has not been identified	(black)	NG-d	(black)	Background	(black)	Background	(black)

Table 3. Classification used in model I

Name	Description	Color
NG	Live NG mat and dead NG leaves	green
Rock	Rocky bottom	red
Sand	sand background	yellow
Background	Fund that does not correspond to any of the classes to be classified or that has not been identified	black

Table 4. Classification used in model II

Name	Description	Color
NG-a	NG bush alive	green
NG-d	NG leaves dead	blue
Rock	Rocky bottom	red
Sand	sand background	yellow
Background	Fund that does not correspond to any of the classes to be classified or that has not been identified	black

Table 5. Classification used in model III

Name	Description	Color
NG-a	Living NG Kill	green
NG-d	dead NG leaves	blue
Rock	Rocky bottom	red
Sand	sand background	yellow
Matte	dead NG bush	magenta
Background	Fund that does not correspond to any of the classes to be classified or that has not been identified	

Model II

When model II was carried out, the classification was increased by one more class with respect to model I. The NG class separates the live NG (NG-a) and the dead NG leaves (NG-d). Table 4 shows the classification used for model II.

Model III

In model III, one more class is increased with respect to model II. I added the matte class to represent the mats of dead NG. Table 5 shows the classification used for model III.

Metrics of a neural network

To determine the quality of the results obtained in the classification of the neural network, a series of metrics such as true positive (TP), true negative (TN), false positive (FP), false negative (FN), accuracy, precision, recall, and F1 are used. These metrics basically consist of a series of calculations that are performed on the results in order to obtain objective information on the behaviour of the neural network.

Results

When training with the collections, the values for the models are obtained. Once with the trained models, the inference is made with the validation collections, the confusion matrix, and the metrics of the models.

Model I

Table 6 shows the confusion matrix for model I, and table 7 shows the metrics obtained from the confusion matrix.

As a result of the results, it can be verified that the metrics of both the NG and the rock are relatively good, above 90% in all metrics. As for the sand class, the results are generally good, but it has precision problems (79.3%), which means that the model is usually wrong more or less 1 time out of 5 when it predicts that a pixel is sand. Also, the value of F1 is not very high, which is why it is worth 86.7% since it is affected by precision. The one that obtains the worst results is the background class; the precision is relatively good, but the recall is quite low. This means that when a background

Table 6. Confusion matrix of model I

		Prediction (pixels)			
		NG	Rock	Sand	Background
Real (píxels)	NG	4963283	60011	67662	2264
	Rock	136687	3664330	50693	20764
	Sand	6340	2051	523967	3047
	Background	159546	321024	7412	100000

Table 7. Model I metrics

	Area (%)	Accuracy(%)	Precision(%)	Recall(%)	F_1(%)
NG	51.5227	96.8262	95.0256	98.8242	96.9267
Rock	39.8226	95.2263	91.7257	95.4245	93.5289
Sand	6.9223	99.8261	80.7258	97.1235	88.1261
Background	7.4268	96.1268	79.1260	17.7236	28.4247

Table 8. Normalized confusion matrix of model I

		Prediction			
		NG	Rock	Sand	Background
Real (%)	NG	98.8212	2.6227	2.7219	1.5273
	Rock	5.2241	95.4228	3.0260	2.0270
	Sand	4.8227	1.8231	97.1235	2.0268
	Background	29.5261	55.8252	2.6260	17.7267

is predicted, it is usually correct, but most of the time, when there is a background, it is not detected.

Table 8 shows the normalized confusion matrix, and from it it is clearly seen that most of the time that there is a background class, it is predicted as rock and sand rather than as background. Of the rest of the classes, it is verified that most of the time it is predicted correctly. Figure 5 shows an example of some predictions made from model I. In the first column are the original images (1a) and (2a), and in the second column are the manually labelled images (1b) and (2b). And finally, in the third column, is the prediction made by the model during the inferences (1c) and (2c). This prediction is shown superimposed on the actual image.

In the images in Figure 5, it can be seen that the NG, the rock, and the sand have been detected with enough precision.

Model II

Table 9 shows the confusion matrix for model II, and table 16 shows the metrics obtained from the confusion matrix.

In this model, one more class is added, distinguishing between living and dead NG. But the number of images containing dead NG is significantly lower than the live ones.

The NG-a, Rock, and Sand have good behaviour, similar to that of the model I. The background class also behaves in a similar way, although it has worsened its behaviour a little more compared to model I. The newly added NG-d class has poor behaviour, similar to Background. Precision, recall, and F1 have values below 20%, which means that this class is not detected very well.

From the normalized confusion matrix in Table 11, it can be seen that most of the times that NG-d should have been predicted were predicted as NG-a. This is due to their great similarity. It can also be seen that many times the NG-d was actually predicted to be sand; this is possibly due to the fact that in the training images, most of the time the NG-d was on sand. Figure 6 shows an example of some predictions made from model II. As in Figure 5, in the first column are the original images (1a) and (2a), in the second the manually labelled ones (1b) and (2b), and finally the prediction made by the model during the inference (1c). and (2c).
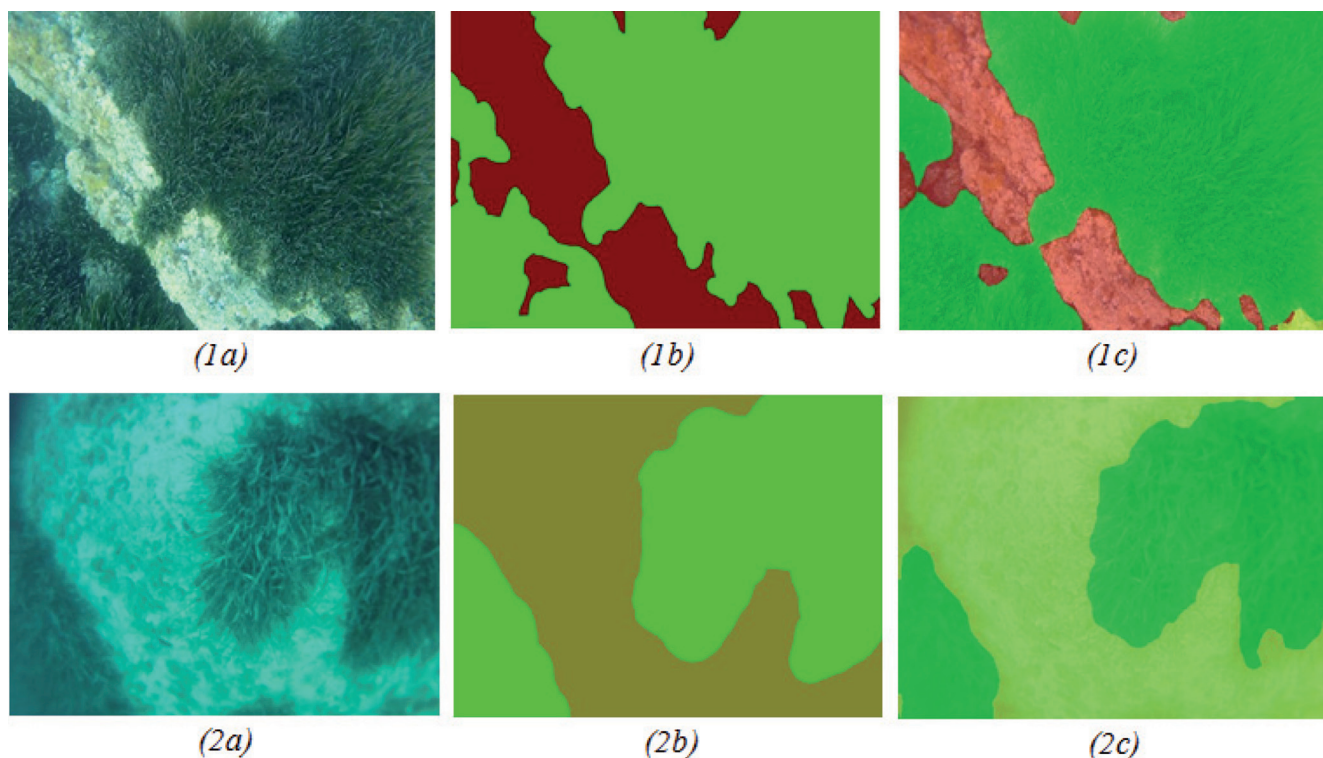

(1a)   (1b)   (1c)

(2a)   (2b)   (2c)

Figure 5. Model I predictions

Table 9. Confusion matrix of model II

		Prediction (pixels)				
		NG-a	NG-d	Rock	Sand	Background
Real (píxeles)	NG-a	4981572	496	58423	14502	1586
	NG-d	13678	50568	7361	8014	0
	Rock	135737	0	3746465	3829	153
	Sand	15949	7287	54085	446606	531
	Background	4981572	0	58423	14502	1586

Table 10. Model II metrics

	Area (%)	Accuracy(%)	Precision(%)	Recall(%)	F1(%)
NG-a	51.1263	97.1263	94.7263	99.9263	97.2263
NG-d	1.8263	100.8263	21.3263	20.5263	20.9263
Rock	39.8263	94.9263	89.5263	97.5263	93.3263
Sand	6.9263	100.1263	95.3263	83.3263	88.9263
Background	51.1263	97.1263	94.7263	99.9263	97.2263

Table 11. Normalized confusion matrix of model II

		Prediction				
		NG-a	NG-d	Rock	Sand	Background
Real (%)	NG-a	99.9263	1.4263	2.6263	1.7263	1.4263
	NG-d	41.0263	20.5263	21.2263	23.0263	1.4263
	Rock	5.2263	1.4263	97.5263	1.5263	1.4263
	Sand	4.5263	6.5263	11.3263	83.3263	1.5263
	Background	99.9263	1.4263	2.6263	1.7263	1.4263

In Figure 6, it can be seen in figure (1c) how sand is no longer detected, as well as in model I, confusing NG-d with sand. On the other hand, the NG and the rock can be seen, and it continues to detect them with enough precision.

4.3 Model III

Table 12 shows the confusion matrix for model III, and table 13 shows the metrics obtained from the confusion matrix.

A new class, Matte (dead NG kill), has been added to this model. For this class, as for the NG-d, it does not appear many times in the images used during training.

The NG-a and Rock and Sand classes, despite having worsened the predictions a bit, continue to behave quite well. The sand class is the one that has worsened the most, although it continues to behave in an acceptable way. The new Matte class does not behave well, as do the NG-d and
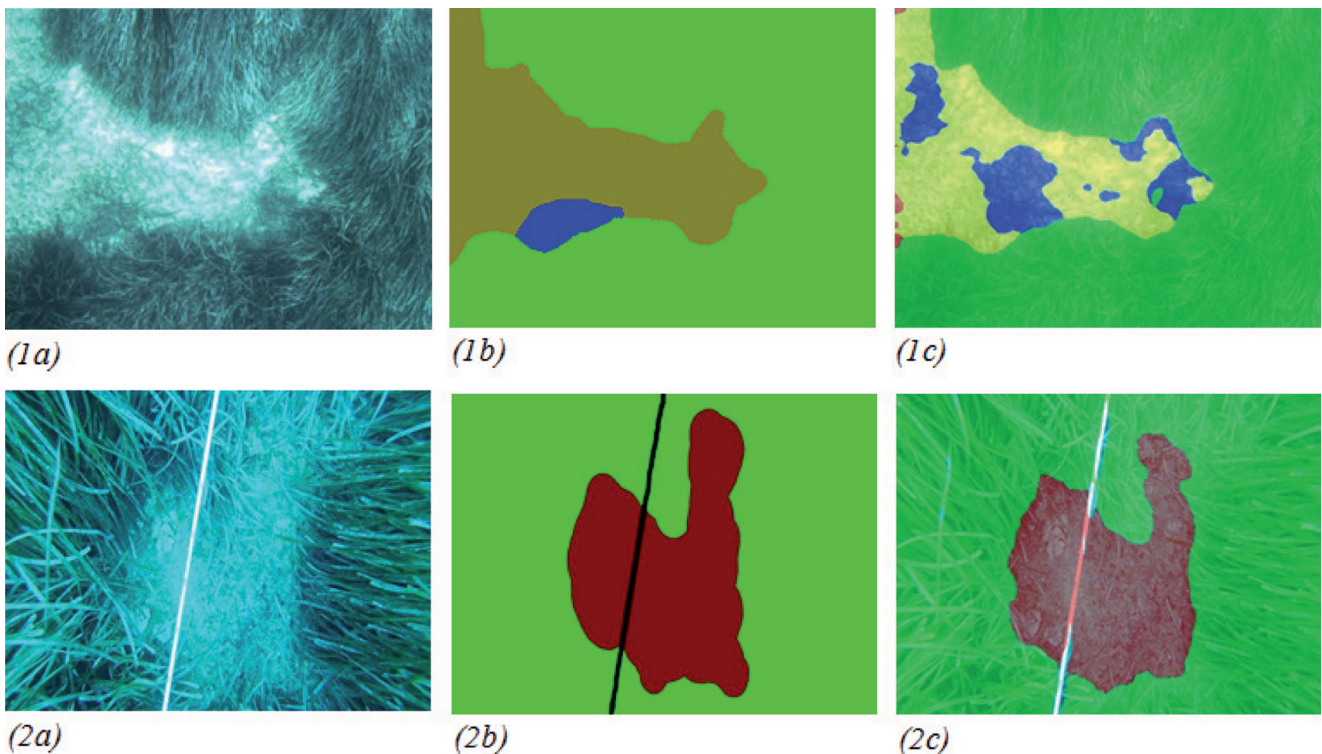

Figure 6. Model II predictions

Table 12. Confusion matrix of model III

		Prediction (pixels)					
		NG-a	NG-d	Rock	Sand	Matte	Background
Real (pixeles)	NG-a	4732028	2173	127895	74669	76	7443
	NG-d	6388	13065	3306	14282	0	209
	Rock	66907	0	3619081	166670	0	40151
	Sand	3833	25656	4074	452823	1625	476
	Matte	4999	23741	0	40620	4176	0
	Background	142627	0	309794	12298	0	134469

Table 13. Model III metrics

	Area (%)	Accuracy(%)	Precision(%)	Recall(%)	F1(%)
NG-a	51.1261	97.0250	96.7223	97.2225	96.9227
NG-d	1.8253	100.6261	21.0283	36.3217	26.5214
Rock	39.7232	94.1226	90.1214	94.1228	92.1268
Sand	6.2221	98.0224	60.8216	93.6227	73.7260
Matte	51.1234	97.0268	96.7267	97.2223	96.9223
Background	1.8225	100.6262	21.0260	36.3213	26.5217

Table 14. Normalized confusion matrix of model III

		Prediction					
		NG-a	NG-d	Rock	Sand	Matte	Background
Real (%)	NG-a	97.2263	0.0000	3.9263	2.9263	0.0000	1.6263
	NG-d	18.6263	36.3263	10.5263	39.6263	0.0000	2.0263
	Rock	3.4263	0.0000	94.1263	5.7263	0.0000	2.4263
	Sand	2.2263	6.9263	2.5263	93.6263	1.8263	1.5263
	Matte	8.2263	34.7263	1.4263	55.6263	7.1263	1.4263
	Background	24.9263	0.0000	54.0263	3.4263	1.4263	23.3263

Background classes. This is due to the few images that are in the training for these classes.

In the normalized confusion matrix of Table 14, it can be seen that the classes NG-a, Sand, and Rock tend to be correct with the predictions. On the other hand, the background and NG-d classes continue to fail a lot; the NG-d class has improved a bit compared to the II model, but they are still not acceptable values, and in addition to being confused with the NG-d and Sand, it is also confused in the predictions with Matt. The matte class also doesn't do well when mixed up, especially with the sand and NG-d classes. This is due, as for NG-d and background, to the few images that are available to

(1a)   *(1b)*   *(1c)*
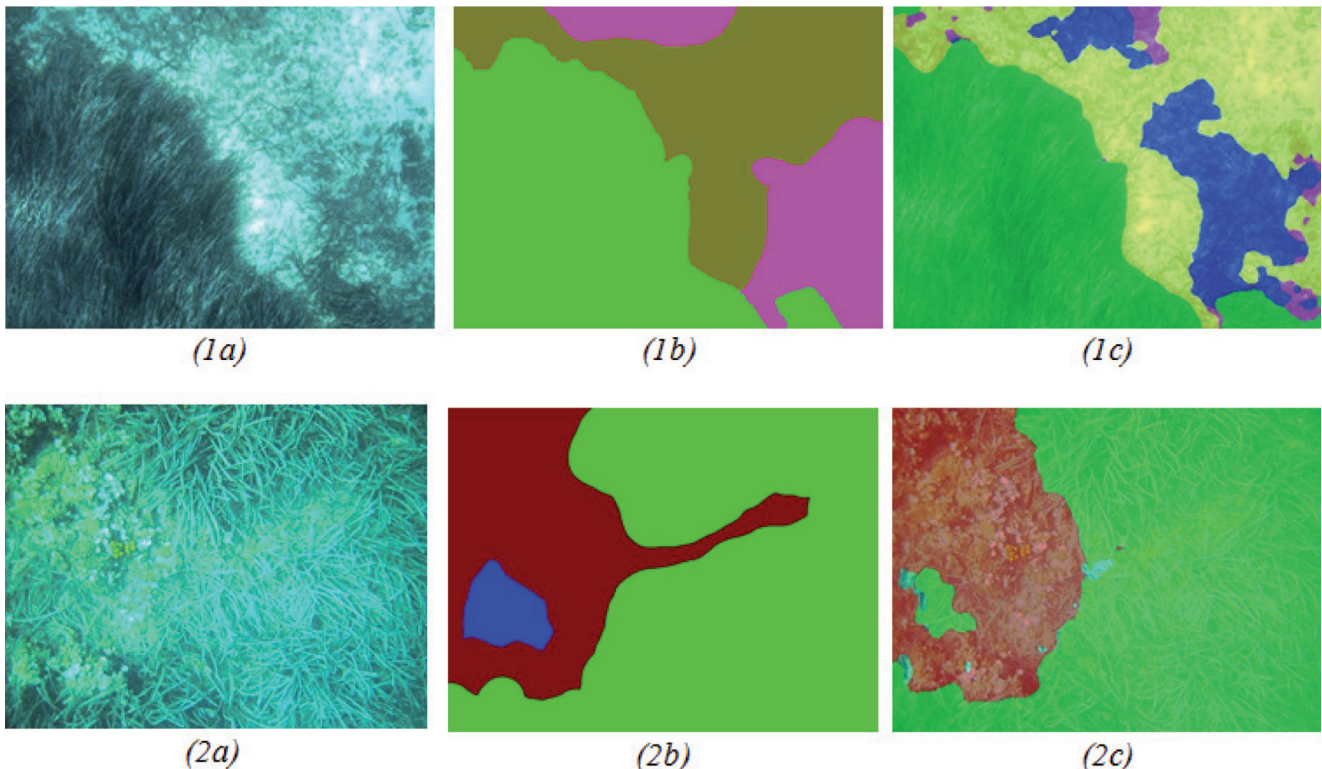
(2a)   *(2b)*   *(2c)*

Fig. 7: Model III predictions

train this class. Figure 7 shows an example of some predictions made from model II. As in Figure 5, in the first column are the original images (1a) and (2a), in the second the manually labelled ones (1b) and (2b), and finally the prediction made by the model during the inference (1c). and (2c).

In Figure 17, it can be seen that rock and NG are still detectable, but sand is sometimes confused with other classes, and both NG-d and matte do not quite identify them correctly.

Analysis of the results

The results obtained are relatively satisfactory, especially in the detection of NG, sand, and rock. Although the rest of the classes have not been able to be detected in a reliable way. The biggest reason why this happens is that the number of available images used in the trainings did not reach 250 for all classes. Since most of the images were of NG, it has led to the best detection of this class. Normally, in this type of classification, image collections of several thousand are used for each class that is desired to be able to detect. Not having so many images has favoured a decrease in the performance of the results obtained by the models. Another error that has been introduced in the collection of images has been during labelling. The labelling has been done by hand, and when labelling the boundaries between classes, the contours have not been exhaustively outlined. Also, different people would not mark exactly the same class boundary in an image. The labelling of certain classes has also been complicated, especially with the matte class and with some images where certain areas did not have sufficient quality. In these cases, there are quite a few discrepancies in how two people would classify the areas of the same image. These labelling errors introduce a decrease in the performance of the trained models.

Conclusion

Despite the fact that not all classes have been detected with sufficient reliability, the most relevant classes (NG, Sand, and Rock) have been successfully detected, obtaining in these cases an F1 of around 90%. In addition, the classification problems could be corrected by expanding the collection of images used in the training. The implemented system presents a series of advantages compared to other seabed detection processes, such as, for example, that it allows segmentation for each pixel of the image without suffering loss of information or requiring any type of post-processing, allowing this task to be carried out in real time. The implementation carried out would not only serve to classify images of the seabed; changing the collection of images and the configuration file of the model can be easily adapted to classify other types of images.

References

1. Jiang Q, Chen Y, Wang G, Ji T. A novel deep neural network for noise removal from underwater image. Signal Processing. Sept. 2020;87, doi: 10.1016/j.image.2020.115921.

2. O'Byrne M, Pakrashi V, Schoefs F, Ghosh B. A Stereo-matching technique for recovering 3D information from underwater inspection imagery. Comput. Aided Civ. Infrastruct. Eng. 2018;33:193–208.

3. Coyle R, Hardiman G, Driscoll K.O. Microplastics in the marine environment: A review of their sources, distribution processes, uptake and exchange in ecosystems. Case Stud. Chem. Environ. Eng. 2020;2:100010.

4. Honingh D, Van Emmerik T, Uijttewaal W, Kardhana H, Hoes O, Van de Giesen N. Urban River water level increase through plastic the accumulation at a rack structure. Front. Earth Sci. 2020;8:28.

5. Zhang M, Liu C, Wang S, He Q, Wei Q. Lightweight underwater object detection based on YOLO v4 and multi-scale attentional feature fusion. Remote Sensing. 2021;13(22):4706.

6. Xiao Y, Tian Z, Yu J, Zhang Y, Liu S, Du S, Lan X. A review of object detection based on deep learning. Multimed. Tools Appl. 2020;79:23729–23791.

7. Zhao ZQ, Zheng P, Xu ST, Wu X. Object detection with deep learning: A review. IEEE Trans. Neural Netw. Learn. Syst. 2019;30:3212–3232.

8. Ge P, Chen Y, Wang G, Weng G. A hybrid active contour model based on pre-fitting energy and adaptive functions for fast image segmentation. Pattern Recognit. Lett. 2022;158:71–79.

9. Weng G, Dong B, Lei Y. A level set method based on additive bias correction for image segmentation. Expert Syst. Appl. 2021;185:115633.

10. Lin TY, Goyal P, Girshick R, He K, Dollár P. Focal Loss for dense object detection. IEEE Trans. Pattern Anal. Mach. Intell. 2020;42:318–327.

11. Fang W, Wang L, Ren P. Tinier-YOLO: a real-time object detection method for constrained environments. IEEE Access. 2020;81935–1944.

12. Doherty M, Landowski J, Maynard P, Uber G, Fries D, Maltz F. Side scan sonar object classification algorithms. Proceedings of the 6th International Symposium on Unmanned Untethered Submersible Technology; IEEE. 1989;34:417–424.

13. Bello MG, Markov random-field-based anomaly screening algorithm. in SPIE's 1995 Symposium on OE/Aerospace Sensing and Dual Use Photonics. International Society for Optics and Photonics, 1995;34:466–474.

14. Mignotte M, Collet C, Pérez P, Bouthemy P. Markov random field and fuzzy logic modeling in sonar imagery: application to the classification of underwater floor. Computer Vision and Image Understanding. 2000;79(1):4–24.

15. Mignotte M, Collet C, Pérez P, Bouthemy P. Three-class markovian segmentation of high-resolution sonar images. Computer Vision and Image Understanding. 1999;76(3):191–204.

16. Mignotte M, Collet C, Pérez P, Bouthemy P. Statistical model and genetic optimization: application to pattern detection in sonar images. In: Proceedings of the IEEE International Conference on Acoustics, Speech and Signal Processing. IEEE. 1998;5:2741–2744,

17. Mignotte M, Collet C, Pérez P, Bouthemy P. Unsupervised markovian segmentation of sonar images. In: Proceedings of the IEEE International Conference on Acoustics, Speech, and Signal Processing. IEEE. 1997;4:2781–2784.

18. Reed S, Petillot Y, Bell J. An automatic approach to the detection and extraction of mine features in sidescan sonar. IEEE Journal of Oceanic Engineering. 2003;28(1):90–105.

19. Bell J, Petillot Y, Lebart K, Reed S, Coiras E, Mignotte P, Rohou H. Target recognition in synthetic aperture and high resolution sidescan sonar. In: High Resolution Imaging and Target Classification. The Institution of Engineering and Technology Seminar. IET. 2006;99–106.

20. Reed S, Petillot Y, Bell J. Automated approach to classification of mine-like objects in sidescan sonar using highlight and shadow information. IEE Proceedings Radar, Sonar and Navigation. 2004;151(1):48–56.

21. Daniell O, Petillot Y, Reed S, Vazquez J, Frau A. Reducing false alarms in automated target recognition using local sea-floor characteristics. In: Sensor Signal Processing for Defence (SSPD), 2014.

22. Calder B, Linnett L, Carmichael D. Spatial stochastic models for seabed object detection. In: AeroSense'97. International Society for Optics and Photonics. 1997;172–182.

23. Calder B, Linnett L, Carmichael D. Bayesian approach to object detection in sidescan sonar. IEE Proceedings-Vision, Image and Signal Processing. 1998;145(3):221–228.

24. Maussang F, Chanussota J, Histetb A. Automated segmentation of sas images using the mean–standard deviation plane for the detection of underwater mines. In: Proc. of MTS/IEEE Oceans 03 conference, 2003.

25. Maussang F, Chanussot J, Hétet A, Amate M. Mean-standard deviation representation of sonar images for echo detection: Application to sas images. IEEE Journal of Oceanic Engineering. 2007;32(4);956–970.

26. Linnett L, Carmichael D, Clarke S, Tress A. Texture analysis of sidescan sonar data. In: Texture analysis in radar and sonar, IEE Seminar on. 1993;2–1.

27. Bell J M, Linnett L. Simulation and analysis of synthetic sidescan sonar images. IEE Proceedings-radar, sonar and navigation. 1997;144(4):219–226.

28. Atallah L, Shang C, Bates R. Object detection at different resolution in archaeological side-scan sonar images. In: Europe Oceans. IEEE. 2005;1:287–292.

29. Michael TG, Tucker JD. Canonical correlation analysis for coherent change detection in synthetic aperture sonar imagery. Institute of Acoustics Proceedings. 2010;32(4);117–122.

30. Williams DP. Fast target detection in synthetic aperture sonar imagery: A new algorithm and large-scale performance analysis. IEEE Journal of Oceanic Engineering. 40, no. 1; 71–92, 2015.

31. Reed S, Ruiz IT, Capus C, Petillot Y, The fusion of large scale classified side-scan sonar image mosaics IEEE Transactions on Image Processing. 2006;15(7):2049– 2060.

Original article

Haemostatic biomaterial based on expired platelets for medical applications

VALENTINA NISTOR[1,2,*], LARISA IONITA[3], ALEXANDRINA RUGINA[4], DAN RAZVAN BENTIA[5], VIOLETA TURCUS[1], CORALIA ADINA COTORACI[6], DANIELA BRATOSIN[1]

[1]Vasile Goldiş Western University of Arad, Faculty of Medicine, Department of Biology and Life Sciences, Arad, Romania

[2]Tulcea County Hospital, Tulcea, Romania

[3]Romanian Doping Control Laboratory, Bucharest, Romania

[4]National Institute for Biological Science Research & Development, Bucharest, Romania

[5]Sanador Clinical Hospital, Department of Neurosurgery, Bucharest, Romania, Titu Maiorescu University, Faculty of Medicine, Bucharest, Romania

[6]Vasile Goldiş Western University of Arad, Faculty of Medicine, Department of General Medicine, Arad, Romania

Abstract

Blood loss has been a concern especially in surgery and bleeding control and a number of haemostatic agents and tissue sealants have been developed and applied in various surgical disciplines. The first steps to stop bleeding due to a vascular lesion, limit blood loss and allow healing are ensured by platelets that play an essential role in forming the primary haemostatic plug. After this, the clot is consolidated by the formation of a fibrin network organized around platelet aggregates.

In this study we tested for the treatment of external haemorrhagic lesions a new biomaterial based on expired platelets from blood banks immobilized on a collagen support. These platelets are no longer used for transfusions, are safe (tested for viral and bacterial contamination) and still have local haemostatic activity. Collagen is non-toxic, non-antigenic and promotes cell adhesion. Platelets bind to the collagen support and subsequently form clots through the intrinsic coagulation pathway.

✉   *Corresponding author: Valentina Nistor, Vasile Goldiş Western University of Arad, Faculty of Medicine, Department of Biology and Life Sciences, Arad, str. Liviu Rebreanu, no. 86, postal code 310414, Arad, Romania; email: nistorvalentina23@gmail.com; phone: +40 743 897711.

Introduction

The body's ability to clot blood is essential to beings and it is what allows us to survive an injury. The clotting process helps wound close up to prevent the injured person from losing too much blood. A healthy body has a specific and effective defence mechanism to prevent excessive blood loss during injuries. The coagulation system is activated very quickly. This leads to the formation of blood clots which will clump together at the lesion to stop the bleeding (haemostasis) [1, 2, 3].

Haemostasis is a vital step and quick haemostasis is important for trauma and surgical operation and other situations in emergency medical care.

The amount of blood in a normal human is approximately 7-8% of the total body weight and when blood loss reaches 20% of total blood volume, it is difficult to maintain normal blood volume and blood pressure. If the extent of blood loss exceeds 40% in a short time, this is the leading cause of trauma-related deaths. 15% of all trauma deaths are caused by a post-traumatic haemorrhage [4]. Adequate haemostasis is an essential strategy to prevent bleeding to avoid death and is the first step in wound healing. Haemostasis is the process of stopping bleeding at the injury site by a haemostatic system consisted of elements that are always present in the blood in an inactive state (platelets and soluble coagulation factors) that are activated immediately after an injury [5].

Platelets play an essential role in maintaining haemostasis, as they form the first line of haemostatic defence by forming the primary haemostatic plug.

Platelets are small pieces of cytoplasm that are shed from the cytoplasm of mature megakaryocytes and these participate in haemostasis and coagulation. Glycoprotein Ib (GPIb) and phospholipid surface of platelets participate to increasing the speed of the clotting response. Under normal circumstances, rapid haemostasis can be achieved in the presence of a large number of local adherent platelets and clotting factors. During processing and storage, platelet activation markers were observed such as the release of specific granular contents in plasma (β thromboglobulin, platelet factor 4 and RANTES), changes in GP expression on the surface of platelets (GPIB, GPIIb and GPIIIa), protein expression, sequestered granular membranes (P-selectin -CD62P, CD63 and CD40L) and the externalization of phosphatidylserine (determined by annexin V binding) [6]. Platelet, platelet-derived nano-vesicles and synthetic platelet mimics can be used to develop haemostatic materials.

With rapid developments in science and technology, various haemostatic materials have been developed with the hope of enhancing the haemostatic effect by activating different coagulation mechanisms. Therefore, developing safe, effective, and convenient haemostatic materials is important. Active haemostatic agents currently used in the field of haemostasis can be natural polymers, synthetic polymers, inorganic materials, and metal-containing materials based on activation of different coagulation mechanisms [7]. Today, the available natural polymeric haemostatic materials are polysaccharides and collagens. These materials are also widely used to manufacture artificial skin, absorbable sutures and drug carriers. Regarding the research status in this field, the design of composite haemostatic materials should conform to the requirement according to which multiple coagulation mechanisms can be simultaneously activated in order to enhance the haemostatic effect [8].

In this study, we aimed to obtain a new biomaterial based on the use of platelets from blood banks at the end of the storage period (hPL-e), immobilized on a collagen support, with good regeneration and healing properties for the treatment of external haemorrhagic lesions. These platelets are no longer used for transfusions, are safe (being tested for viral and bacterial contamination) and still have local haemostatic activity.

Materials and methods

Biological materials

Blood samples were collected from healthy donors into heparinized tubes and tested immediately after sampling. Cells were sedimented by centrifugation, 350 g at 4°C for 5 min, for the removal of plasma, platelets and leukocytes. Platelets concentrate (CUT) and plasma were provided by Tulcea County Hospital, Tulcea, Romania.

Chemicals

Fluorescein conjugated annexin-V (Annexin-V-FITC), HEPES binding buffer (HEPES buffer pH 7.4 containing 2.5 mM calcium chloride), were obtained from Pharmingen (San Diego, CA, USA).

Methods

Obtaining of haemostatic biomaterial

The first phase of the research consisted in testing the coagulation capacity of expired platelets (hPL-e), preserved for 5 days, at the end of this period. The platelet suspension was deposited in glass plates with wells, in the presence or absence of plasma and the supernatant was removed after sedimentation and fixed in cacodylate (0.1 M, pH of 7.2) and 1.25% glutaraldehyde buffer or 70% ethanol for 4 hours. The addition of freshly collected blood on heparin in the wells with immobilized platelets was analysed, after washing with

PBS, for the attachment of red blood cells to platelets and preservation of the capacity to participate in clot formation by optical microscopy and SEM analysis.

In the stage 2 of research, we proposed to use a collagen film as a support for immobilization of platelets (hPL-e), in order to obtain a haemostatic product applicable to wounds at the dermal level.

Cells may be immobilized by a number of methods for a variety of purposes. Although the study of cell immobilization is comparatively novel, the methods that have been developed are very effective and there are few indications that further, greatly superior techniques are likely to evolve [9, 10]. Cells are best immobilized by aggregation, by adsorption onto a support material or by entrapment within gels, of which the natural supports have proved the most useful.

The immobilization of the sedimented platelets on the collagen gel was done with a buffer containing 2.5% glutaraldehyde, in the presence or absence of plasma, followed by washing the collagen/platelet film product with distilled water. On top of the obtained haemostatic supports, freshly collected blood on heparin was later added and after incubation for 5 minutes, removing by washing with PBS of the red blood cells not attached to the support. In all cases, the samples were analysed by scanning electron microscopy.

Scanning Electron Microscopy (SEM) analysis. Fresh erythrocytes and platelets were fixed for 4 hours in 1.25% glutaraldehyde in cacodylate buffer (0.1 M, pH of 7.2), washed 3 times with distilled water, filtered through 0.2 μm Anodisc filters and analysed at a Hitachi SU 1510.

Flow cytometric analyses

Cells (RBCs and platelets) were analysed by flow cytometry according to Bratosin *et al*., 2007[11], and by Scanning Electron Microscopy. Flow cytometric analyses were performed on a Becton Dickinson FACScan cytometer equipped with an argon-ion excitation laser 488 nm using Cell Quest Pro software for acquisition and analysis of results. Cells were gated for the light scatter channels on linear gains, and the fluorescence channels were set on a logarithmic scale.

Morphological changes assessment of platelets by light scattered measurements

Analysis of the scattered light by flow cytometry in the mode FSC/SSC provides information about cell size and structure. The intensity of light scattered in a forward direction (FSC) correlates with cell size and the intensity of scattered light measured at a right angle from the laser beam (SSC) correlates with granularity, refractiveness and presence of intracellular structures that can reflect the light, being associated with cell shrinkage. Platelets suspension in

isotonic PBS buffer, pH 7.4, was gated under forward and side scatter parameters (FSC versus SSC).

Flow cytometric analysis of phosphatidylserine exposure

Phosphatidylserine exposure on platelets was assessed using Annexin-V-FITC. Platelets were suspended (10^6 cells) in HEPES buffer pH 7.4 containing 2.5 mM calcium chloride with 10 μL (0.1 μg) of Annexin-V-FITC solution and incubated for 15 min at room temperature in the dark. The cells were gated for biparametric histograms FL1 (FITC fluorescence) versus FL2 (platelets autofluorescence).

Scanning Electron Microscopy (SEM) analysis

The stages of biological sample preparation for SEM imaging were as follows: Samples of biomaterial were fixed for 4 hours in 1.25% glutaraldehyde in cacodylate buffer (0.1 M, pH of 7.2), washed 3 times with distilled water, filtered through onto 0.2 μm Anodisc filters and analysed directly with a HITACHI SU 1510 scanning electron microscope.

Results

Morphological changes analyses of expired platelets by flow cytometry and scanning electron microscopy (SEM)

Flow cytometric analyses of expired platelets (hPL-e)

Flow cytometry is a widely accepted method for the detection of platelet activation [12]. Expired platelets (hPL-e), preserved for 5 days, were analysed at the end of this period for morphological changes by light scattered, in the mode FSC/SSC that provides information about cell size and structure and for phosphatidylserine (PS) exposure using Annexin-V-FITC compared with fresh platelets. Activation of platelets was observed as a morphological change from the discoid state to activated spherical cells with pseudopods.

As shown in Figure 1, the image given for the dot-plot test contains 2 areas, namely viable platelets and senescent cells whose morphological parameters have changed, having a decrease in size and density, according to cells undergoing apoptosis. This picture evolves during storage, from day 1 to day 5, with the zone of viable platelets rapidly retreating to apoptotic cells for platelets preserved in transfusion centres.

These morphological changes have led to the dot-plot different from that obtained for the control platelets (Fig 1).

It has also been shown that the morphological changes are accompanied by PS externalisation, correlating the results obtained by the dot-plot analysis with the results provided by the Annexin-V-FITC test. A higher percentage of approximately 31% and 44% PS is observed for day 2 and
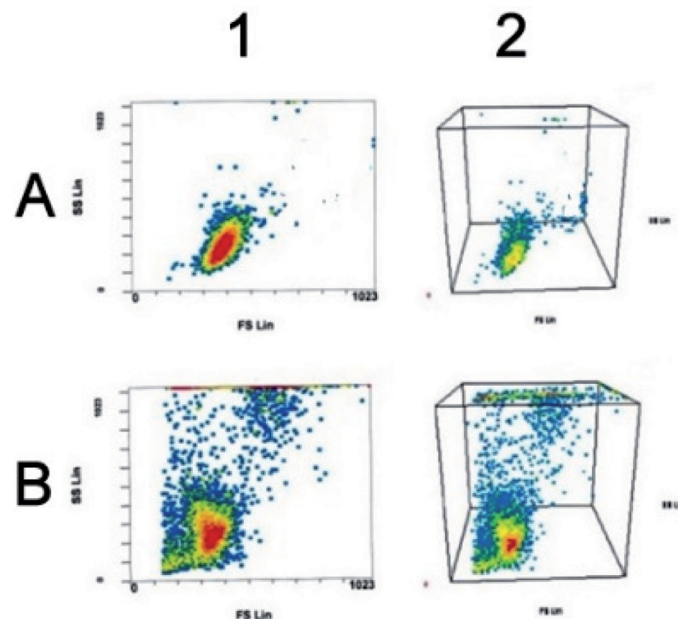
Fig 1. Flow cytometric analysis of fresh (A) and expired platelets *(hPL-e)* (B); (1) Dot-plot analysis Forward Scatter (FSC Lin) versus Side Scatter (SSC Lin); (2) 3D-plot analysis FSC Lin/ SSC Lin /vertically number of cells

day 3, and 65% to 83% PS in platelets preserved on day 5 and 7, compared to 5% - 10% PS in platelets at the time of their collection was obtained.

This morphological change, possibly together with a high percentage of platelets externalizing PS demonstrated that platelet concentrate stored at 20 °C (room temperature) for 5 days storage, (the storage temperature currently used in blood banks), shows a loss of their integrity and functionality, known as the platelet storage lesion.

Scanning Electron Microscopy (SEM) analysis of expired platelets

Scanning electron microscopy showed modification of platelets at the end of the preservation period losing their initial discoidal shape, almost entirely showing the appearance of cells in apoptosis, with vesicles, pseudopodia formation and membrane blebbing. Freshly platelets have a discoid shape, whereas expired platelets are much smaller, mostly with a spherical morphology (Fig 2).

Platelets were activated, since pseudopodia were prominent and interactions, especially platelet–platelet interaction, could be distinguished. This shows that platelets are activated and release their granules. Platelet pseudopodia formation is the initial morphological change associated with adhesion and aggregation. These processes are suggested to aid adherence to other platelets and the forming fibrin strands. The increased pseudopodia formation seen during storage, and the visible interaction of the processes with other platelets, therefore support platelet adhesion and aggregation.

Subsequent granule release will recruit additional platelets and trigger the formation of the fibrin network to form

the stable, secondary haemostatic plug. The observed membrane blebbing can therefore be the result of elevated thrombin concentrations. However, no thrombin was added to the platelet samples. It can be deduced that elevated thrombin concentrations were present in the plasma. It is known that elevated thrombin induces platelet activation, resulting in blebbing of the membrane similar to apoptosis. Membrane blebbing is one of the traits of apoptosis. Scanning electron microscopy confirms the results obtained by flow cytometry.

In vitro haemostasis evaluation and characterisation of biomaterial by SEM analysis

Haemostasis analysis obtained in the first stage of the research consisted in testing the coagulation capacities of platelets preserved for 5 days, at the end of this period. (hPL-e) were deposited as a suspension in glass plates with wells, in the presence or absence of plasma. After sedimentation, supernatant was removed and platelets adhered to the glass were fixed with cacodylate/glutaraldehyde buffer or 70% ethanol for 4 hours. Freshly collected blood on heparin it was added for testing of their haemostatic capacities.

The attachment of red blood cells to platelets was measured by measuring the capacity to participate in the clot formation as preservation of haemostatic properties. The best results were obtained when hPL-e were fixed with glutaraldehyde and observed by optical microscopic analysis (data not shown).

If the platelets were fixed on a collagen support, as shown in Figure 3, a first analysis was conducted by scanning electron microscopy of the attachment of red blood
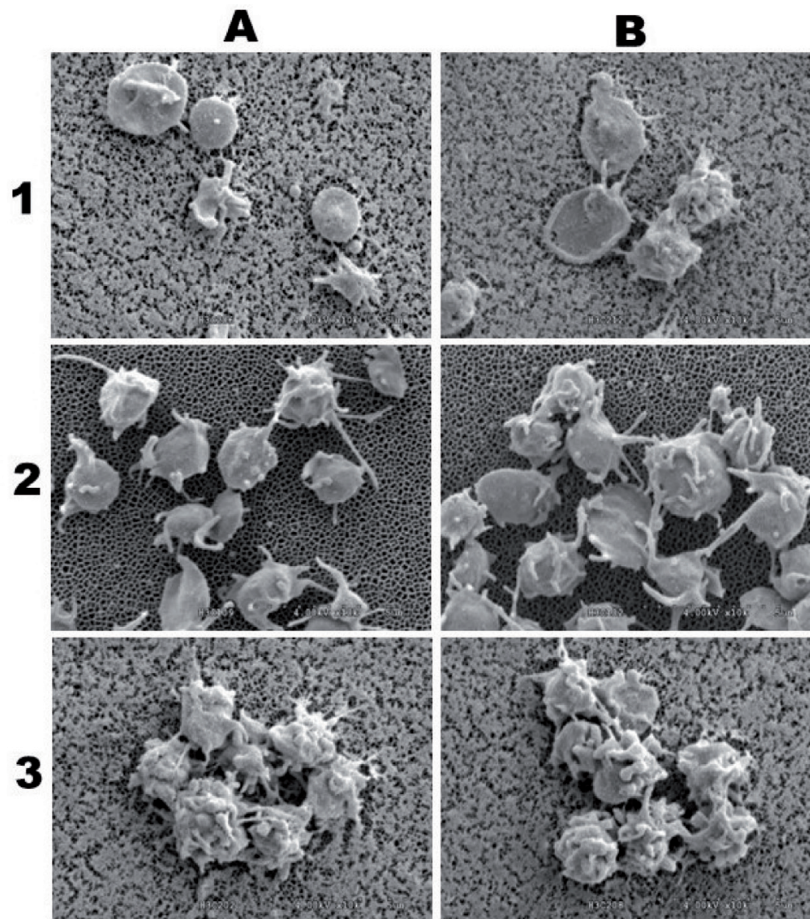
Fig 2. Analysis by Scanning Electronic Microscopy (SEM) of expired platelets (hPL-e), preserved in transfusion centers for 3-day storage (2-A and B) and 5-day storage (3-A and B) compared with freshly normal (hPL) at time zero sampling (1-A and B). Data shown are representative for similar results.
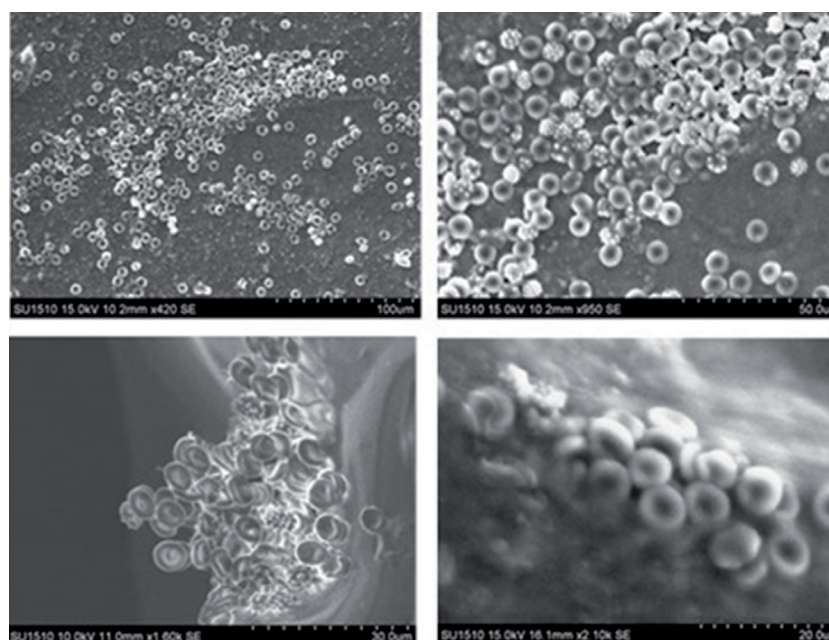

Fig 3. Scanning Electronic Microscopy analysis of *in vitro* haemostasis evaluation and clot formation of expired platelets (hPL-e) fixed on a collagen support. Data shown are representative for similar results.

cells to platelets and clot formation, and the best results were obtained when platelets were fixed with glutaraldehyde in the presence of plasma.

Discussion

Blood loss has always been a concern especially in surgery and bleeding control methods. Over the past years, a number of haemostatic agents and tissue sealants have been developed and are currently used in various surgical disciplines.

The efficacy of some products has been established, but others are awaiting further evaluation and confirmation. Haemostatic treatments include fibrin sealants, microfibrillar collagen, gelatin, haemostatic agents, oxidized regenerated cellulose and cyanoacrylates adhesives [13, 14].

The research and development of haemostatic materials are prerequisite for effective haemostasis. Chitosan with a good biodegradability, biocompatibility and nontoxicity and excellent haemostatic properties led to the appearance of new haemostatic materials based on chitosan widely applied in medicine [8]. Haemostatic agents work by forming blood clots at bleeding site of vessel injury either mechanically or by increasing the coagulation cascade [14]. The first steps to take to stop bleeding due a vascular lesion, limit blood loss and allow healing is ensured by the platelets. After the platelets have formed a first barrier limiting bleeding, the clot is consolidated by the formation of a fibrin network organized around aggregates platelets [15].

Collagen is an extracellular-matrix protein that plays an important role in the formation of tissues and organs and it is non-toxic, non-antigenic, favours cell adhesion, proliferation, and differentiation to mimic the natural cell environment [16]. Erythrocytes and platelets have in their membrane structure Annexin-V, known for its ability to bind to PS. Thus, RBCs recognize the large number of PS residues in the membrane of expired platelets or membrane annexin-V of hPL-e is fixed by PS of RBCs and generate the formation of a thrombus phosphatidylserine [17, 18, 19, 15]. Platelets bind to the collagen framework and subsequently form clots via the intrinsic coagulation pathway. Haemostasis is usually achieved in 2-5 minutes.

The development of medical services requires an increased effort for new haemostatic materials performance, efficiency, security, designed for easy transport.

Conclusions

In conclusion, advances were achieved in the field through our haemostatic biomaterial based on expired platelets, which are safe (platelets were tested for viral and bacterial contamination) and still have local haemostatic activity. Collagen is non-toxic, non-antigenic and promotes cell adhesion. Eryth-rocytes from blood bind to the expired platelets fixed on collagen support and subsequently form clots through the intrinsic coagulation pathway. Our haemostatic biomaterial can contribute to solving the current needs in medical practice.

Acknowledgments

References

1. O'Donnell JS, O'Sullivan JM, Preston RJS. Advances in understanding the molecular mechanisms that maintain normal haemostasis. Br J Haematol. 2019; 186(1): 24–36. doi: 10.1111/bjh.15872

2. Peng HT. Biomaterials for haemorrhage control. Trends Biomater Artif Organs. June 2010; 24(1):27-68.

3. Grover SP, Mackman N. Intrinsic pathway of coagulation and thrombosis. Arterioscler Thromb Vasc Biol. 2019; 39(3): 331–38. doi: 10.1161/ATVBAHA.118.312130

4. Mabry R, McManus JG. Prehospital advances in the management of severe penetrating trauma. Crit Care Med. 2008; 36(7): 258–266. doi: 10.1097/CCM.0b013e31817da674

5. Koupenova M, Clancy L, Corkrey HA, Freedman JE. Circulating platelets as mediators of immunity, inflammation, and thrombosis. Circ Res. 2018; 122(2): 337-351. doi: 10.1161/CIRCRESAHA.117.310795

6. Vassallo RR. Recognition and management of antibodies to human platelet antigens in platelet transfusion-refractory patients. Imunohematology. 2009; 25(3):119-124. doi.org/10.21307/immunohematology-2019-244

7. Guo Y, Wang M, Qi L, Guoliang L et al. Recent advances in the medical applications of haemostatic materials. Theranostics. 2023; 13(1): 161–196. doi: 10.7150/thno.79639

8. Hu Z, Zhang D-Y, Lu S-T, Li P-W et al.'. Chitosan-Based Composite Materials for Prospective Hemostatic Applications. Mar Drugs. 2018; 16(8): 273. doi:10.3390/md16080273

9. Bucke C, Brown DE. Immobilized Cells [and Discusion]. Philosophical Transactions of the Royal Society of London. Series B. Biol Sci . 1983; 300(1100): 369-389. doi : http://www.jstor.org/stable/2395831

10. Caiyun Z , Qingyan Z, SaHu P, Wendong W et al.'. Research status and development potential of composite hemostatic materials, J Mater Chem B; 2020 Jul 1; 8(25):5395-5410

11. Bratosin D. Exploring by flow cytometry the structure and cellular functions. V. Goldis University Press, Arad. 2007; ISBN: 978-973-664-213-5.

12. Devine DV, Bradley AJ, Maurer E, Levin E et al.'. Effects of prestorage white cell reduction on platelet aggregate formation and the activation state of platelet and plasma enzyme systems. Transfusion. 1999; 39: 724-734. doi: https://doi.org/10.1046/j.1537-2995.1999.39070724.x

13. Masci E, Santoleri L, Belloni F, Bottero L et al.'. Topical hemostatic agents in surgical practice. Transfus Apher Sci. 2011; 45(3), 305-311. doi: 10.1016/j.transci.2011.10.013

14. Traver MA, Assimos DG. New Generation Tissue Sealants and Hemostatic Agents: Innovative Urologic Applications. Rev Urol. 2006; 8(3):104-111

15. Jandrot-Perrus M, Nurden P. Des fonctions plaquettaires aux implications thérapeutiques. From platelet functions to therapy. Rev Med Interne. 2010; 31(3): 319-323. doi: 10.1016/j.revmed.2010.09.020

16. Shoulders MD, Raines RT. Collagen structure and stability. Annu Rev Biochem. 2009; 78: 929–958, doi: 10.1146/annurev.biochem.77.032207.120833

17. Seghatchian J, Krailadsiri P. Red cell storage lesion assessed by the levels of potassium, hemoglobin and annexin V in supernatants. Transf Aph Sci. 2002; 26(2):139–143. doi: 10.1016/s1473-0502(01)00155-0

18. Herr C, Clemen CS, Lehnert G, Kutschkow R et al. Function, expression and localization of annexin A7 in platelets and red blood cells: Insights derived from an annexin A7 mutant mouse. BMC Biochem. 2003; 4: 8. doi:10.1186/1471-2091-4-8

19. Sparrow RL, Healey G, Patton KA, Veale MF. Red blood cell age determines the impact of storage and leukocyte burden on cell adhesion molecules, glycophorin A and the release of annexin V. Transfus Apher Sci. 2006; 34(1):15–23. doi: 10.1016/j.transci.2005.09.006

Original article

Microbiological and nutritional quality of banku a fermented maize and cassava-based food consumed in West Africa

**EKOUA REGINA KRABI[1], KOFFI MAÏZAN JEAN-PAUL BOUATENIN[2,*],
KOHI ALFRED KOUAMÉ[2], INZA FRÉDÉRIC FOFANA[2], MARINA KOUSSEMON[2]**

[1]Félix Houphouët-Boigny University, UFR Biosciences, Laboratory of Biotechnology, 22 BP 582 Abidjan 22, Côte d'Ivoire.

[2]Food Sciences and Technology, Laboratory of Biotechnology and food Microbiology, Nangui Abrogoua University, 02 BP 801 Abidjan, Côte d'Ivoire.

Abstract   Banku is a food made of fermented maize flour and fermented cassava dough. It is produced and consumed by the Togolese, Nigerian and Ghanaian peoples living in Côte d'Ivoire. Not only is this food less known by the original inhabitants of the Côte d'Ivoire but the nutritional and sanitary quality of this food is not defined. However, its preparation remains empirical and is done in unhygienic conditions. Thus, objective of this study is to promote banku through its nutritional and sanitary characteristics in order to ensure consumer safety. Two localities (Grand-Bassam and Gonzagueville) of Côte d'Ivoire where there is a strong foreign community were chosen to take the various samples. The analyses were carried out by biochemical and microbial properties during the production of banku. The results showed that the fermented maize flour had the highest titratable acidity with a value of $0.31 \pm 0.01\%$. The phytate content was lower in the mixture of fermented maize flour and cassava dough with a value of 8.81 ± 0.57 mg/100 g DM. After cooking, the mesophilic aerobic germs load in the banku indicated $(5.6 \pm 0.4) \times 10^3$ CFU/g which is below the standard prescribed by CODINORM. The promotion of banku in Côte d'Ivoire would contribute to food self-sufficiency and growth of the country's economy. The nutritional and microbiological properties are in accordance with the CODINORM (2001) standard. Banku can be safely consumed in Côte d'Ivoire and worldwide.

✉   *Corresponding author: Jean-Paul Bouatenin, Food Sciences and Technology, Laboratory of Biotechnology and food Microbiology, Nangui Abrogoua University, Abidjan, Côte d'Ivoire, 02 BP 801 Abidjan 02, email: bouateninkoffi@gmail.com; phone: +225 0708070253.

Introduction

Fermentation is also used by indigenous populations in developing countries, particularly in the many traditional technologies for processing cassava and maize [1]. Fermented products derived from cassava (*Manihot utilissima*) and maize (*Zea mays L.*) include *banku*. *Banku* is a Ghana dish that is prepared with a mixture of fermented maize and cassava contained in a smooth whitish paste, cooked in boiling water [2]. *Banku* is served as a side dish with soup, stew, or in a pepper sauce with fish [3]. In Côte d'Ivoire, this dish is produced and consumed by the Togolese, Nigerian and Ghanaian people. It is an unknown food in Côte d'Ivoire and its production relies on empirical knowledge, based on the traditional experience of the foreign producer. Its production involves a combination of steps in which the mixture of maize flour and cassava dough is fermented for three days before being kneaded by hand to obtain a suitable consistency for subsequent cooking. This method of production does not seem to offer a guarantee to curb the proliferation of microorganisms. For example, hand-kneading or numerous hand manipulations during production are favorable to the contamination and growth of many microorganisms [4]. According to [5], food safety in Africa is crucial. This concerns fermented foods in particular. They are produced in the absence of hygiene practices, production and marketing. In addition, the production sites are not very healthy and the premises are not very adequate. Other problems are often encountered by producers, such as the lack of control over manufacturing parameters such as temperature, fermentation processes, etc. [5]. Fermentation is an ancestral process of food processing that has three major advantages overall, namely improving the nutritional quality of food; improving the sanitary quality of food, improving the organoleptic quality of food. These benefits are produced by certain microorganisms of interest to the food industry. These include lactic acid bacteria and yeasts. In fact, lactic acid bacteria, thanks to the organic acids they produce, guarantee food safety, as well as providing it with specific flavor and texture characteristics. Work carried out by [6] showed that lactic acid bacteria help to reduce cyanide levels in cassava and are responsible for the sour taste in fermented products due to the production of lactic and acetic acids. Yeasts had previously been identified as the second most predominant germs involved in cassava-based foods, after lactic acid bacteria. Cassava-based foods after lactic acid bacteria capable of contributing to flavor development in fermented products [7]. A poorly done fermentation, often leads to a product of inconsistent quality, poor hygiene, low nutritional value and short shelf life [8]. Similarly, the presence of antinutritonal substances can reduce the nutritional value of foods by interfering with the absorption of certain minerals (iron, calcium, zinc), and the digestibility of proteins and carbohydrates. In some cases, they can potentially cause toxicity and health problems when present in the body in excessive quantities. Thus, to ensure the health of consumers and to promote a new traditional food on the Ivorian territory, it is necessary to know the microbiological and nutritional characteristics of *banku*. On the one hand, this study will allow us to put in place strategies for rapid and early detection of microbiological and anti-nutritional hazards and prevention of food-borne diseases for the production of *banku* of consistent and healthy quality. On the other hand to solve the problem of food self-sufficiency in Côte d'Ivoire. Until today, there are no studies on the biochemical composition and the sanitary quality of this food which could be integrated in the food habits of the people of Côte d'Ivoire and even in the whole world. Therefore, the general objective of this study is to valorize the *banku* in order to promote its consumption on the African continent and in the whole world.

Materials and methods

Sample source and collection

The material consisted of four (04) samples taken during the production of *banku*: the maize flour obtained after fermentation, the fermented cassava dough, the mixture of the maize flour and the fermented cassava dough and finally the product obtained after cooking « the banku ». Fermentations were carried out in ROUND plastic bowls D. 36 8L POLA of 28 cm in diameter and 12.5 in height covered tightly with clean and sterile linen or in GILAC HACCP food plastic bins - volume 12 to 55 L, of height 18 cm and diameter 32,5 cm. These samples were taken in two (02) localities (Grand-Bassam and Gonzagueville). These localities were chosen because they are home to Togolese, Nigerian and Ghanaian *banku* consumers. Gonzagueville is a district of the commune of Port Bouėt (Abidjan). While Grand-Bassam is a city located 14 km from Gonzagueville. In each locality, five producers were selected. For each visit, four samples were taken from a producer: 500g of fermented maize flour, 500g of fermented cassava dough, 500g of the mixture of fermented maize flour and fermented cassava dough and finally 500g of the product obtained after cooking (the *banku*). Three visits were made to each producer. A total of 120 samples were taken from the 10 women farmers, 12 samples per farmer. These samples were packaged in sterile "Stomacher" bags, placed in a cooler containing carbohydrate ice at 4°C and transported to the central laboratory of the NANGUI AB-ROGOUA University in Abidjan, Côte d'Ivoire where they were refrigerated at 4°C before any analysis.

Production follow-up

For production monitoring, all production units participated. Grand Bassam and Gonzagueville were chosen as the production zones. The banku processors were observed during production in order to learn about the different stages of banku production. This monitoring helped to explain certain results in this study.

Biochemical analysis

Sample acidity

pH and titratable acidity were determined by the method of [9]. Forty grams of samples were ground in 300 ml of distilled water in a porcelain mortar and then centrifuged at 4000 tours/min for 30 min. The pH was determined on 50 ml of the supernatant using a pH-meter (P107 Consort). Total titratable acidity (TTA) was determined by titrating 10 ml of supernatant used for pH determination against 0.1 M NaOH using phenolphthalein as indicator. TTA was calculated as percentage.

Macronutrient contents

The dry matter content were determined gravimetrically in an oven at 105 °C and every 24 hours the weight of the sample was determined until a stable weight was obtained [10]. Watersoluble carbohydrates were determined by the phenol sulphuric acid method according to [11] and the values were expressed in mg/100 g of dry matter, while the reducing sugars were quantified as described by [12] and expressed in mg 100 g^{-1} of dry matter.

Phenolic compounds content

Total polyphenol contents were determined using the colorimetric method of Folin-Ciocalteu [13]. The absorbance was read at 725 nm against a blank without extract taken as reference. Quantification of total polyphenols is done according to a linear calibration line (y= ax + b) performed by a standard extract gallic acid at different concentrations (0 to 1000 µg ml^{-1}). Polyphenol content is expressed as gallic acid equivalents in milligrams per 100 grams of dry matter.

$$Polyph\acute{e}nols \ (mg/100g) = \frac{OD_{725} \times 5 \ \times 10^3}{5,04 \times m_e}$$

Calibration line: OD_725 = 5.04, mass (mg) Gallic acid, **R2** = 0.992, **me :** mass (g) of the sample.

Flavonoid content was measured by colorimetric assay using the method described by [14] using aluminum chloride. To a volume of 0.5 mL of each methanolic extract was successively added 0.5 mL distilled water, 0.5 mL aluminum chloride (10%, w/v), 0.5 mL sodium acetate (1M), and 2 mL distilled water. Then, the tubes were allowed to stand for 30 min at room temperature. The optical density reading was taken by spectrophotometer at 415 nm (BK-UV1000

spectrophotometer, Biobase, Qingdao, China), compared to a control containing distilled water instead of methanolic extract. Finally a concentration range of quercetin from 0 to 0.1 mg/mL was performed for the calibration curve. The total flavonoid content was expressed as mg quercetin equivalent per 100 g dry matter

$$Flavonoids \ (mg/100g) = \frac{OD_{415} \times 2 \ \times 10^3}{18,12 \times m_e}$$

Calibration line: OD_415 = 18.12, mass (mg) Quercetin, **R2** = 0.99. **me :** mass (g) of the sample.

Anti-nutritional compounds

The determination of phytates in the sample was performed according to the method described by [15] Latta and Eskin (1980) using Wade's reagent. One (1) g of sample was homogenized in 20 ml of HCl (0.65 N) under stirring for 12 h at room temperature. The mixture was centrifuged at 3000 rpm for 40 min using a centrifuge (SIGMA 3-16P, Germany). A 0.5-ml sample of each supernatant was taken followed by addition of 3 ml of Wade's reagent. Then the tubes were allowed to stand for 20 min in the dark and the absorbance reading was done with a spectrophotometer (BK-UV1000 spectrophotometer, Biobase, Qingdao, China) at 490 nm against the control containing no extract. Finally, a calibration curve was performed using a phytic acid range of concentration from 0 to 10 mg/mL. Results were expressed as mg phytic acid equivalent (PAE)/100 g dry matter (DM).

$$Phytates \ (mg/100g) = \frac{OD_{490} \times 4}{0,033 \times m_e}$$

Calibration line: OD_490 = 0.033 mass (µg) Phytate sodium, **R2** = 0.99., **me :** mass (g) of the sample.

The method used for the determination of oxalates is that described by [16]. Two (2) grams of sample were dried and ground and homogenized in 25 mL of H2SO4 (3M) under magnetic stirring for 1 h at room temperature. The mixture was then filtered through Whatman filter paper or paper towels. Then, a 25 mL volume of this filtrate was titrated under heat with 0.05 M potassium permanganate (KMnO$_4$) solution until a persistent pink turn for 30 seconds. The oxalate content expressed in mg 100 g^{-1} dry matter was obtained by the following equation**:**

$$Oxalates \ (mg/100g) = \frac{2,2 \times V_{eq} \times 100}{m_e}$$

Veq: volume (mL) of KMnO$_4$ poured at the equivalence, **me:** mass (g) of the sample.

The determination of tannins was performed as described by [17] A volume of 1 mL of methanolic extract was taken and to this volume was added 5 mL of vanillin reagent (0.1 mg vanillin in 70% (v/v) hydrochloric acid). Then, the tubes were allowed to stand for 20 min in the dark and the

absorbance reading on a spectrophotometer (BK-UV1000 spectrophotometer, Biobase, Qingdao, China) was taken at 500 nm against the blank containing distilled water in place of the methanolic extract. Finally, a calibration curve was performed using a tannic acid range of concentration from 0 to 0.1 mg mL-1. The results were expressed as mg tannic acid equivalent (TEA)/100 g dry matter (DM).

$$Tannins \; (mg/100g) = \frac{OD_{500} \times 10^3}{3,11 \times m_e}$$

Calibration line: OD_500 = 3.11, mass (mg) Tannins acid, **R2** = 0.99, **me :** mass (g) of the sample.

Microbial analysis

The samples of our food to be analyzed were prepared in the proportions (g/mL), according to the technique described by French Standard (NF) ISO 6887-V08-010-6 (2013). Ten (10) grams of our food were introduced into a sterile glass bottle containing 90 mL of buffered peptone water (Conda, Spain) previously autoclaved (121 °C, 45 min, 1bar). The mixture obtained after manual homogenization by shaking for 2 min corresponds to the stock solution. Successive decimal dilutions were then prepared from this stock solution ranging from 10^{-1} to 10^{-8}.

In accordance with standard NF ISO 4833-2003, 1 mL of the stock suspension and 1 mL of the decimal dilutions produced were duplicated on different empty petri dishes, then added to PCA (Plate Count Agar) agar medium supercooled at 45°C. After homogenization and solidification, a second layer of PCA medium was poured into each dish. Petri dishes were then incubated at 30 °C in an oven for 24 to 72 h after solidification. To count mesophilic aerobic germs on PCA agar, petri dishes containing 30 to 300 were selected for counting.

In accordance with NF ISO 7954-1988, 0.1 mL of inoculum corresponding to dilutions 10^{-3}, 10^{-4} was surface-seeded in a Petri dish containing 15 mL of Sabouraud chloramphenicol medium. Incubation took place at 37 °C for 3 to 5 days. Petri dishes of Sabouraud chloramphenicol agar containing 15 to 150 characteristic yeast colonies were considered for enumeration. Yeast colonies appeared whitish, smooth and bulging, with a diameter of 0.5 to 2 mm.

The medium used for lactic acid bacteria enumeration is MRS (Man Rogosa Sharp) agar in accordance with ISO 15 214 (1998). Seeding was done by spreading 0.1 mL stock suspension or decimal dilutions retained on the surface of the agar previously poured and cooled in a petri dish. Petri dishes were incubated anaerobically in jars for 48 h at 30 °C. Plates with colony counts between 15 and 150 were counted.

Neutral red crystal violet bile lactose agar (VRBL agar) was used for coliform enumeration. Inoculation was car-

ried out in the mass with 1 mL of inoculum in sterile Petri dishes. Then 12 to 15 mL of supercooled medium at 45 °C was poured into the Petri dishes containing the inoculum. The resulting mixture was homogenized by gentle manual agitation. After solidification, a second layer of 4 mL of the same medium was poured. Incubation was carried out for 24 h at 30°C for total coliforms (NF ISO 4832 (V08-015), 2006) and 44 °C for fecal coliforms (NF ISO 4832 (V08-060), 2009). Colonies appeared red, purplish and round. All characteristic colonies present in plates containing 15 to 150 colonies were counted.

Bacillus was counted on plates Mossel agar (AES Laboratoire, COMBOURG France). The stock solution or decimal dilutions were placed in an 80 °C water bath for 10 min, then cooled immediately. This treatment destroys the vegetative forms of the microorganisms. The medium used for *Bacillus* research and enumeration was Mossel agar. Inoculation was carried out by spreading 0.1 mL of the mother suspension or decimal dilutions on the surface of agar previously poured and cooled in petri dishes. Incubation took place at 30 °C for 24 to 48 h. *Bacillus* colonies on Mossel agar are pink with the presence of a clear, opaque halo around the culture, or yellow with the absence of an opaque halo. Presumptive *Bacillus* colonies present in plates containing 15 to 150 colonies were counted.

According to NF ISO 16140, 2003, *E. coli* inoculation was carried out by spreading 0.1 mL of the mother suspension or decimal dilutions on the surface of RAPID'*E. coli* agar, previously poured and cooled in petri dishes. Incubation took place at 37 °C for 24 h.. On RAPID'*E. coli* agar, *E. coli* colonies appear purple to pink. *E. coli* colonies present in plates containing 15 to 150 colonies were counted.

Salmonella was detected using [18] multi-stage method: pre-enrichment on non-selective medium, followed by enrichment on selective medium and isolation on selective agar. For pre-enrichment on non-selective medium, 25 g of our sample is added to 90 mL of peptone water in a sterile flask. The well-homogenized mixture is incubated at 37 °C for 24 hours. Then, for enrichment in selective medium, 1 mL of the pre-enriched culture was pipetted into 10 mL of sterile Rappaport Vassiliadis broth. Incubation took place for 24 h at 37 °C. Each enrichment culture was streaked onto *Shigella-Salmonella* agar (SS, Oxoid). Incubation took place at 37°C for 24 h. On SS agar, presumptive colonies were colorless, transparent with or without a black center.

According to NF ISO 6888-1/ 1999, inoculation was carried out by spreading 0.1 mL of the mother suspension or decimal dilutions on the surface of Baird Parker agar, which had been poured and cooled in petri dishes. Incubation took place at 37°C for 48 h. On Baird Parker agar, presumptive

S. aureus colonies were either shiny black, entire, convex, surrounded by clear zones extending into the opaque medium, or shiny black, entire, convex, without well-defined clear zones, or dark grey. Presumptive *Staphylococcus aureus* colonies on plates containing 15 to 150 colonies were counted.

Tryptone Sulfite Cycloserine agar is recommended for the detection and enumeration of *Clostridium perfringens*. For petri dish culture, heat the product to be tested to destroy vegetative forms and activate spores. Place 1 mL of the product to be tested, or its decimal dilutions, in sterile Petri dishes and add 15 ml of liquefied TSC agar to each dish within 15 min, mix thoroughly and leave to solidify. Incubation takes place anaerobically at 37 °C for 24 h. Finally, count the colonies surrounded by a black halo, due to the reduction of sulfite to iron sulfide precipitate. Take the reading very soon after removal from the jar.

Statistical analysis

The assays were performed in triplicate and the data presented are the means and standard deviations of these three determinations calculated with Excel 2016. Means obtained after different treatments were compared by analysis of variance (ANOVA) using Duncan's multiple comparison test at 5% level of significance.

Results and Discussion

Production of *banku*

Banku is a little-known food in Côte d'Ivoire, unlike in other countries such as Togo, Nigeria and Ghana. It is a Ghanaian dish prepared with a mixture of fermented maize and cassava contained in a smooth, whitish paste, cooked in boiling water [2]. Its preparation involves soaking the raw material (a mixture of maize and manioc) in water for 24 hours. After grinding, the maize flour and cassava dough are placed in a large container (the maize flour and cassava paste) with just enough hot water to moisten it completely. There are no strict rules regarding the ratio of maize flour to cassava dough. In most cases, 3 to 4 volumes of corn paste are mixed with 1 volume of cassava paste. The mixture is mixed well by hand and the container is covered with a clean cloth for a three-day fermentation in a warm place at 37°C or in the upper part of the refrigerator. When properly fermented, it should have a slightly sour, but not unpleasant aroma, like a rising bread dough. An over-fermented mixture does not taste good. The fermented dough should be stirred and kneaded continuously with the hands to obtain a suitable consistency for the subsequent baking at 100 °C. To cook, the fermented dough is put in a large pot and left steam-cooked for twenty minutes or more, stirring constantly and

vigorously. The *banku* should become thick and stiff. If it becomes too dry, water can be added if necessary. Form the *banku* into balls about the size of tennis balls. *Banku* can be served hot or cold at room temperature (Figure. 1).

Biochemical parameters during *banku* production

To ensure consumer health and to promote a traditional food that is new to Côte d'Ivoire, the nutritional and health parameters of the flour, dough, flour-dough mixture and the finished product called *banku* were studied. Thus, the fermented maize flour shows a pH of 4.18 ± 0.52 with an acidity level of 0.31 ± 0.01 %. While the fermented cassava dough records a pH of 3.58 ± 0.04 with an acidity level of 0.27 ± 0.04. Under the same storage conditions, the pH of the mixture of fermented cassava flour and fermented cassava dough 3.53 ± 0.04 with an acidity level of 0.18 ± 0.01. However, the pH of the final product (*bankou*) is 4.07 ± 0.08 with an acidity level of 0.05 ± 0.01 (Table 1).

Table 1. Samples acidification

Samples	pH	Titratable Acidity (%)
FMF	4.18 ± 0.52[a]	0.31 ± 0.01[a]
FCD	3.58 ± 0.04[b]	0.27 ± 0.04[a]
MMCF	3.53 ± 0.04[b]	0.18 ± 0.01[b]
FP	4.07 ± 0.08[a]	0.05 ± 0.01[c]

Notes: Values are means of triplicate samples, each analyzed in triplicate (n =9) ± standard deviation Within the same column; mean values followed by a different alphabetical letter are statistically different (p≤ 0.05) (Duncan multiple t-test); **FMF :** Fermented maize flour ; **FCD :** Fermented cassava dough ; **MMCF :** Mixture of fermented maize flour and fermented cassava dough ; **FP :** Final product .

These pH values observed in the fermented samples and in the *banku* could be explained by the production of organic acids, notably lactic acid and acetic acid by lactic bacteria. In fact, lactic acid bacteria constitute the majority flora of fermented cassava and corn products. Similar remarks were obtained in the study conducted by [19] and [20] on the physicochemical characteristics of fermented cereal-based foods. It should be noted that the acidity obtained in the final product (banku) complies with the requirements of the Ivorian standard NI 03-08-003 on attiéké, the results of [21] on attiéké and those of other work on fermented cassava-based foods [22, 23].

In other hand, the dry matter content or water content undergoes changes during the preparation of *banku*. The highest dry matter content observed during *banku* production was in the fermented maize flour 61.25 ± 3.69 g 100/g FM and the lowest in the final product 25.16 ± 3.49 g100/g FM. The observed differences are significant at the 5 % level. Also, the results show the presence of total sugars in

the four samples studied and the highest value was found in the fermented maize flour 7.74 ± 0.05 mg 100/g DM, and the lowest was in the final product 0.51 ± 0.04 mg 100 g^{-1} DM. However, reducing sugars were found only in the fermented maize flour with a content of 9.17 ± 0.50 mg 100/g DM. The observed differences are significant at the 5% level (Table 2).

Table 2. Content of some macronutrients

Samples	Dry matter (g/100g FM)	Total sugars (mg/100g DM)	Reducing sugars (mg/100g DM)
FMF	61.25 ± 3.69^a	7.74 ± 0.05^a	9.17 ± 0.50^a
FCD	41.95 ± 4.82^b	0.59 ± 0.13^b	0.00 ± 0.00^b
MMCF	41.54 ± 2.03^b	1.17 ± 0.15^c	0.00 ± 0.00^b
FP	25.16 ± 3.49^c	0.51 ± 0.04^b	0.00 ± 0.00^b

Notes: Values are means of triplicate samples, each analyzed in triplicate (n =9) $\pm$ standard deviation. Within the same
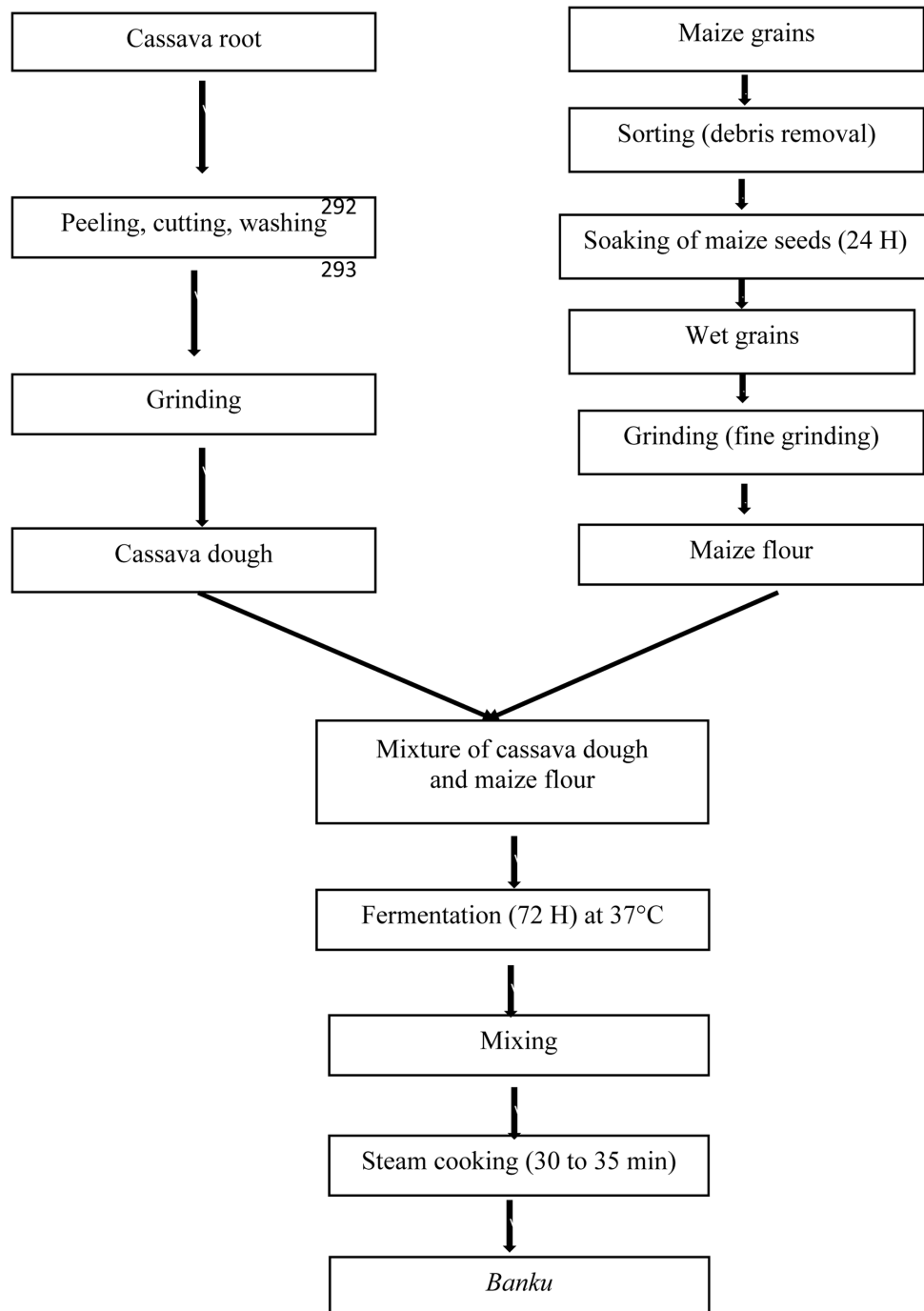
Fig. 1. Production diagram of *banku*

Remark : Cassava dough and maize flour can be fermented separately for 72 hours at 37°C and then mixed together after fermentation.

column; mean values followed by a different alphabetical letter are statistically different (p≤ 0.05) (Duncan multiple t-test); **FMF :** Fermented maize flour ; **FCD :** Fermented cassava dough ; **MMCF :** Mixture of fermented maize flour and fermented cassava dough ; **FP :** Final product ; **DM:** Dry matter ; **FM:** Fresh matter.

Indeed, the different levels of dry matter and sugars encountered during the production of *banku* would not only be related to the raw material but also and especially to certain unit operations such as fermentation and cooking where a large amount of water is eliminated during the preparation of the fermented food [24]. During this production process, an elimination of these substances, especially starch, occurs during the fermentation stage, which allows a degradation of starch into fermentable sugars. This observation is also made by [25] and [8], during the fermentation of cassava dough.

Similarly, the reduction of phenolic compounds changes from 342.26 ± 4.55 to 47.95 ± 2.50 mg100/g DM for total polyphenols and 40.65 ± 0.46 to 7.77 ± 0.39 mg 100/g DM for total Flavonoids (Table 3).

Table 3. Phenolic compounds content

Sample	Total polyphenols (mg/100g DM)	Total flavonoids (mg/100g DM)
FMF	342.26 ± 4.55^a	40.65 ± 0.46^a
FCD	108.13 ± 2.62^b	11.26 ± 0.66^b
MMCF	108.80 ± 3.48^b	14.13 ± 0.40^b
FP	47.95 ± 2.50^c	7.77 ± 0.39^c

Notes: Values are means of triplicate samples, each analyzed in triplicate (n =9) ± standard deviation. Within the same column; mean values followed by a different alphabetical letter are statistically different (p≤ 0.05) (Duncan multiple t-test); **FMF :** Fermented maize flour ; **FCD :** Fermented cassava dough ; **MMCF :** Mixture of fermented maize flour and fermented cassava dough ; **FP :** Final product ; **DM:** Dry matter

Anti-nutritional compounds notably Phytates, àxalates, tannin are also reduced during fermentation. The highest phytate content was found in the final product (86.42 ± 1.63) mg 100/g DM. While the highest oxalate content was in the fermented maize meal (132.00 ± 5.50) mg 100/g DM and the highest tannin content was found in the fermented corn meal (185.32 ± 2.41) mg100/g DM (Table 4).

Table 4. Anti-nutritional compounds content

Sample	Phytates (mg/100 g DM)	Oxalates (mg/100 g DM)	Tanins (mg/100 g DM)
FMF	84.93 ± 0.62^a	132.00 ± 5.50^a	185.32 ± 2.41^a
FCD	85.29 ± 1.86^a	40.33 ± 3.18^b	22.94 ± 1.59^b
MMCF	84.81 ± 0.57^a	31.17 ± 3.18^b	54.77 ± 1.52^c
FP	86.42 ± 1.63^a	25.67 ± 3.18^c	22.51 ± 1.47^b

Notes: Values are means of triplicate samples, each analyzed in triplicate (n =9) ± standard deviation. Within the same column; mean values followed by a different alphabetical letter are statistically different (p≤ 0.05) (Duncan multiple t-test); **FMF :** Fermented maize flour ; **FCD :** Fermented cassava dough ; **MMCF :** Mixture of fermented maize flour and fermented cassava dough ; **FP :** Final product ; **DM:** Dry matter

The reduction of phenolic compounds and Anti-nutritional compounds observed during the preparation of the *banku* would be due to the fermentation step of the different foods used content varied during the production of *banku*. Indeed, according to [26], it is known that spontaneous fermentation reduces the concentration of anti-nutritional substances and phenolic compounds. However, the analysis of physico-chemical parameters indicates that the analyzed *banku* complies with the [27] CODINORM (2001) standard.

Microbial analysis during *banku* production

Concerning microbiological analysis, the table 5 shows the evolution of the microorganism load of fermented maize flour, fermented cassava dough, the mixture of maize flour

Table 5. Microbiological analysis

Germs	Microbial load of samples (CFU/g)			
	FMF	FCD	MMCF	FP (*Banku*)
AMG	$(1.2 \pm 1.1) \times 10^{7a}$	$(2.6 \pm 2.8) \times 10^{8a}$	$(1.5 \pm 1.3) \times 10^{8a}$	$(5.6 \pm 0.4) \times 10^{3a}$
TC	ND	ND	$(2.7 \pm 1.9) \times 10^{0a}$	ND
FC	ND	ND	$(9 \pm 0.1) \times 10^{1a}$	ND
Yeasts	$(4.3 \pm 0.4) \times 10^{4b}$	$(5.4 \pm 0.4) \times 10^{4b}$	$(6.4 \pm 0.6) \times 10^{5b}$	ND
LAB	$(2.2 \pm 4.4) \times 10^{7a}$	$(1.9 \pm 0.5) \times 10^{6a}$	$(6.4 \pm 0.6) \times 10^{6a}$	ND
E. coli	ND	ND	ND	ND
S. aureus	$(2.8 \pm 0.9) \times 10^{3b}$	ND	$(9.5 \pm 0.9) \times 10^{0b}$	ND
Bacillus	$(5.9 \pm 1.5) \times 10^{2b}$	$(2.2 \pm 0.3) \times 10^{2c}$	$(5.2 \pm 0.2) \times 10^{3a}$	ND
Clostridium	ND	ND	ND	ND
Salmonella	Absent	Absent	Absent	Absent

Notes: Values are means of triplicate samples, each analyzed in triplicate (n =9) ± standard deviation. On the same line; mean values followed by a different alphabetical letter are statistically different (p≤ 0.05) (Duncan multiple t-test). **AMG:** Aerobic mesophilic germs; ***E. coli:*** *Escherichia coli;* ***S. aureus:*** *Staphylococcus aureus*; **TC:** Total coliforms, **FC:** Fecal coliforms, **LAB:** Lactic acid bacteria **ND:** Not detected, **FMF :** Fermented maize flour ; **FCD :** Fermented cassava dough ; **MMCF :** Mixture of fermented maize flour and fermented cassava dough ; **FP :** Final product.

and fermented cassava dough and the final product during the production process. The loads of aerobic mesophilic germs (AMG) varied with values ranging from (1.2 ± 1.1) $\times 10^7$ CFU/g in the fermented maize flour and (2.6 ± 2.8) $\times 10^8$ CFU/g in the fermented cassava dough. After mixing the maize flour and the fermented cassava dough, the loads of AMGs were $(1.5 \pm 1.3) \times 10^8$ CFU/g. In the final product, the aerobic mesophilic germs (AMG) load decreased to $(5.6 \pm 0.4) \times 10^3$ CFU/g (Table 5).

This microbial load was composed of coliforms, lactic acid bacteria, *Bacillus, Salmonella,* yeast and *Staphylococcus aureus*. According to [28] the total aerobic mesophilic flora is the primary contamination flora of food and the source of contamination of foodstuffs comes from the environment, dust, cross contamination and contamination due to handling. This flora of contamination is often made up of enterobacteria, *Bacillus*, Staphylococci, lactic bacteria or other potentially pathogenic agents. Their presence beyond the standards is due to a lack of hygiene in processing and poor storage conditions [28]. The presence of certain microorganisms in the mixture could be due to contamination of the ingredients by the hands of female producers during production, but also by domestic animals. These germs provide information on the lack of hygienic handling, inefficiency of processes, lack of ownership of premises and equipment used for production [29].

After cooking, the *banku* (final product) recorded a microbial load in mesophilic aerobic germs indicating the absence of coliforms, lactic acid bacteria, *Bacillus*, *Salmonella,* yeast and *Staphylococcus aureus*. The absence of all these germs searched shows that these microorganisms were eliminated during cooking. According to [28], the cooking temperature of 88 ± 3.33 °C and a cooking time of 35 ± 1.37 min are sufficient to eliminate all vegetative forms except spore forming forms. The observed mesophilic aerobic germs value indicates the presence of others in the *banku* that were not sought in our study. However, this mesophilic aerobic germs load in the *banku* is largely lower than the requirements of the Ivorian standard on fermented foods. The microbiological quality of the *banku* would be satisfactory and could therefore be consumed without danger to the health of the consumer. It should be noted that in all samples analyzed, clostridia and *E. coli* were not detected. This indicates that the lactic acid bacteria would have produced enough lactic acid during the fermentation to inhibit the development of *Clostridium* and *E. coli*. Indeed, lactic acid bacteria, thanks to the organic acids they produce, prevent the growth of most pathogenic germs [30, 31] and guarantee food safety, as well as providing them with very specific characteristics of flavour and texture.

Conclusion

The present study evaluated the biochemical and microbiological characteristics of *banku*, a fermented food consumed by living foreigners in Côte d'Ivoire. From a nutritional point of view, *banku*, a product of fermented maize flour and cassava ferment, would contribute significantly to improving the calorific intake of West African populations. In poor families, it could find its place as a substitute for some food, since its nutritional properties are in accordance with the CODINORM 2001 standard. In terms of sanitary quality, not only does *banku* contain no pathogens but also its level of contamination in mesophilic aerobic germs is lower than the microbiological criteria prescribed by CODINORM 2001. In sum, the microbiological quality of the *banku* is satisfactory. Other studies could follow on from this, such as setting up an HACCP system for production or using selected starters to help control the flavor and aroma of these products. Above all, producers need to be made aware of and trained in the basic rules of hygiene, the microbial hazards involved in poor hygiene practices, and the means of preventive and corrective action. We also need to train producers in Good Manufacturing Practices (GMP) and Good Hygiene Practices (GHP).

Disclosure statement

No potential conflict of interest was reported by the authors.

References

1. CIRAD, Salon international de l'agriculture à Paris sur le thème "Souveraineté alimentaire : une histoire de diversité". https://www.cirad.fr/les-actualites-du-cirad/agenda/2023/salon-international-de-l-agriculture.

2. Briggs P, K. Rushton. The Bradt Travel Guide. 2007;73

3. Steven S, Toyin F. Culture and customs of Ghana. Greenwood Press. Westport. Conn. 2002;109.

4. Kouame A.K, Djeni T.N, N'Guessan F.K, Dje M.K. Post-processing microflora of commercial attieke (a fermented cassava product) produced in the south of Côte d'Ivoire, Letters in Applied Microbiology. 2013; 56:44-50.

5. FAOSTAT. Estimate FAO Statistics Division 2007/ 23 may 2007. http://faostat.fao.org/

6. Steinkraus KH. Nutritional Significance of Fermented Foods, Food Research International. 1994;27:259–267.

7. Tankoano A, Diop M.B, Sawadogo-Lingani H, Kaoré D, Savadogo A. Les aspects technologiques, microbiologiques et nutritionnels d'aliments fermentés à base de lait de mil en Afrique de l'Ouest, International Journal of Advanced Research. 2017;5:1509-1526.

8. Bouatenin KMJP. Mise en place de starters selections specifiques aux trois principaux types d'attiéké (Adjoukrou, Alladjan et Ebrié) en Côte d'Ivoire, Thèse unique de doctorat, Univercité Nangui Abrogoua. 2013;192

9. Kimaryo V.M, Massawi G.A, Olasupo N.A, Holzapfel W.H. The use of a starter culture in the fermentation of cassava for the production of 'Kivunde', a traditional Tanzanian food product, International Journal of Food Microbiology. 2000;56:179–190.

10. AOAC (Association of Official Analvtical Chemist). Official methods of Analysis of the Association Chemists International, (16edn). AOAC International Arlington, VA. 250. 1995.

11. Dubois M, Gilles K, Hamilton J, Rebers P, Smith F. Calorimetric method for deterrnination of su gars and related substances, Analytical Chemistry. 1956;28:350-356.

12. Bernfeld P, Amylase and Protcases. In: Colswick SP and Kaplan NO (Editors). Methods in Enzyrnology. Academic Press, New York, USA. 1955;149-154.

13. Singleton VL, Orthofer R, Lamuela-Raventos RM, Analysis of total phenols and other oxidation substrates and antioxidants by means of Folin–Ciocalteu reagent, Methods in Enzymology. 1999; 299:152–178.

14. Meda A, Lamien CE, Romito M, Millogo J, Nacoulma OG. Determination of the Total Phenolic, Flavonoid and Proline Contents in Burkina Fasan Honey, as Well as Their Radical Scavenging Activity, Food Chemistry. 2005;91:571-577.

15. Latta M, Eskin M. A Simple and Rapid Colorimetric Method for Phytate Determination, Journal of Agricultural and Food Chemistry. 1980;28:1313-1315.

16. Day RA, Underwood AI. Quantitative Analysis (5th Edn). Prentice & Hall Publication, London. 1986;701.

17. Bainbridge Z, Tomlins K, Wellings K, Westby A. Methods for assessing quality characteristics of non-grains starch (Part. 3. Laboratory methods). 1996;13.

18. Hendriksen RS. Laboratory Protocols Level 1: Training Course Isolation of Salmonella. A Global Salmonella Surveillance and Laboratory Support Project of the World Health Organization, 4th edn. Geneva: WHO. 2003.

19. Louembe D, Keleke S, Kobawila SC. Bactéries lactiques de la pâte fermentée de maïs, Tropicultura. 2003;1:3-9.

20. Yao NB, Ehouman AGS, Adingra KM-D, Aka KSP, Tano K. Effect of Fermentation on the Biochemical Composition of Soybean (*Glycine max* L.) and Red Bean (*Vigna unguiculata* L.) Consumed in the City of Daloa (Côte d'Ivoire). Int.J. Curr.Microbiol. App.Sci. 2021;10:572-583.

21. Coulin P, Farah Z, Assanvo J, Spillman H, Puhan Z. Characterisation of the microflora of attiéké, a fermented cassava product during traditional small-scale production. International Journal of Food Microbiology.2006;106:131-136.

22. Obilie EM, Tano D, Amoa-Awua WKA. Souring and breakdown of cynogenic glucosides during the processing of cassava into Akyeke, International Journal of Food Microbiology. 2004;93:115-121.

23. Tape JS. Etude comparative de deux types de ferments traditionnels utilises dans la transformation du manioc en Attiéké et placali, Mémoire de Master, Université Nangui Abrogoua. 2014;53.

24. Hounhouigan DJ, Nout MJR, Nago CM, Houben JH, Rambouts FM. Composition and microbiological and physical Attributes of mawè, a fermented maize dough from Bénin, Inter. J. Food Sei. Technol. 1993a;28:513-517.

25. Djeni NT. Typologie de l'attiéké de trois zones de production de Côte d'Ivoire et analyse des propriétés des levains traditionnels utilisés pour sa préparation, Thèse unique de Doctorat, Universite´ Abobo-Adjame´. 2009;170.

26. Blandino A, Al-Aseeri ME, Pandiella SS, Cantero D, Webb C,Cereal-Based Fermented Foods and Beverages, Food Research International. 2003;6:527–543.

27. CODINORM, Projet de norme Ivoirienne sur l'attiéké, Attiéké-Spécification PNI 03-08-001. 2001.

28. Kouame KA, Identification des dangers et des points critiques de contrôle pour la mise en place d'un système HACCP pour la production de l'attiéké en Côte d'Ivoire, Thèse unique de doctorat, Université Abobo-Adjamé. 2013;147.

29. Kluytmans J, Van Belkum A, Verbrugh H. Nasal Carriage of Staphylococcus aureus: Epidemiology, Underlying Mechanisms, and Associated Risks, Clinical Microbiology Reviews. 1997;10:505-520.

30. Tchekessi CKC, Yaou IB, Agbangla C, Adeoti K, Dossou-Yovo P, Assogba E, Caractérisations physicochimiques et microbiologiques d'une pâte traditionnelle "gowé" fabriquée à base de maïs au Bénin, Journal Recherche Science Universel. 2013;2:377-387.

31. Kouame KA, Bouatenin KMJ-P, Coulibaly WH, DK. Marcellin. Biochemical and microbiological characterization of "Soumbara" from African locust bean (Parkia biglobosa) seeds consumed in Abidjan (Côte d'Ivoire). The North African Journal of Food and Nutrition Research. 2021;5 :35-42.

Original article

Antibacterial, Antidiabetic, Antioxidant and DNA cleavage studies of novel N(3-(bis(pyridine-2ylmethyl)amino)-2-hydroxypropyl) benzene sulphonamide ligand

R VIJAYAKUMAR[1], R TAMILARASAN[2,*]

[1]Assistant Professor, Department of Chemistry, Thiruvalluvar College of Engineering & Technology, Vandavasi, 604505, India.

[2]Assistant Professor Department of Chemistry, University College of Engineering, Pattukkottai, Thanjavur, Tamilnadu, India.

Abstract   The novel N (3-(bis(pyridine-2ylmethyl)amino)-2-hydroxypropyl) benzene sulphonamide ligand have been synthesized from 1,3-Diamino-propan-2-ol. The structure of the ligand was confirmed by Mass spectroscopy and ^{1}H NMR spectroscopy. The synthesized Schiff base ligand was tested for their in vitro anti bacterial action with Gram-positive and negative bacteria. The anti-diabetic activities have been tested with α-amylase inhibition method and antioxidant effect of the compound was established using DPPH method. Thus all the studies reveals that the synthesised Schiff base compound has significant antibacterial, antidiabetic and antioxidant activities. The DNA cleavage studies shown that, the DNA binding nature of the ligand was appreciably good. The Molecular docking characteristics were supported that the binding approach of the effective inhibitors with the active site of enzymes.

✉ *Corresponding author: R Tamilarasan, Assistant Professor Department of Chemistry, University College of Engineering, Pattukkottai, Thanjavur, Tamilnadu, India; email: rrtamilk@yahoo.co.in.

Introduction

As the last decade, researchers focusing on the synthesis of <u>Schiff base,</u> has risen extensively due to their beneficial applications in significant fields. The Schiff base are synthesized by condensation reaction by using the substituted aldehydes or ketones with aliphatic and aromatic amines that produced mostly in presence either acid or base catalysis or necessary heat[1]. The Schiff bases were initially reported by German chemist Nobel Laureate Hugo Schiff in 1864. Later a variety of Schiff bases were reported by different researchers [2-4]. The Schiff base ligands encompasses with the several donor atoms like nitrogen, Sulphur and oxygen [5]. Amongst the Schiff bases, 2-pyridyl aldehyde derived imines are exhibits large number of biological activities either alone or with metal complexes [6]. These legends with metal complexes were employed in drugs and possess appreciable biological activities like antibacterial [7], antifungal [8], antiviral[9], anti-inflammatory[10] and antitumor activities[11], antifertility[12], antioxidant[13], herbicidal[14] and antiproliferative [15]. Schiff base ligands have enticed countless attention owing to their potential applications in DNA recognition. This also have the good fluorescence [16], aggregation[17]a potentiometric cation caring[18], anthelmintic[19] and photoluminescence[19] properties. The numerous applications of Schiff base in dye, pharmaceutical, food, analytical, catalysis, fungicidal, agroindustry and biological field were reported by the various researchers [21].

In this article we have selected 1,3-diamino-propan-2-ol based Schiff base was prepared due the nature and excellent biological activity from the literature[32]. The sulphonamide and amide functional groups present in the schiff base is similarly contain the many of the drug molecules, aggregation[17] a potentiometric cation caring[18], and anthelmintic[19] and photoluminescence[20] properties.

Materials and methods

Apparatus and chemicals

The chemicals, such as raw materials and solvents with highest purity were purchased from Sigma Aldrich products and were used without any purification. The Mel-Tem (Mitamura Riken Kogyo) melting point apparatus was used to find out the melting points of the product. The FTIR-8300 Shimadzu Spectrophotometer with KBr pellet was employed for the determination of infrared(FTIR)spectrum of the product in the frequency range of 4000–200 cm⁻¹.The UV– Visible spectra were chronicledwithTCC-240- A instrument, using chloroform as solvent for 200– 1100 nm range. A Bruker 400 MHz spectrometer with DMSO-d6 as solvent was used

to determine ^{1}H and ^{13}CNMR spectra. Mass spectra of the samples were recorded with Micromass UK PLATFORM II LC-MS spectrometer.

Experimental procedure

Preparation of N(3-(bis(pyridine-2ylmethyl) amino)-2-hydroxypropyl)benzenesulfonamide (Ligand-1):

Step-1: Synthesis of (3-Amino-2-hydroxy-propyl)-carbamic acid tert-butyl ester (3):

1,3-Diamino-propan-2-ol (**1**) (10 g, 0.11 moles 1 eq) and dry DCM (150 mL) was taken in 250 ml 3 neck RB flask with constant stirring. Under N$_2$ atm, Et$_3$N was added to it and then cooled for 0°C. To the reaction mixture BOC anhydride (24.2 g, 0.11 moles, 1 eq) was added slowly in the temperature range from 0 to 5 °C for 30 min. After the adding all reagents the reaction mixture was allowed for uniform stirring in RT for 2 h. Then DCM (250 mL) was used for dilution and water (125 mL) was used to washing of the contents. The layer of DCM was separated and dried with sodium sulphate. Then it was concentrated in reduced pressure condition the crude product was obtained. The obtained product was ground to a fine powder with diethyl ether. The white solid mass was filtered and dried to get the (3-Amino-2-hydroxy-propyl)- carbamic acid tert-butyl ester (**3**) as a white solid mass (15 g, Yield=71%). LCMS: (M+H)$^{+}$: 191.3; 1H NMR (400 MHz, DMSO-d$_6$): δ 6.68 (t, J = 5.6 Hz, 1H), 3.35 (m, 1H), 2.96 (m, 2H), 2.51 (m, 1H), 2.39 (m, 1H), 1.32 (s, 9H) ppm.

Step-2: Synthesis of (3-Benzenesulfonylamino-2-hydroxy-propyl)-carbamic acid tert-butyl ester (5):

(3-Amino-2-hydroxy-propyl)-carbamic acid tert-butyl ester (1 g, 0.005 moles, 1 eq) and dry DCM (15 mL) was taken in 100 mL 3 neck RB flask with uniform stirring of the solution. Under N$_2$ atm Et$_3$N (0.9 mL, 0.006 moles, 1.2 eq) was added and cooled to 0 °C. Benzene sulphonyl chloride (**4**) (0.95 g, 0.005 moles, 1 eq) was added slowly to maintaining the temperature below 0 °C. All the reagents were added in the reaction mixture then it was kept with constant stirring at RT about 3 h. DCM (75 mL) was used to diluting the contents and then washed with water (25 mL). The separated DCM layer was dried with sodium sulphate. Under reduced pressure the product was concentrated then the crude product was obtained. The product was ground with diethyl ether, a white product (solid) was obtained. It was filtered and dried to get the (3-Benzene sulfonylamino-2-hydroxy-propyl)-carbamic acid tert-butyl ester (**5**) as a white colored solid product (1.4 g, Yield=82%). LCMS: (M+H)+: 331.5; ^{1}H NMR (400 MHz, DMSO-d$_6$): δ 7.83 (d, J = 8 Hz, 2H), 7.62 (m, 3H), 5.62 (broad s, 2H), 3.76 (m, 1H), 2.93 (m, 1H), 2.76 (m, 2H), 2.63 (m, 1H) ppm.

Step-3: Synthesis of N- (3- Amino-2-hydroxy-propyl)-benzene sulfonamide(6):

(3-Benzenesulfonylamino-2-hydroxy-propyl)-carbamic acid tert- butyl ester (1 g, 0.0030 moles, 1 eq) and dry DCM was taken in 50 mL single neck RB flask with a constant stirred solution. Under N_2 atm 4N HCl in dioxane (3.5 mL, 0.0121 moles, 4 eq) was added at 0 °C. Subsequently the addition was completed then it was kept with constant stirring at RT for 2 h. Under reduced pressure the reaction mixture was concentrated to get the crude product. The obtained product was dried to get the N-(3-Amino-2-hydroxy-propyl)-benzene sulfonamide hydrochloride salt (**6**) as a white colored solid (0.6 g, Yield=87), it was taken for subsequent step without purification. LCMS: (M+H)$^{+}$: 231.4; ^{1}H NMR (400 MHz, DMSO-d$_6$): δ 7.90, (broad s, 4H), 7.83 (d, J = 8 Hz, 2H), 7.62 (m, 3H), 5.62 (broad s, 1H), 3.76 (m, 1H), 2.93 (m, 1H), 2.76 (m, 2H), 2.63 (m, 1H) ppm.

Step-4: Synthesis of N(3-(bis(pyridine-2ylmethyl)amino)-2-hydroxypropyl) benzene sulfonamide (Ligand-1):

N-(3-Amino-2-hydroxy-propyl)-benzene sulfonamide hydrochloride salt (**6**) (0.25 g, 0.0011 moles, 1 eq) in absolute ethanol (10 mL) was taken in 50 mL single neck RB flask with a uniform stirred solution. Under N_2 atm, Pyridine-2-carbaldehyde (0.48 g, 0.0023 moles, 2.1eq) was added. The entire mixture was heated about 80 °C and agitated for 2 h. Then the mixture was cooled to room temperature. The reaction mixture was stirred for 1h at RT after the addition of NaBH$_4$ (0.167 g, 0.0022 mmol, 2 eq). The reaction mixture was concentrated under reduced pressure and the obtained crude product was diluted with EtOAc and water. The EtOAc layer was separated, washed with brine water solution and dried over sodium sulphate. The product obtained was purified by silica column purification to get the N(3-(bis(pyridine-2ylmethyl)amino)-2-hydroxypropyl) benzene sulfonamide (0.35 g, Yield=75%). LCMS: (M+H)+: 413.0; 1H NMR (400 MHz, DMSO-d$_6$): δ 8.50, (d, 2H), 7.96 (t, 1H), 7.78-7.97 (m, 2H), 7.77-7.7.70 (m, 3H), 7.69-7.63 (m, 3H), 7.62-7.557 (m, 2H), 7.34-7.7.33 (d, J=7.6 Hz, 2H), 7.26-7.23 (m, 2H), 4.99 (m, 1H), 4.11 (m, 1H), 3.73 (s, 4 H), 3.19 (m, 2H), 2.88-2.82 (m, 2H), 2.68-2.63 (m, 1H), 2.62-2.57 (m, 1H) ppm.

Biological studies:

Antioxidant activity (Total antioxidant activity):

The Reactive oxygen species (ROS) are produced as a natural by products of oxidative cellular metabolism reactions in our body system the produced ROS are significantly play important roles in the modulation of cell existence and other cell activities. The ROS radical such as hydroxyl radical, superoxide anion, and H_2O_2 are more active and effectively destruct the chemical groups. The ROS effect on lipids, proteins, and nucleic acids may create a variety of chronicle damages, like coronary heart disease, atherosclerosis and cancer[44]. Therefore, it is essential to avoid the free radical action in our body, we can use immunise drugs which possess rich in antioxidants. The inhibitors along with antioxidant performance have been a supreme therapeutic prospective, in view of the fact that oxidative damage and swelling are shows a basic mechanism to asses a numeral of human health disorders, including diabetes[34-37].

Determination of Total antioxidant activity:

The total antioxidant ability of ligands was measured by using the following procedure. To the analytical samples with different concentrations 3ml of antioxidant reagent - (28 mM Na_3PO_4, 0.6 M H_2SO_4 and 4 mM ammonium molybdate) was added. Then the analytical sample was achieved appropriate diffusion with phosphomolybdenum reagent when it was incubated for 95°C and a period of 90 min in a water bath. The total antioxidant ability of samples and vitamin C standard of drug were determined using spectrophotometer[38] in the absorbance range of 695 nm. Schiff base was appreciably shown the antioxidant action owing the presence of various
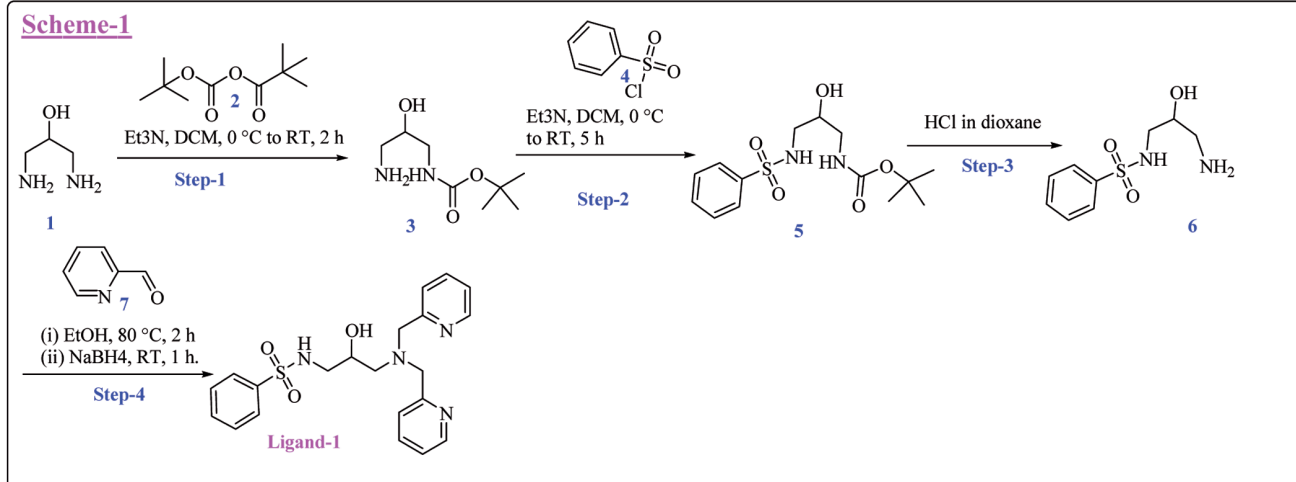
Scheme-1

Scheme 1. Synthesis of N(3-(bis(pyridine-2ylmethyl)amino)-2-hydroxypropyl)benzenesulfonamide.

functional groups like, hydroxy, phenoxy, and amino groups in its structure[38] , therefore the following formula was used to calculate the total antioxidant activities.

$$TOA = [(A_t - A_c)/A_t] \times 100.$$

Antidiabetic activity (α-amylase inhibitory method)

Experimental section; α-Amylase- inhibition technique:

The α-amylase inhibition technique was employed to determine the anti-diabetic activity of the ligand. In this technique the standard solution and 0.5 mg/ml of amylase was incubated for 10 min with extract and without extract about 25∘C in 20 mM sodium phosphate buffer solution (pH 6.9)[42]. Then 1mL of starch solution (1%) was added and the contents were incubated for another 30 min at 25∘C. The DNSA reagent (1mL) was added as the color reagent to bring to a close the enzymatic reaction, and then it was incubated in a hot water bath for 15min. After attaining to room temperature, the spectrophotometer instrument[32-33] was employed to determine the absorbance in the range of 540 nm. The experimental absorbance value was compared with Absorbance control. The % of inhibition was calculated using the following formula.

% α -Amylase inhibition = Absorbance of control –Absorbance of complex X100

Absorbance of control

Stability study:

1 mM concentration of the ligand was dissolved in phosphate buffer (pH =7.4, 5mL) (PPA). From that, 200 μL of the sample was diluted in 2 mL of phosphate buffer. The diluted sample was incubated at 37 °C for 10 min[28]. The absorbance study was carried out in the range of 270 nm for the degradation and the experiment was repeated nearly 24 hours with different time intervals at 37 ^{0}C. The PPA stability was calculated from the diminishing values of the absorbance[29].

Antibacterial activity Results:

Antibacterial activity:

In vitro antibacterial screening of the Schiff base and its metal complexes (Table 1) were examined against Gram-positive bacteria, namely, Enterococcus faecalis and Staphylococcus aureus and Gram-negative bacteria, namely, Escherichia coli, and Pseudomonas aeruginosa using disc diffusion method[24-25].

Disc-diffusion method:

It is very important aim to preparation of antimicrobial substance which inhibiting the basic microbe exclusive of any side effects to the patients. The significance of the dis-

tinctive character of the Schiff base, it can be proficient to apply securely in the treatment of diseases. It is observed that the increasing concentration of test solution significantly increase biological activity. The lowest inhibitory concentration (LIC) values of the substance were shown in the Table 1.The experimentally found LIC values specify that the compound having superior antimicrobial activity.

The disc diffusion method was adopted for the determination of antibacterial activity of prepared sample. The target bacteria was grown-up in Nutrient broth and incubated for 24 hrs. The diluted bacterial strain was cultured using Petri dishes containing Nutrient agar (NA) medium. The primed discs were kept on the culture medium. To the sterile disc[26] examination samples (500μg, 1000μg and 2000 μg) were introduced. Streptomycin (Std drug) (20μg) was employed as a affirmative reference standard. Then the immunized plates were incubated about 37 °C for 24 h. The clear zone around the disc diameter was determined and given in mm since its antibacterial activity[27-30].The activity of compound RV2 showed excellent activity against all organisms.

DNA Cleavage Assay

It is a reaction that ruptures any one of the covalent bond in a sugar-phosphate linkages among nucleotides in the sugar phosphate of DNA. It is catalysed by employing either enzyme or chemical or by radiation. Cleavage or rupturing whether exo-nucleolytic it might be removes the end nucleotide, or endo-nucleolytic then it splits the strand into two[12].

The various Studies relating to DNA cleavage by artificial reagents are of substantial attention due to their efficacy as biological tools in all organisms. The super coiled pBR322 DNA endorsed by metal complex was ensued by adding of substance (20μl). The 20μl of the mixture have pBR322 DNA, 10mM H_2O_2, 50mm NaCl and 50 mM Tris–HCl then followed by the addition Millipore water. All the contents were incubated at 37º C for 1 hr. Agarose electrophoresis method[42] was employed for the analysis.

Results and discussion

Synthesis

It is reported that the synthesis of novel N(3-(bis(pyridine-2ylmethyl)amino)-2-hydroxy propyl) benzene sulfonamide (Ligand-1) as shown in **Scheme 1.** The synthesis started with 1,3-diamino propane-2-ol treated with Boc anhydride in the presence of triethylamine base in dichloromethane solvent at room temperature conditions to get compound 3 as mono Boc-protected compound with excellent yield and purity. It was treated with triethylamine base along with dichloromethane solvent and benzoyl chloride to get compound 5 with good yield. Then compound 5 treated with HCl in

dioxane gave deprotected amine hydrochloride compound 6. It was then reductive aminated with Pyrdine-2-carboxaldhydeunder NaBH4 reducing agent gave N(3-(bis(pyridine-2ylmethyl)amino)-2-hydroxy propyl) benzene sulfonamide with considerable amount of yield.

Characterization

The Intermediates and N(3-(bis(pyridine-2ylmethyl) amino)-2-hydroxypropyl) benzene sulfonamide (ligand-1) were checked by NMR spectroscopy. The ligand was furthermore analysed by LCMS spectral investigations. The observed results were compared with literature.

¹H NMR spectral analysis of HL1ligand

The ¹H NMR spectra of the Ligand-1 examined, it was found that the symmetric pyridine protons were appeared as 2 set of protons. Down field doublet of 2 protons with 6.0 Hz at δ 8.50 represent the protons of the C2-pyridine rings. A broad proton at δ 4.99 represents the proton from OH group. A triplet with 6.0 Hz at δ 7.96 of 1 proton represents the presence of sulfonamide NH proton. The pyridine attached N-CH2 protons are appeared at δ 3.70 with 4 protons. In the aromatic side, 14 protons (including sulfonamide proton) were appeared. In the aliphatic side, 10 protons (Including hydroxyl proton) were appeared .¹H NMR signal denoted 21 protons, and furthermore it shown 7 sets of proton signals. The spectrum of the ligand was verified on comparison with intermediate-6. The NMR spectra and the corresponding interpretations were shown in Fig-1 and Fig-2.

LC-MS spectra of the ligand HL1

The LC-MS spectrum of the hydro chloride salted ligand was confirmed and displayed in the molecular ion peak at m/z value at 413.0 shown in Fig.3.

Biological studies

In vitro antioxidant activity (DPPH scavenging assay)

The antioxidant activity of the Ligand-1 was determined by DPPH free radical scavenging method. To check the activities Vitamin - C was used as a reference material. Different concentrations (10-500 mM) were used to check the antioxidant activity of the Ligand-1 and reference material. The Ligand-1 and reference results are shown in Fig.4. It was observed that t 10-500 mM concentrations Ligand-1 showed equal activity to the standard in DPPH free radical scavenging studies. The N-(3-Amino-2-hydroxy-propyl)-benzamide hydrochloride containing NH possibly will act as hydrogen donor to slake with the DPPH in addition it produce an aryl radical could stabilize in the pyridine azonylphynyl conjugated system. These inference imply that Ligand-1 have awfully antioxidant activity.
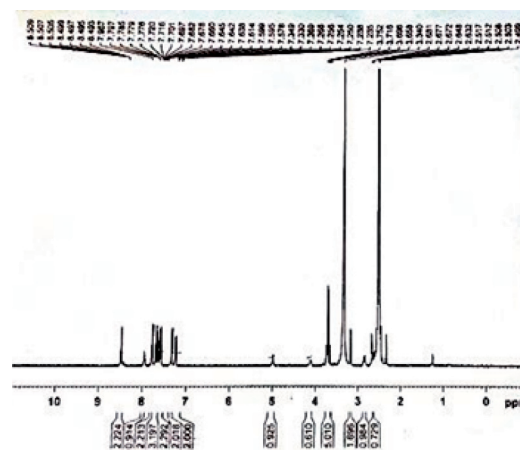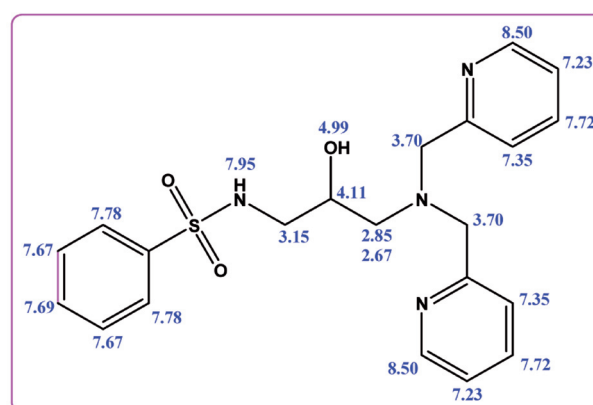

Fig. 1. ¹H NMR full spectra

Fig. 2. ¹H NMR chemical shifts values of Ligand-1.

Table 1 Antioxident properties of DPPH scavenging assay (STD: Vitamin - C)

S.No	Ligand-1 Concentration (µg/mL)	Inhibition %	STD
1	10	4.42	25.25
2	50	13.38	42.44
3	100	18.21	65.9
4	250	23.85	82.97
5	500	31.86	95.72

Antidiabetic activity

The α-amylase enzyme inhibition method was employed for the determination of antidiabetic activity of Ligand-1. Here the standard drug was used as Acarbose which is advised to control the blood glucose level[43]. Various concentrations of acarbose and Ligand-1 of VK-1 (10, 25, 50, 100 and 500 mM) was treated to the inhibition activity of the α -amylase enzyme under suitable condition. The inhibition activity of Ligand-1 was significant value and its values were close proximity with the standard acarbose. A variety of concentrations and inhibition activity percentage were presented in Fig. 5.
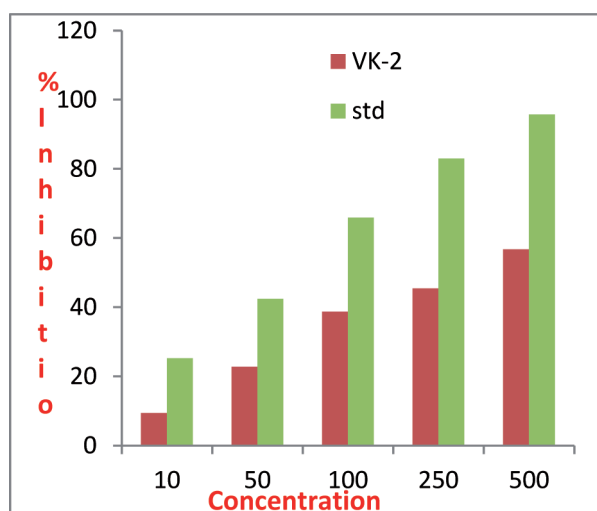
Fig. 4 Antioxidant activity of Ligand-1 (VK2) ligand: DPPH Free radical scavenging activity Standard: Vitamin C

Fig. 5. Antidiabetic activity: α -amylase inhibitory activity ofLigand-1 (VK2). Standard: Acarbose

Stability study

The bioavailability was limited by the poor stability so it is essential to determine the stability study by performing with reported method[44].

The variation in absorption of Ligand-1 was calculated in the presence of Tris-HCl buffer solution to maintain the pH 7.4 at 37 °C. UV-Vis spectrometer was employed with various interval of time (0, 4, 6, 8, 16, 20 and 24 h) used for the degradation effect of Ligand-1. From the observation of the experiment, within 24 h in a buffer solution 7.88% of ligand was degraded and 92.12% of the Ligand-1 compound was more stable under the experimental condition. It suggests that the Ligand possess excellent stability and it was presented in Fig. 6.

Antibacterial activity:

In vitro antibacterial inhibition efficiencies of the Ligand-1 (Table 3) were tested with Gram-positive bacteria, namely, Enterococcus faecalis and negative bacterium, the Ligand-1 exhibited significant effectiveness for gram negative (P. aeruginosa bacterium) than that of the other three gram negative and positive bacterium. Therefore the consequence of Ligand-1 counter ions comprises comparatively superior inhibition activity than the other ligands.
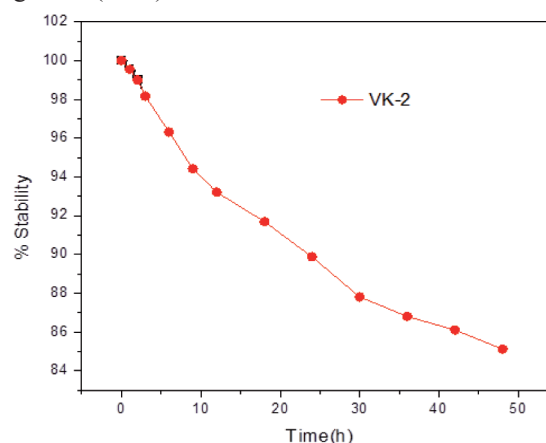

Fig. 6. Stability of Ligand-1 (VK2) ligand

Antibacterial activity outcome:

The Gram-positive like *Enterococcus faecalis*, *Staphytococcus aureus* and Gram-negative bacteria like *Escherichia coli*, *Pseudomonas aeruginosa* were used for the determination of inhibition efficiencies of the Schiff's base ligands.

The solvent DMSO does not show any zone of inhibition and does not interferes with the results so it was reserved as control in all plates in the antimicrobial activity for microorganisms. The investigational result was revealed in Table 3 which specify that Ligand-1 ligand having higher inhibition efficiency is due to chelate formation mechanism. During the investigation of antimicrobial activity of Ligand-1 The following factors [18] were contemplated. They are (i) the chelating effect of ligands; (ii) the nature of the N-donar ligands; (iii) charge of the complex; (iv) existence of ion with counterbalance potential of the ionic complex and (v) the nuclearity of the central metal ion in the complex. The chelation effect may decrease the polarization of ligand owing to the overlapping of the ligand orbital with inequitable contribution of the positive charge of the central metal ion. In addition that

Table .2. Antidiabetic properties of DPPH scavenging assay (STD: Vitamin - C)

S.No	Ligand-1 Concentrations (VK-1) (μg/mL)	Inhibition %	STD
1	10	15.2	17.22
2	50	18.7	23.84
3	100	27.61	45.51
4	250	59.22	62.19
5	500	82.35	89.71

the delocalization of p-electrons over the entire chelate ring and develops the lipophilicity of the entire complexes. This enhanced lipophilicity develops the carrying of the ligand and complexes into lipid membrane. With the comparison of gram positive and *Staphylococcus aureus* and Gram-negative bacteria, namely, *Escherichia coli* and *Pseudomonas aeruginosa* using disc diffusion method[45-46].

DNA Cleavage Assay

The cleavage effectiveness determination was done by the capability of the Ligand-1 to modified as super coiled DNA (Form-I) and it can open a spherical form or purloined form (Form-II). As it was shown in Fig. 7 indicates a significant quantity of increased intensity of bands in exposed circular form in the occasion of the ligand [47]. The various DNA cleavage efficacy was observed in the Ligand-1 mainly owes the dissimilar binding attraction of the HL1 to DNA.
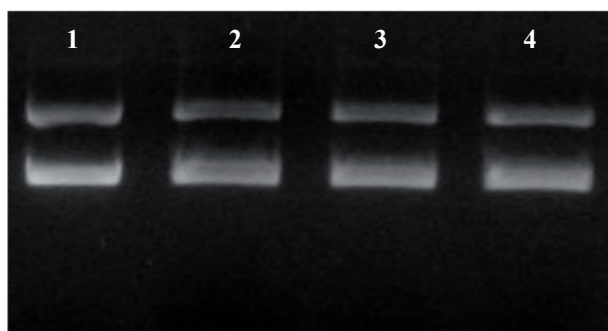

Fig .7. DNA cleavage Activity of the ligand HL1 (RV-2): L 1 –PUC 18 DNA – Control; L 2 –DNA + H2O2 (1mM); L 3 – DNA + H_2O_2 (1mM) + RV-2 (1µL); L 4 – DNA + H_2O_2 (1mM) + RV-2 (2µL)

DNA cleavage Activity:

Molecular docking study with α - amylase

It is a very important tool for design of drug delivery system in human or animal biology[31].

The objective of molecular docking is to forecast the various mode of binding interactions like Hydrogen bonding, hydrophobic and electrostatic energies of the ligand into bio molecules for more familiar 3D structure[31]. The 3D structure of the enzymes were collected from the protein data bank[21,22]. Auto dock tool (version 4.2) was used for the α-amylase enzyme. The benzamide ligand **HL1** revealed optimum binding energies with 1 HNY exhibited binary hydrogen bonding interactions with different amino acid residues such as HIS101(2.83Å) and ASP300 (2.64Å) respectively in HL1R ligand. The pyridyl CH with hydroxyl oxygen of HIS101 has the conventional hydrogen bonding interactions and their bond distance is acknowledged as 2.83Å Å.

The hydrogen bonding interaction between amide NH with Sulphonamide groupASP300 has the bond distance is found to be 2.64Å their inhibition constant is found to be 4.18 µM. Moreover, the molecular docking interaction of acarbose was done in contradiction of 1HNY.

The HL1S exhibited poor inhibition constant and binding energy than HL1R ligand.

The quantity of hydrogen bond attraction was found to be less than HL1 ligand. The docking outcomes such as inhibition constant, hydrogen bond interactions and binding energy, are summarized in Table. 4 and also the interaction between HL1 and acarbose with 1HNY is presented in Fig.8 & Fig.9.
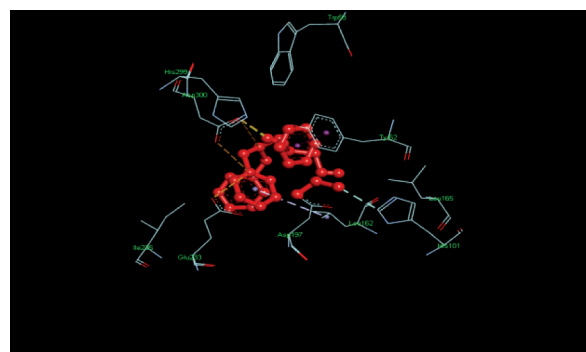

Fig.8.Interaction of HL1R in the active site pocket of 1HNY.pdb

Table 3. Ligands and its complexes antibacterial activity studies

Sample	Zone of Inhibition (mm)											
	E. faecalis			*S. aureus*			*E. coli*			*P. aeruginosa*		
	500 µg	1000 µg	2000 µg	500 µg	1000 µg	2000 µg	500 µg	1000 µg	2000 µg	500 µg	1000 µg	2000 µg
RV2	-	-	9	-	-	8	-	-	-	-	-	9
STD	24			23			24			24		

STD:Streptomycin (20 µg)

Table 4. Docking results of synthesized compounds in the active site pocket of 1HNY.pdb.

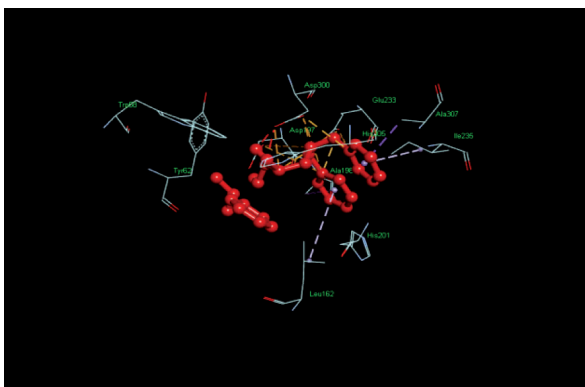| Sample code	Binding energy kcal/mol	Inhibition constant	No of hydrogen bonding	Hydrogen bonding amino acid residue
L1	-7.34 kcal/mol	4.18 µM	2	HIS101(2.83Å) carbon hydrogen bonding interaction ASP300 (2.64Å) Conventional hydrogen bonding interaction
L2	-8.24 kcal/mol	913.11 nM	-	-

Fig.9 Interaction of HL1S in the active site pocket of 1HNY.pdb

Conclusion

In the present work we successfully synthesized novel N(3-(bis(pyridine-2ylmethyl)amino)-2-hydroxypropyl) benzene sulfonamide ligand. The ligand have been characterized well with spectral techniques. The result of DNA cleavage study reveals that significant activity. In addition to the result of antibacterial activity exhibited very good activity against S.aureus and E. faecalis are the gram positive and Pseudomonas aeruginosa are the gram negative bacteria. Further it has very high potential application in pharmaceuticals and in medicinal chemistry. Its synthetic compound's antioxidant action and α-Amylase inhibition efficiency are feasibly extraordinary profits to govern the complication of diabetic patients. In vitro stability of the synthesized compounds has also been significant improvement.

References

1. More MS, Joshi PG, Mishra YK, Khanna PK. Metal complexes driven from Schiff bases and semicarbazones for biomedical and allied applications: a review. Mat Today Chem,2019,14: 100195.

2. Maher KA, Mohammed SR, Metal Complexes of Schiff Base Derived from Salicylaldehyde A Review, Int J. Current Res and Review 2015.17(2) ;6-16.

3. Introduzioneallo studio dellachimica [Introduction to the study of chemistry], series of Schiff's lessons at the Museo di Scienze Naturali, Edizioni Loescher, Torino, 1876.

4. Einführung in das Studium der Chemie [Introduction to the study of chemistry], Prof. Hugo Schiff, Ed. Verlag von Theobald Grieben, Berlin, 1876.

5. Mahasin A, Huda K, Carolin S.Synthesis physical characterization and biological evaluation of Schiff base M(II) complexes. J .Asso. Arab Universities for Basic and App Sci,2014,15; 28-34.

6. Booysena IN, Maikooa S, Akermana MP, Xulua B, Munro O. Ruthenium(II/IV) complexes with potentialy tridentate Schiff base chelates containing the uracil moiety J Coord Chem 2013,66 ; 3673.

7. Fatma NS, Ashraf MA, Somia MS, Omar MM, Gehad GM. Design, spectroscopic characterization, DFT, molecular docking, and different applications: Anti-corrosion and antioxidant of novel metal complexes derived from ofloxacin-based Schiff base,J Organomet Chem 2023, 993; 122698

8. Anshita V, Mishra AP. Synthesis spectral characterization, computational studies, antifungal, DNA interaction, antioxidant and fluorescence property of novel Schiff base ligand and its metal chelates. Spectrochem Acta Part A Mol and Biomol Spect, 2023, 297; 122765

9. Creaven BS, Czegl´edi E, Devereux M. Biological activity and coordination modes of copper(II) complexes of Schiff base-derived coumarin ligands. Dalton Transac,2010, 39 ;10854–10865.

10. Jarrahpour A, Khalili D, De Clerq E, Salmi C, Brunel JM. Molecules, 12, 2007; 1720–1730

11. Priyanka D, Kiran S, Bhupender K, Jahnavi KS. Synthesis, spectroscopic, antimicrobial and *in vitro* anticancer activity of Co^{+2}, Ni^{+2}, Cu^{+2} and Zn^{+2} metal complexes with novel Schiff base, Inorg Chem Comm, 2023,152; 110674

12. Manjunatha M, Naik VH, Kulkarni AD, Patil SA. DNA cleavage, antimicrobial, anti-inflammatory anthelmintic activities, and spectroscopic studies of Co(II), Ni(II), and Cu(II) complexes of biologically potential coumarin Schiff bases. J Coord Chem, 2011, 64; 4264– 4275.

13. Fatma NS, Ashraf MA, Somia MS, Omar MM, Gehad GM, Design, spectroscopic characterization, DFT, molecular docking, and different applications: Anti-corrosion and antioxidant of novel metal complexes derived from ofloxacin-based Schiff base,J. Organomet. Chem. 2023; 993; 122698

14. Anacona JR, Noriega N & Camus J, Synthesis, characterization and antibacterial activity of a tridentate Schiff base derived from cephalothin and sulfadiazine, and its transition metal complexes. Spectrochem Acta - Part A Mol Bio mole Spect 2015;137: 16–22.

15. Abdullah MA, Salman AK, Hadi MM, Kamlesh S, Synthesis, spectroscopic and physicochemical investigations of environmentally benign heterocyclic Schiff base derivatives as antibacterial agents on the bases of *in vitro* and density functional theory.J Photochem and Photo bio 2013;120: 82-89.

16. Anshita V, Mishra AP Synthesis, spectral characterization, computational studies, antifungal, DNA interaction, antioxidant and fluorescence property of novel Schiff base ligand and its metal chelates. Spectrochem Acta Part A Mol and BiomolSpect2023; 297: 122765

17. Pandiarajan S, Easwaramoorthy D, Hajarabeevi N &Karthikeyan R, Antimicrobial activity and corrosion inhibition property of Schiff bases derived from Imidazole. IndJ Chem Tech 2020; 27: 311- 318.

18. Rao NVS, Choudhury TD, Deb R, Paul MK &Rao TR, Fluorescent lanthanide complexes of Schiff base ligands possessing N-aryl moiety: influence of chain length on crossover (calamitic to discotic) phase behaviour. LiqCrys 2010; 37: 1393-1410.

19. Priyanka D, Kiran S, Bhupender K, Jahnavi KS Synthesis, spectroscopic, antimicrobial and *in vitro* anticancer activity of Co^{+2}, Ni^{+2}, Cu^{+2} and Zn^{+2} metal complexes with novel Schiff base. Inorg Chem Commn2023;152: 110674

20. Fatma NS, Ashraf MA, Somia MS, Omar MM, GehadGM,Design, spectroscopic characterization, DFT, molecular docking, and different applications: Anti-corrosion and antioxidant of novel metal complexes derived from ofloxacin-based Schiff base,JOrganometChem2023; 993; 122698

21. Ohorodnik YM, Alexander SA &Khomenko DM, Synthesis, structural characterization and anticancer properties of *p*-cymene Ru(II) complexes with 2-(N-methyl-*1-H*-1,2,4-triazol-3-yl)pyridines. Transit Met Chem 2022; 47: 213–221.

22. Guha A, Adhikary J, Mondal T & Das D, Zinc and cadmium complexes of a Schiff base ligand derived from diaminomaleonitrile and salicylaldehyde: Syntheses, characterization, photoluminescence properties and DFT study. Ind J Chem2011; 50:1463-1468.

23. Howard JKA & Allen FH (Eds) (1999), Implication Of molecular and materials structure for new technologies, kluwer, Dordrecht.

24. Sambrook J, Fritsch EF &Maniatis T, Molecular cloning, A Laboratory Manual, (1989) Cold Spring Harbor Laboratory press.

25. Kavithasharma, Singh GP &Vikas Kumar, Macrocyclic divalent transition metal complexes of cobalt, nickel, copper and zinc with their antimicrobial, spectroscopic studies. Ind J Chem Tech 2017; 24: 534 – 540.

26. Kiehlbauch J, Hannett G, Salfinger M, Use of the National Committee for Clinical Laboratory Standards Guidelines for Disk Diffusion Susceptibility Testing in New York State Laboratories. J Clin Microbiol 2000: 38:3341–3348.

27. Mellem J, Baijnath H &Odhav B,Antidiabetic potential of brachylaenadis colour. Afr Tradit Complement Altern Med 2015; 12: 38-44.

28. Shukla S N, Gaur P, Mathews S, Khan S &Srivastava A, Synthesis, characterization, catalytic and biological

29. Pelczar M J, Chan E C S & Krieg N R, Text Book of Microbiology, 5th Ed, McGraw-Hill Publishing Company Ltd, New Delhi, India, (2001) 138.

activity of some bimetallic selenocyanate Lewis acid derivatives of N, N'- *bis* (2-chlorobenzylidene)ethylene diamine. J Coord Chem 2008; 61: 3913-3921.

30. Chuengsamarn S, Rattanamongkolgul S, Luechapudiporn R, Phisalaphong C &Jirawatnotai S, Curcumin extract for prevention of type 2 diabetes, Diab Care 2012;35: 2121–2127.

31. Hong J, Bose M, Ju J, Ryu J H, Chen X, Sang S, Lee M J & Yang C S, Modulation of arachidonic acid metabolism by curcumin and related beta-diketone derivatives: effects on cytosolic phospholipase A(2), cyclooxygenases and 5-lipoxygenase. Carcinogenesis 2004: 25: 1671–1679.

32. Raman N, Antibacterial Study of the Mannich Base, N-(1-morpholino-benzyl)semicarbazide and its Transition metal(II) Complexes. Res J Chem Environ 2005; 9: 79–80.

33. Yousefi R, Alavian-Mehr MM, Mokhtari F, Panahi F, Mehraban MH &Khalafi-Nezhad A, Pyrimidine-fused heterocycle derivatives as a novel class of inhibitors for α-glucosidase. J Enzyme InhibMed Chem 2013; 28: 1228–1235.

34. Banuppriya G, Sribalan R &Padmini V, Synthesis and characterization of curcumin-sulfonamide hybrids:

35. Biological evaluation and molecular docking studies. J MolStruct2018; 1155: 90-100.

36. Zafar H, Ahmad A, Khan AU & Khan TA,Synthesis, characterization and antimicrobial studies of Schiff base complexes. J Mol Struct 2015; 1097:129–135.

37. Olszowy-Tomczyk, M. How to express the antioxidant properties of substances properly?. *Chem. Pap.* 2021; 75: 6157–6167.

38. Mustafa D, Cuneyt T, Mesut I, Yeliz D, Ali S, Ali K, AbdussamatG,Sukru B, Suleyman A, Sameh MO, Zeid A Claudiu TS Synthesis, characterisation, biological evaluation and in silico studies of sulphonamide Schiff bases. J EnzymInhib Med Chem2020; 35: 950–962

39. Akila E, Usharani M &Rajavel R, Metal (II) complexes of bioinorganic and medicinal relevance: Antibacterial, antioxidant and dna cleavage studies of tetradentate complexes involving o, n-donor environment of 3, 3′-dihydroxybenzidine-based schiff bases. Int J Pharm PharmSci 2013; 5: 573–581.

40. Oyedemi S O, Bradley G &Afolayan A J,Antibacterial and antioxidant activities of hydroalcoholic stem bark extract of *Schotialatifolia* . Asian Pac J Trop Med 2011;4:952–958.

41. NCCLS/CLSI—National Committee for Clinical Laboratory Standards. Methods for Dilution Antimicrobial Susceptibility Tests for Bacteria that Grow Aerobically, Approved Standard 6th ed.:M07-A6; Clinical and Laboratory Standards Institute: Wayne, PA, USA, 2004.

42. Sribalan R, Shakambari G, Banuppriya G, Varalakshmi P, Subramanian E, Sudhakar&Padmini V, Synthesis of a Water-Soluble PyrazoleCurcumin Derivative: *In Vitro* and *In Vivo* AGE Inhibitory Activity and Its Mechanism.ChemistrySelect 2017; 2: 1122–1128.

43. Amer S, El-Wakiel N, & El-Ghamry H,Synthesis, spectral, antitumor and antimicrobial studies on Cu(II) complexes of purine and triazole Schiff base derivatives. J MolStruct.2013;1049: 326–335.

44. Omar M M, Mohamed G G, &Hindy A M M, Transition metal complexes of heterocyclic Schiff base biological activity, spectroscopic and thermal characterization. J Therm Anal Cal, 86 (2006) 315-325.

45. ZangadeS,Shinde A, Chavan S &Vibhute y, Solvent-free, environmentally benign syntheses of some imines and antioxidant activity J Chem, 7 (2015) 208-214.

46. Manjula B & Anthony Arul S, Antimicrobial screening of Transition Metal complexes of 4-aminoantipyrine Schiff base Res.J.chem.sci, 3 (2013) 22-28.

47. Li Y, Yang Z Y, & Wu J C, Synthesis, crystal structures, biological activities and fluorescence studies of transition metal complexes with 3-carbaldehyde chromonethiosemicarbazone Eur. J Med Chem, 45 (2010) 5692-5701.

48. 47. Consiglio G, Failla S, Finocchiaro P, Oliveri I P & Bella S D,Aggregation properties of Bis (salicylaldiminato) zinc(ɪɪ) Schiff-base complexes and their Lewis acidic Character Dalton Trans, 41 (2012) 387-395

Original article

Kinetic and thermodynamic parameters of urease in soils with different fertilization regimes

CARMEN POSTOLACHE[1]*, FLORINA BOTEZ[1], HORIA DOMNARIU[1,2], CHETAN FELICIA[3], CRISTIAN-ALIN CUCU[4]

[1] Department of Systems Ecology and Sustainability, Faculty of Biology, University of Bucharest, Splaiul Independenței no. 91-95, District 5, Bucharest, Romania, Postal code: 050095

[2] Soil Biology Laboratory, National Research and Development Institute for Soil Science, Agrochemistry and Environment – ICPA, Bd. Mărăști, no. 61, Bucharest, Romania, Postal code: 011464

[3] Agricultural Research and Development Station Turda, Agriculturii Street 27, 401100 Turda, Romania

[4] Faculty of Biology, University of Bucharest, Splaiul Independenței no. 91-95, District 5, Bucharest, Romania, Postal code: 050095

Abstract

In recent years the growing demand for food led to intensification of agricultural practices, especially by the excessive use of fertilizers, which increased the environmental pollution. Therefore, pollution control by improving the efficiency of fertilizers and reducing their application is of great interest. Urease is one of the most active hydrolases in soil, having an important role in soil N cycle and being used as an indicator of soil quality. The objective of this study was to assess the urease activity in soils with different fertilization treatment, as well as its kinetic and thermodynamic parameters to better understand its driving factors. The results show a better enzymatic activity in soils treated with combined manure and mineral fertilizers. Soil urease has two optimal pH values, in the neutral and basic domains. Enzymatic activity has a steep increase with the temperature in the interval 45–65°C. The K_M values increase with temperature from 11 to 23.5 mM, indicating a lower substrate affinity. The activation enthalpies for enzyme-substrate formation as well as for the rate limiting step are 7.59 and 14.18 kcal/mol respectively. The relationship between urease activity and microbial biomass will be further investigated.

✉ *Corresponding author:* Carmen Postolache, Splaiul Independenței no. 91-95, District 5, Bucharest, Romania,
email: carmen.postolache@bio.unibuc.ro; phone: +40744495917
horia.domnariu@gmail.com; felicia.chetan@scdaturda.ro; cristian.cucu.002@student.uni.lu

Introduction

Enzymes play an essential role in all processes that take place in organisms and in the environment [1]. They catalyze biochemical reactions that thus take place with an order of magnitude higher than in their absence. Thus, life on Earth could not exist without the rapid unfolding of biochemical processes. Enzymes are involved in many edaphic processes like organic matter decomposition, forming of humic substances, xenobiotic degradation, nitrogen fixation among others [2]. Therefore, ecological functions like biomass production and soil decontamination, are highly dependent on enzymes activity, as they are directly involved in biogeochemical cycles of C, N, P and S. Among them, due to their function, hydrolases – proteases, phosphatases and ureases are the most studied soil enzymes [3]. A major agricultural topic of recent research is food security, and it is closely related to soil health. One of the important indicators of soil quality is soil biological activity. It has been suggested that activity of soil enzymes is a potential indicator of soil quality because of their relationship with soil biology and rapid response to changes in soil management [4].

Urease is a key catalytic enzyme involved in urea hydrolysis, widely distributed in nature in plants, animals and microorganisms [5; 6]. It has an important role in the use of urea fertilizer, is involved in the N cycle, and the changes of its activity can be used as an indirect indicator of N pool and availability in soils. But, by increasing the use of urea as fertilizer, there is an intensification of the activity of soil urease, and an increase of ammonia volatilization, soil alkalinization, and nitrous oxide generation, the 3rd greenhouse gas, or even the degradation of aquatic ecosystems, through eutrophication [7; 8]. Low urease activity, on the other hand, causes environmental pollution through leaching of additional urea. To mitigate these problems the understanding of urease mechanism and kinetics is crucial because it can give information on compounds that could inhibit soil urease activity and reduce urea hydrolysis in case of its use as fertilizer. There is still little knowledge about the kinetic and thermodynamic characteristics of soil urease with amendment of urease inhibitors and different environmental conditions [9].

It has been revealed the influence of individual environmental factors like temperature, water content, nitrogen application rates on urease activity, but the integrated effect of these factors is not clear. In agricultural soils, with different temporal and spatial environmental conditions, the impact of these factors on urea hydrolysis has different consequences. Urea hydrolysis is a first order kinetic process, and the rate constant is an important parameter. Nitrogen transportation and transformation simulation studies use the value of this kinetic parameter at a fixed moisture content, temperature and nitrogen concentration [10.

Previous studies mentioned that there is variation in the stabilities of urease in the heterogeneous soil systems, especially thermal stability, due to the complexation of enzyme with organic colloids or adsorption on clay particles [11]. These differences were attributed to soil pH and adsorptive properties of soils [12].

Therefore, in this study we assessed the kinetic and thermodynamic parameters of soil urease and compared it to extracted urease "*jack bean urease*". There are no comprehensive studies on soil urease activity and kinetics in Romania and this kind of information is important in establishing agricultural strategies with special consideration on urea decomposition rate and its environmental consequences. We expect that this study will generate useful information to assess and develop strategies for sustainable nitrogen management and a useful indicator of soil health.

Materials and methods

Description of the research area and sampling

The agricultural field selected for this study belongs to o a long-term experiment established in 1962 and managed by Agricultural Research and Development Station Turda (ARDS Turda), having the following geographical coordinates: 46° 35' 12.3" lat. N, 23° 48' 3.42" long. E. The experiment consists of 7 fertilization treatments (combinations of N, P and manure fertilizers) each in three field replicates with an area of 50 m^2. The rotation system involves a three-crop sequence based on maize, soybean and wheat. Topsoil (0-20 cm) samples were collected in April 2021 being composited out of six subsamples that were extracted by the means of a soil auger.

From each batch (subjected to a certain combination of fertilizers) 5 replicates were taken from a depth of 20 cm. Each replicate was obtained by homogenizing the soil taken from 5-6 injections. The kinetic analysis of urease was performed on the sample taken from the plot fertilized annually with 50 t/ha of N, 25 t/ha of P and 60 t/ha of manure. Before any analysis, samples were processed by grounding and sieving with a sieve with a diameter of 4 mm.

Physicochemical properties

Physicochemical parameters determined for the soil samples were pH, moisture, organic matter, ammonia nitrogen, nitrate nitrogen, phosphorus in the form of phosphate and urease activity. The pH was measured on a suspension soil-water in 1 to 2.5 ratio [13], using a WTW 3000 pH-meter. Soil water content was determined gravimetrically

and organic matter content of soil samples through loss on ignition at 550°C. Inorganic nitrogen compounds were extracted from soils with a solution of potassium chloride (KCl) 0.2 M. Ammonia nitrogen was determined by indophenol-blue method [14], nitrate with the phenol disulphonic acid method, and phosphate by green malachite method [15], using a Helios Gamma UV-VIS spectrophotometer [16]. All analytical results were normalized to dry soil weight.

Urease activity assay

Urease activity was assayed following the procedure described by Tabatabai and Bremner [17]. Five grams of soil were incubated with 10 ml buffer solution (pH in the range 5.4 -11) and 1 ml urea of different concentrations for 2 hours at 37°C. Different urea concentrations between 2 and 160mM were used to assess kinetic parameters, as well as different temperature for determination of thermodynamic parameters. The reaction was stopped by the addition of KCl solution 1M. A volume of 1 mL was taken from the supernatant to determine the ammonium concentration by the indophenol-blue method. The kinetic and thermodynamic parameters were carried out on an average sample made from the 3 replicates taken from lot 4, fertilized annually with 50 t/ha N, 25 t/ha P and 60 t/ha manure.

Michaelis kinetic parameters

The kinetic parameters K_M and V_{0max} were calculated by Hanes-Woolf equation [18]:

$$\frac{[S]}{V_0} = \frac{1}{V_{0max}} \cdot [S] + \frac{K_M}{V_{0max}},$$

where V_{0max} is the enzyme maximum initial velocity, [S] is the concentration of substrate (mM), K_M is the Michaelis constant.

Thus, the variation of K_M with temperature allows the determination of the enthalpy of formation of the ES complex, and the variation of k_2 with temperature on that of the enthalpy of activation of the velocity-determining step, that of the decomposition of the ES complex into products and

Fig. 1. Energy diagram of the enzymatic reaction

enzyme. These parameters are represented in the energy diagram in Figure 1. The enthalpy of formation of the ES complex is calculated based on the van't Hoff relation:

$$\frac{d lnK_{eq}}{dT} = \frac{\Delta_r H^\emptyset}{RT^2},$$

which, through integration, leads to:

$$lnK = \frac{-\Delta H^\emptyset}{RT} + \frac{\Delta S^\emptyset}{R}$$

and the plot of lnK = f(1/T) is a straight line with the slope -ΔH/R.

The temperature dependence of the rate constant k_2 with temperature, according to the well-known Arrhenius equations [19]:

$$k = A \cdot e^{-\frac{E_a}{RT}},$$

where E_a is the activation energy (kJ/mol), A is the preexponential factor, R is the gas constant ($J \cdot mol^{-1} \cdot K^{-1}$) and T is the absolute temperature (K). The plot of $lnk_2 = f(1/T)$ allows the determination of the activation energy and activation enthalpy, according to the equation: $\Delta H_2^* = Ea - RT$.

Results and discussion

Physicochemical characterization of soils

Prior to the evaluation of urease, the physicochemical characterization of the samples taken from the 7 plots subjected to different fertilization treatments was carried out. It was reported that physical, chemical and biological composition of soils, together with type of crops and management practices influence soil enzymatic activities [20]. Table 1 shows the average results obtained from the analysis of the 3 replicates from each plot.

Table 1. Average values of the physicochemical parameters of soil samples taken from plots with different fertilization treatments

Tratament (t/ha/year)	pH	N-NH₄⁺ µg/g soil	N-NO₃⁻ µg/g soil	P-PO₄³⁻ µg/g soil	MO%	U%
1: 150N, 60P	5.08	0.92	1.88	11.25	8.89	18.19
2: 120N, 50P, 20t manure	5.10	0.94	1.76	18.08	8.93	16.19
3: 80N, 30P, 40t manure	5.17	0.82	3.02	23.64	9.42	17.34
4: 50N, 25P, 60t manure	5.08	1.11	2.81	19.98	9.01	19.13
5: 20t manure	5.19	2.06	1.99	10.23	9.24	19.05
6: 40t manure	5.14	2.99	1.30	11.14	9.05	16.46
7: not fertilized	5.27	1.07	0.97	2.69	8.65	18.24

The analysis of the results indicates that the soil has a slightly acidic reaction, the pH values being between 5.08-5.27. In general, agricultural soils are characterized by a more acidic reaction than untilled soils because of the application of fertilizers. The humidity varies in the range
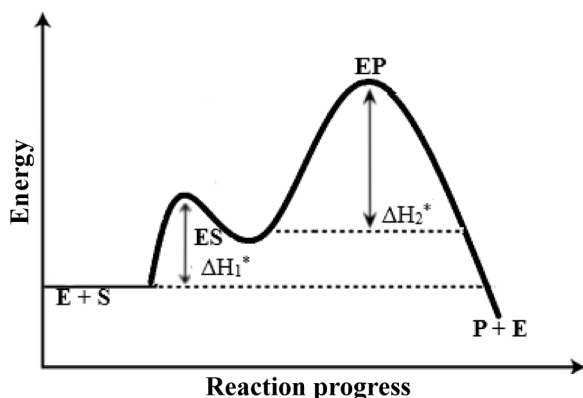
of 16.19-19.13%, and the organic matter in the range of 8.65-9.42%. In terms of nutrient content (N and P), the not fertilized soil is differentiated, having the lowest inorganic nitrogen (DIN) content, of 2.04 µg N/g dry soil and reactive phosphorus (in the form of PO_4^{3-}) of 2.69 µg P/g dry soil. Soils treated only with manure have, as expected, the highest ammonia nitrogen content (above 2 µg N-NH_4^+/g dry soil) but the lowest phosphorus content (except for not fertilized soil).

Determination of urease activity in agricultural soils subjected to different fertilization treatments

The results obtained from the analysis of the urease activity are presented in Table 2. As can be observed, the enzymatic activity (expressed as maximum initial reaction rate) presents small differences for the 7 fertilization treatments, varying between 0.44 and 0.61 mM/h, at 37°C, pH = 8, $[S]_0$ = 80 mM. The higher values of enzymatic urease were obtained for soil samples of plots 3 and 4, fertilized with high amounts of organic fertilizer combined with mineral fertilizers, which is in accordance with data described in literature. Some authors reported a decrease of urease activity with long-term nitrogen fertilization [3]. This was explained by the absorption of inorganic nitrogen by soil microorganisms [21]. But urease activity was also reported to increase with addition of nitrogen and organic fertilizers [22]. It was also noted that application of both organic and mineral fertilizers enhances urease and phosphatase activities in soils cultivated with beans [23]. The increase was attributed to a combined effect of higher degree of enzyme stabilization with formation of organomineral complexes and increase of microbial biomass because of organic carbon content [24]. Soil sampled from plot 4 are characterized by the highest water content and high organic matter.

Kinetic and thermodynamic studies were performed on soils from plot 4. The choice of soil samples from this plot was based on the values obtained for urease activity which were the highest and the fertilization treatment is the most complex, including, in addition to mineral fertilizers, the largest amount of organic fertilizer.

Table 2. Values of the maximum initial velocity at pH = 8 and 37°C of the catalyzed reaction of urease

Plot (treatment)	C (µg N-NH_4^+)	V0 (mM/h)
1	10.98	0.571
2	10.74	0.558
3	11.23	0.583
4	11.72	0.609
5	8.53	0.443
6	10.63	0.552
7	10.18	0.529

Characterization of kinetic and thermodynamic parameters of urease in agricultural soil

1. Variation of the initial reaction rate with pH

Variation of the enzymatic rate of reaction with pH was investigated on the pH range 5-10. Phosphate buffer solutions have been used for the pH range 5-8 and borate buffer solutions for the range 8.4 -10. Although the assays are usually performed in phosphate buffer and/or in borate buffer, in the literature it is indicated that the phosphate buffer at pH < 7.5 manifests inhibition by the $H_2PO_4^-$ ion [25], as well as the borate buffer manifests inhibition with increasing pH [26]. Boric acid exhibits maximum inhibition at pH 5 and minimum at pH 10 [27]. Phosphoric and boric acid are competitive inhibitors, admittedly, with low inhibitory activity.

The variation of the soil urease activity with pH shows two maximum values corresponding to pH 7.4 and 10.8 (Figure 2), as opposed to the dynamics mentioned in literature for the purified *jack bean urease* which shows only one maximum, with a bell shape and an optimal pH 7-7.5, according to Krajewska (2009a). The bell shape is specific to many enzymes, and in *jack bean urease* the existence of three functional groups has been demonstrated, with pKa of 5.3, 6.6 (associated with a molecule of His in catalytic active center), and 9.1 (either W2 or WB) [28]. Optimal pH reported in literature for soil urease is between 6.5-7, but values above 8.8 and even below 5.8 have been reported [29]. The optimal pH depends on the buffer used, but also on the nature of the enzyme. We assume that the differences from the *jack bean enzyme,* for which we obtained a maximum value at pH of 7.2 using the same buffers, are due to the different origin of the enzymes in the soil. According to various reports, urease can originate from multiples sources, including bacteria, fungi, plant and animal tissues and animal waste [30]. The hypothesis is supported by the fact that the soil we took into analysis was fertilized with 60 t/ha/year of manure. The same literature study mentions that microbial urease is controlled by N fluxes in the soil. At the same time, even the optimal pH value of jack bean urease can be considerately higher, if the enzyme gets immobilized on certain types of clay minerals as shown by Lai and Tabatabai [31].

2. Variation of the initial reaction rate with the substrate and temperature

In this study the variation of soil urease activity with temperature shows a maximum at a temperature of 65°C (pH=10, $[S]_0$ = 160 mM), like many enzymes. From 15 to 45°C, the increase of the initial rate is about 1.8 times over each 10°C, followed by a steep increase from 45°C to 65°C, of 3.5 times (Figure 3). Other studies [32] showed different response of urease activity to temperature [33], with two
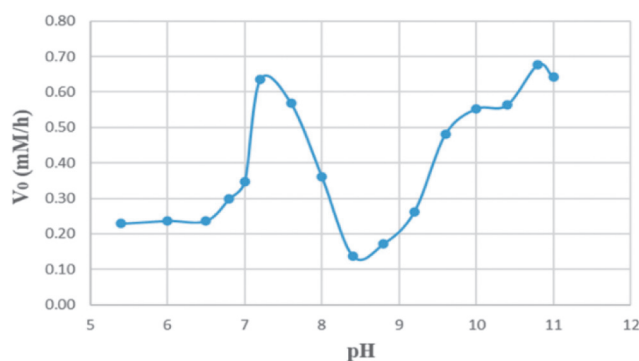
Fig. 2. Variation of the initial rate of the soil urease catalyzed reaction with pH

or three times increases from 15°C to 35°C or only 0.15-0.62 times for the same temperature interval [34]. The optimal temperature mentioned in the literature was 60°C [35]. By choosing a high concentration of substrate, the thermal stability of the enzyme is increased. At temperatures above 65°C, the initial velocity decreases because the enzyme is largely denatured. It was reported that, even if the inactivation of urease activity occurs in 65-70°C, it is not completely destroyed up to 105°C [36], its greater thermal stability being explained by adsorption on clay colloids or complexation with organic colloids [11]. Other studies showed that soil enzymes are generally more resistant to thermal denaturation in the heterogeneous soil systems [37]. The effect of temperature on soil enzyme activities leads generally to changes in substrate affinity, enzyme stability and kinetics through its influence on size and activity of microbial biomass. Urease activity has been shown to be dependent on soil temperature and moisture content, but not on soil nitrogen concentration [38], but the influence of nitrogen application rate was also mentioned in literature [34]. Many studies revealed the influence of single factors on urease activity, however the effect of interaction between factors should not be ignored. Our results also suggest that fertilization treatment influences urease activity, which was greater in soils treated with the highest amounts of organic fertilizer (Table 2).

Regarding the influence of the substrate concentration on the maximum initial velocity, the urea concentration range 2-160 mM was used. The working temperatures were
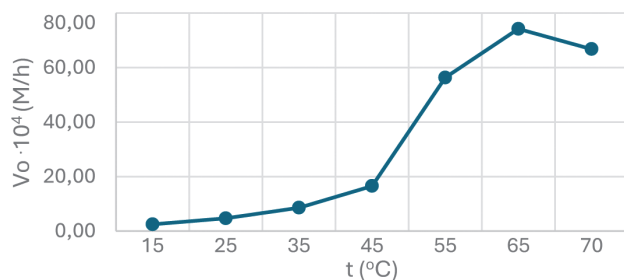

Fig. 3. Variation of the initial rate of reaction catalyzed by soil urease with temperature

in the range of 15-55°C, but due to the low enzymatic activity at low temperatures, it was difficult to obtain a clear variation of the kinetic parameters (K_M and V_{0max}). Thus, only the results at temperatures of 35, 45 and 55°C were interpreted, respectively. The parameters kept constant were pH=10, t = 2h. The graphical representation clearly shows that a Michaelis-Menten kinetic is observed, reaching a plateau at high concentrations of urea (Figure 4).
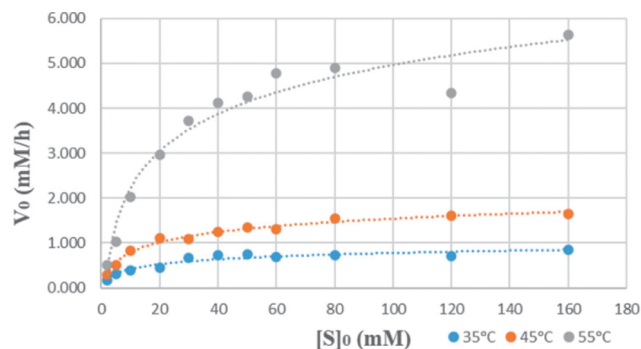

Fig. 4. Variation of the initial rate of the reaction catalyzed by soil urease with substrate and temperature

The Hanes-Woolf linearization (Figure 5) equation was used to determine the kinetic parameters K_M and V_{0max}.

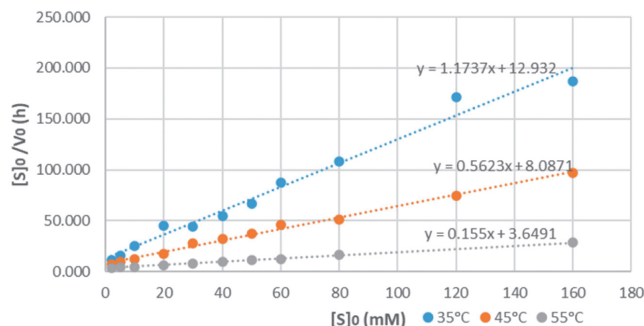$$\frac{[S]}{V_0} = \frac{1}{V_{0max}} \cdot [S] + \frac{K_M}{V_{0max}}$$

Fig. 5. Hanes-Woolf linearization of the initial rate variation of the catalyzed reaction by soil urease

The values of V_{0max} for temperatures in the range 35-55°C were obtained from the graph slope and K_M from the free term of equation.

The K_M values obtained in our study vary between 11–23.5 mM, increasing with temperature, and fall within the very wide range of variation of this constant mentioned in the literature, between 1.2-330 mM (Table 3).

Table 3. Kinetic parameters (K_M, V_{0max} and k_2) at different temperatures of the reaction catalyzed by the urease enzyme

T (K)	1/T (K⁻¹)	$K_M \cdot 10^3$ (M)	V_{0max} (M/h)	lnK_M	k_2 (s⁻¹)	lnk_2
308	0.0032	11.02	0.852	-4.508	3.156	1.149
318	0.0031	14.38	1.778	-4.242	6.585	1.885
328	0.0030	23.54	6.452	-3.749	23.896	3.174

This constant is an indication of enzyme affinity for substrate, a lower value of K_M indicating a higher affinity. Its value is increasing with incubation temperature, probably because of the reduced amount of enzyme active sites covered by humus accompanied with temperature [9]. The same authors hypothesized that soil urease could be trapped by higher soil organic C content and slow down the diffusion of substrate, impeding the enzyme-substrate interaction. The humic substances present in the soil modify the K_M and V_{0max} values in relation to the purified enzyme, which explains the large variations of the K_M constant depending on the organic matter content and the type and quantity of clay in the soil [29]. The formation of different inhibitor-urease complexes has the same effect, as well as conformational changes in enzyme structure, decreasing the accessibility of its active sites [39]. These large variations have not been fully explained, but it has been found that the enzyme can be stabilized by the formation of urease organo-mineral complexes or clay-enzyme associations in some soils. Fidaleo and Lavecchia [40] concluded that value of K_M is influenced by temperature, substrate properties, pH and ionic strength.

The values of the kinetic parameters V_{0max}, K_M and k_2 of the soil urease hydrolysis reaction at different temperatures allowed the determination of activation parameters of the reaction.

Enthalpy of ES complex formation (ΔH_1) was obtained by the variation of lnK_M with temperature (Figure 6), and the enthalpy of activation of the rate-determining step (ΔH_2^*) was obtained from the variation of lnk_2 with temperature (Figure 7), which correspond to the decomposition of the ES complex into products and enzyme (Figure 1).

The value obtained for the enthalpy of formation of the ES complex is 31.75 kJ/mol, more than 3 times higher than that we obtained for the formation of the complex with the purified "*jack bean urease*". This value suggests that the process is more endothermic in the case of the enzyme in the soil. Our results are very close to values reported
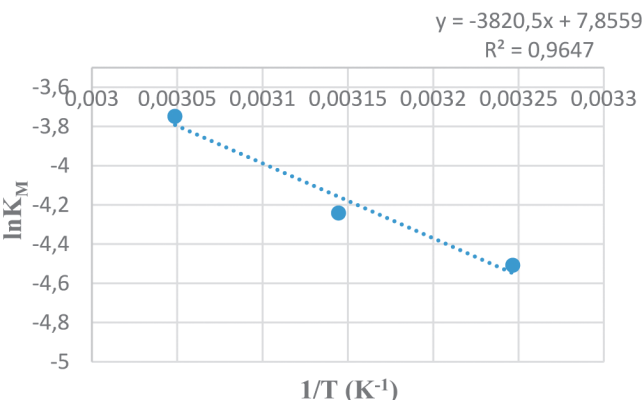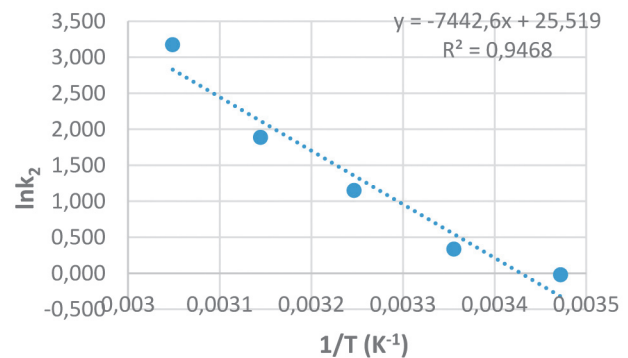

Fig. 7. Plot of lnk2 with temperature for determination of enthalpy of activation of the rate-determining step (ΔH_2^*)

in literature, which vary between 37.96 to 49.70 kJ/mol in loamy sand soil and from 32.04-44.34 kJ/mol in silty clay soil [41]. Other researchers [31] reported values of activation enthalpy of about 36 kJ/mol, whereas Juan et al. (2010) mentioned values between 19.08-21.64 kJ/mol. Same authors [31] hypothesized that a large enthalpy of activation is an indication that for the formation of activated state, many stretching, squeezing and probably breaking of chemical bonds are necessary. Moyo et al. [32] concluded that values reported in literature for activation energy for soil urease are dependent on pH, urea concentration, water content and even assay techniques used that can influence differently the energy requirements for the formation of enzyme-substrate.

Proceeding further to calculate the activation energy of the rate-determining step (ΔH_2^*), the formation of reaction products from the ES complex, an enthalpy of activation of 59.29 kJ/mol was obtained. This value is significantly higher than that obtained for "*jack bean urease*" ((ΔH_2^* = 17.01 kJ/mol), indicating that the energy barrier of this process is higher, so the reaction occurs more slowly in the case of urea hydrolysis under the action of the enzyme in the soil.

Comparing the values obtained in this study with those mentioned by other studies (Table 4), we find that the results fall within the (very wide) ranges of variation mentioned in the literature.

Fig. 6. Plot of lnK_M with temperature, for enthalpy determination of the ES complex formation

Table 4. Comparative values of the kinetic and thermodynamic parameters of the hydrolysis reaction of urea catalyzed by the purified and native enzyme in soil [29] [42; 43]

	K_M (mM)	V_{0max} (µM/s)	ΔH_1^* (kcal/mol)	ΔH_2^* (kcal/mol)
Jack bean urease this study	19.8	2.77	2.05	4.07
Soil urease this study	14.38	10.84 µg N/g soil/h	7.59	14.18
Literature - jack bean)	2.7-45	0.75	-	1.5-9.6
Literature - soil enzyme (free bound)	1.3-330	14-143 µg N/g soil/h	-	5.7-9.8

There are obviously differences in the units of measurement used to express the maximum reaction rates in the case of the enzymatic reaction catalyzed by the purified enzyme and the one catalyzed by the enzymes in the soil. As for the activation enthalpy of the limited rate step of products formation, in the case of purified urease our value is consistent with those reported in the literature, while in the case of the analyzed soil urease, the obtained value is slightly higher.

Conclusion

Results of our study showed that urease activity was stimulated by the application of organic fertilizer in combination with mineral fertilizers. The lowest enzymatic activity was obtained for plots fertilized with only manure in low amounts. Soil urease activity has two optimal pH values, at neutral and basic domains, which suggest different originate sources, which must be investigated. Temperature has a great effect on enzyme activity, influencing biochemical transformation of nutrient catalyzed by soil urease. The increase of K_M value with temperature shows a decrease in enzyme affinity for urea. The larger activation enthalpy we obtained for the soil urease indicates a lower probability of the activated complex enzyme-substrate of progressing towards reaction products.

Future studies are required to analyze the relationship between urease and microbial biomass for different agricultural ecosystems, leading to better understanding of soil health and development of N management strategies.

Funding

Acknowledgements

Conflicts of interest

The authors declare no conflict of interest.

References

1. Karigar CS, Rao SS. Role of microbial enzymes in the bioremediation of pollutants: a review. Enzyme research. 2011;2011(1):805187. https://doi.org/10.4061/2011/805187

2. Das SK, Varma A. Role of enzymes in maintaining soil health. In: Shukla, G., Varma, A. (eds.) Soil Enzymology, Soil Biology 22. Springer Verlag Berlin Heidelberg. 384 p. 2011 https://doi.org/10.1007/978-3-642-14225-3_2

3. Bautista-Cruz A, Ortiz-Hernández YD. Hydrolytic soil enzymes and their response to fertilization: a short review. Comunicata Scientiae. 2015 Dec 29;6(3):255-62. https://doi.org/10.14295/cs.v6i3.962

4. Kumar A, Srivastava AK, Velmourougane K, Sidhu GS, Mahapatra SK, Singh RS, Sahoo AK, Das K, Das TH, Reza SK, Bhattacharyya T. Urease activity and its kinetics in selected benchmark soils of Indo-Gangetic Plains, India. Proceedings of the National Academy of Sciences, India Section B: Biological Sciences. 2015 Jun;85:407-13. https://doi.org/10.1007/s40011-014-0352-5

5. McCarty GW, Bremner JM. Production of urease by microbial activity in soils under aerobic and anaerobic conditions. Biology and fertility of soils. 1991 Jun;11:228-30. https://doi.org/10.1007/BF00335772

6. Tabatabai MA. Soil enzymes. In: Weaver RW, Angel JS, Bottomley PS (eds.) Methods of soil analysis. Part 2. Microbial and biochemical properties. Soil Science Society of America, Madison, 1994, pp 775-833.

7. Khan FA, Ansari AA. Eutrophication: an ecological vision. The botanical review. 2005 Dec;71(4):449-82. https://doi.org/10.1663/0006-8101-(2005)071 [0449:EAEV]2.0.CO;2

8. Krajewska B. Ureases I. Functional, catalytic and kinetic properties: A review. Journal of molecular catalysis B: Enzymatic. 2009a Jul 1;59(1-3):9-21. https://doi.org/10.1016/j.molcatb.2009.01.003

9. Juan YH, Chen ZH, Chen LJ, Wu ZJ, Wang R, Sun WT, Zhang YL. Kinetic and thermodynamic behaviors of soil urease as affected by urease inhibitors. Revista de la ciencia del suelo y nutrición vegetal. 2010;10(1):1-11. http://dx.doi.org/10.4067/S0718-27912010000100001

10. Xinqiang L, Junli Y, Miaomiao H, Hua L, Liang L, Guangming T. Modeling the fate of fertilizer N in paddy rice systems receiving manure and urea. Geoderma. 2014 Sep 1;228:54-61. https://doi.org/10.1016/j.geoderma.2013.09.002

11. Burns RG., Enzyme activity in soil – Some theoretical and practical considerations, In R.G. Burns(eds.) – Soil Enzymes, Academic Press Inc, New York. 1978

12. O'Toole P, McGarry SJ, Morgan MA. Ammonia volatilization from urea-treated pasture and tillage soils: effects of soil properties. Journal of Soil Science. 1985 Dec;36(4):613-20. https://doi.org/10.1111/j.1365-2389.1985.tb00363.x

13. Wilke BM. Determination of Chemical and Physical Soil Properties. In: Monitoring and Assessing Soil Bioremediation. Soil Biology, vol 5. Springer, Berlin, Heidelberg. 2005. https://doi.org/10.1007/3-540-28904-6_2.

14. Bremner JM. Inorganic forms of nitrogen. Methods of soil analysis: part 2 chemical and microbiological properties. 1965 Jan 1;9:1179-237, Chemical and Microbiological Properties, Black C.A. (Eds.), Madison, Wisconsin, 1179-1237 https://doi.org/10.2134/agronmonogr9.2.c33

15. Fernández JA, Niell FX, Lucena J. A rapid and sensitive automated determination of phosphate in natural waters 1. Limnology and Oceanography. 1985 Jan;30(1):227-30. https://doi.org/10.4319/lo.1985.30.1.0227

16. Jagessar RC, Sooknundun L. Determination of nitrate anion in waste water from nine selected areas of coastal Guyana via a spectrophotometric method. 2011, International Journal of Research and Reviews in Applied Sciences, 7, 203-212.

17. Tabatabai MA, Bremner JM. Assay of urease activity in soils. Soil biology and Biochemistry. 1972 Nov 1;4(4):479-87. https://doi.org/10.1016/0038-0717(72)90064-8

18. Segel IH. Enzyme kinetics: behavior and analysis of rapid equilibrium and steady state enzyme systems. New York: Wiley; 1975 May 26.

19. Trasar-Cepeda C, Gil-Sotres F, Leirós MC. Thermodynamic parameters of enzymes in grassland soils from Galicia, NW Spain. Soil Biology and Biochemistry. 2007 Jan 1;39(1):311-9. https://doi.org/10.1016/j.soilbio.2006.08.002

20. Gianfreda L, Ruggiero P. Enzyme activities in soil. In Nucleic acids and proteins in soil 2006 (pp. 257-311). Berlin, Heidelberg: Springer Berlin Heidelberg.

21. Mohammadi K. Soil microbial activity and biomass as influenced by tillage and fertilization in wheat production. Am. Eurasian J. Agric. Environ. Sci. 2011 Jul 13;10:330-7.

22. Eivazi F, Bayan MR, Schmidt K. Select soil enzyme activities in the historic Sanborn Field as affected by long-term cropping systems. Communications in Soil Science and Plant Analysis. 2003 Aug 1;34(15-16-):2259-75. https://doi.org/10.1081/CSS-120024062

23. Datt N, Dubey YP, Chaudhary R. Studies on impact of organic, inorganic and integrated use of nutrients on symbiotic parameters, yield, quality of Frenchbean (Phaseolus vulgaris L.) vis-à-vis soil properties of an acid Alfisol. African Journal of Agricultural Research. 2013 Jun 13;8(22):2645-54. DOI: 10.5897/AJAR12.942

24. Chang EH, Chung RS, Tsai YH. Effect of different application rates of organic fertilizer on soil enzyme activity and microbial population. Soil Science and Plant Nutrition. 2007 Apr 1;53(2):132-40. https://doi.org/10.1111/j.1747-0765.2007.00122.x

25. Du N, Sheng L, Xu H, Song C, Chen S. Kinetics of competitive inhibition of jack bean urease by boric acid. Journal of Molecular Catalysis B: Enzymatic. 2012 Oct 1;82:53-8. https://doi.org/10.1016/j.molcatb.2012.06.008

26. Krajewska B, Ciurli S. Jack bean (Canavalia ensiformis) urease. Probing acid–base groups of the active site by pH variation. Plant Physiology and Biochemistry. 2005 Jul 1;43(7):651-8. https://doi.org/10.1016/j.plaphy.2005.05.009

27. Ravi Charan Reddy K, Kayastha AM. Boric acid and boronic acids inhibition of pigeonpea urease. Journal of Enzyme Inhibition and Medicinal Chemistry. 2006 Jan 1;21(4):467-70. https://doi.org/10.1080/14756360600638147

28. Krajewska B. A combined temperature-pH study of urease kinetics. Assigning pKa values to ionizable groups of the active site involved in the catalytic reaction. Journal of Molecular Catalysis B: Enzymatic. 2016 Feb 1;124:70-6. https://doi.org/10.1016/j.molcatb.2015.11.021

29. Dharmakeerthi RS, Thenabadu MW. Urease activity in soils: A review. Journal of the National Science Foundation of Sri Lanka. 1996 Sep 30;24(3).

30. Estermann EF, McLaren AD. Contribution of rhizoplane organisms to the total capacity of plants to utilize organic nutrients. Plant and Soil. 1961 Nov;15:243-60. https://doi.org/10.1007/BF01400458

31. Lai CM, Tabatabai MA. Kinetic parameters of immobilized urease, Soil Biology and Biochemistry, 24(3), 225-228., 1992. https://doi.org/10.1016/0038-0717-(92)90222-J

32. Moyo CC, Kissel DE, Cabrera ML. Temperature effects on soil urease activity. Soil Biology and Biochemistry. 1989 Jan 1;21(7):935-8. https://doi.org/10.1016/0038-0717(89)90083-7

33. Kumari JA, Rao PC. Effect of Temperature on Soil Enzyme Urease Activity-Productivity. College of Agriculture, Rajendra Nagar, Hyderabad, Best: International Journal Of Humanities, Arts,Medicine And Sciences (Best: Ijhams) 2017;5(4):65-72

34. Lei T, Gu Q, Guo X, Ma J, Zhang Y, Sun X. Urease activity and urea hydrolysis rate under coupling effects of moisture content, temperature, and nitrogen application rate. International Journal of Agricultural and Biological Engineering. 2018 Mar 31;11(2):132-8. DOI: 10.25165/j.ijabe.20181102.3784

35. Kumar S, Kansal A, Kayastha AM. Immobilization of jack bean (Canavalia ensiformis) urease on gelatin and its characterization. Oriental pharmacy and ex-

perimental medicine. 2005;5(1):43-7. DOI:10.3742/OPEM.2005.5.1.043

36. Zantua MI, Dumenil LC, Bremner JM. Relationships between soil urease activity and other soil properties. Soil Science Society of America Journal. 1977 Mar;41(2):350-2. https://doi.org/10.2136/sssaj1977.03615995004100020036x

37. Pal S, Chhonkar PK. Thermal sensitivity and kinetic properties of soil urease. Journal of the Indian Society of Soil Science. 1979;27(1):43-7.

38. Sardans J, Peñuelas J, Estiarte M. Changes in soil enzymes related to C and N cycle and in soil C and N content under prolonged warming and drought in a Mediterranean shrubland. Applied Soil Ecology. 2008 Jun 1;39(2):223-35. https://doi.org/10.1016/j.apsoil.2007.12.011

39. Juan YH, Chen LJ, Wu ZJ, Wang R. Kinetics of soil urease affected by urease inhibitors at contrasting moisture regimes. Revista de la ciencia del suelo y nutrición vegetal. 2009;9(2):125-33. http://dx.doi.org/10.4067/S0718-27912009000200004

40. Fidaleo M, Lavecchia R. Kinetic study of enzymatic urea hydrolysis in the pH range 4-9. Chemical and biochemical engineering quarterly. 2003 Dec 1;17(4):311-8.

41. Al-Ansari AS, Abdulkareem MA, Kadhum SJ. Activity and thermodynamic parameters of urease in soils amended with organic residues. Iraqi Journal of Agricultural Sciences. 2019 May 1;50(3) https://doi.org/10.36103/ijas.v50i3.695

42. Kandeler E, Gerber H. Short-term assay of soil urease activity using colorimetric determination of ammonium. Biology and fertility of Soils. 1988 Mar;6:68-72. https://doi.org/10.1007/BF00257924

43. Krajewska B. Ureases. II. Properties and their customizing by enzyme immobilizations: a review. Journal of Molecular Catalysis B: Enzymatic. 2009b Jul 1;59(1-3):22-40. https://doi.org/10.1016/j.molcatb.2009.01.004

Original article

Shifts in the nitrogen cycle under different fertilizer management practices

FLORINA BOTEZ[1,*], CARMEN POSTOLACHE[1], HORIA DOMNARIU[1,2], ALEXANDRA LEONTE[3], ANDREEA-GABRIELA DULĂ[4]

[1] Department of Systems Ecology and Sustainability, Faculty of Biology, University of Bucharest, Splaiul Independenței no. 91-95, District 5, Bucharest, Romania, Postal code: 050095

[2] Soil Biology Laboratory, National Research and Development Institute for Soil Science, Agrochemistry and Environment – ICPA, Bd. Mărăști, no. 61, Bucharest, Romania, Postal code: 011464

[3] Agricultural Research and Development Station Secuieni Neamț, Str. Principală, no. 377, Com. Secuieni, Neamț County, Romania, Postal code 617415

[4] Faculty of Biology, University of Bucharest, Splaiul Independenței no. 91-95, District 5, Bucharest, Romania, Postal code: 050095

Abstract

Human population is dependent on agricultural production, but these activities pose multiple threats to soil health and indirectly to ecological sustainability. Synthesis of fertilizers proved to be a miraculous solution to enhance soil productivity, but this advancement came with many unseen risks. Long-term research stations that have decades long experiments with fertilizers additions are paramount in better understanding long-term impact of fertilizer use. Our study focused on ammonium and nitrate levels found in soils in an experiment of inorganic nitrogen addition than began in 1975. We further directed our attention to soil mineralization potential, nitrate reductase activities and densities of two major microbial functional groups: ammonifiers and denitrifiers. Our data suggests that ammonium has a stronger tendency of soil buildup than nitrate and that increased levels of inorganic nitrogen species also impacted molecular compartments and processes such as mineralization potential, soil microbiota and enzymatic activities. Another result indicates that analysed soils reached a storage limit for phosphorus which threatens to overburden other ecosystems.

✉   *Corresponding author: Florina Botez, Splaiul Independenței no. 91-95, District 5, Bucharest, Romania, email: florina.botez@bio.unibuc.ro; phone: +40761501060. carmen.postolache@bio.unibuc.ro; horia.domnariu@gmail.com; andra29nt@yahoo.com; andreea.dula@yahoo.com

Introduction

The extensive use of fertilizers in agriculture, while essential for enhancing crop yields and ensuring food security, poses significant ecological challenges. One of the primary concerns is nutrient runoff, where excess fertilizers, particularly nitrogen and phosphorus, are washed from agricultural fields into nearby water bodies. This runoff leads to eutrophication, a process that results in the over-enrichment of water bodies with nutrients, causing algal blooms and hypoxic conditions, often referred to as "dead zones," where aquatic life cannot survive [1]. Notable examples include the Gulf of Mexico and Lake Erie, where agricultural runoff has severely impacted aquatic ecosystems [2].

The over-application of fertilizers also contributes to soil degradation. Excessive use of chemical fertilizers can alter soil pH, reduce soil organic matter, and disrupt soil microbial communities [3; 4]. These changes can lead to soil acidification and a decline in soil health, making soils less productive over time and more susceptible to erosion [5]. Soil erosion not only reduces agricultural productivity but also contributes to sedimentation in water bodies, further exacerbating water quality issues.

Fertilizer use is also a significant source of greenhouse gas emissions [6; 7]. Nitrous oxide, a potent greenhouse gas, is released from soils following the application of nitrogen-based fertilizers. This gas has a global warming potential approximately 300 times that of carbon dioxide, making it a critical contributor to climate change [8]. The production and transportation of synthetic fertilizers also involve substantial energy use, primarily from fossil fuels, adding to their carbon footprint [9].

Moreover, the reliance on synthetic fertilizers can lead to a dependency that undermines sustainable agricultural practices. Over time, soils can become less fertile naturally, requiring even more fertilizer inputs to maintain crop yields. This cycle can trap farmers in a pattern of increasing fertilizer use, escalating costs, and diminishing returns, which is particularly challenging for smallholder farmers in developing countries [10].

Human health is also at risk due to fertilizer use. Nitrate contamination of drinking water, resulting from fertilizer runoff, poses significant health risks, including methemoglobinemia or "blue baby syndrome" in infants, and potential links to various cancers. Additionally, the volatilization of ammonia from fertilizers can contribute to the formation of fine particulate matter in the atmosphere, which is associated with respiratory and cardiovascular diseases [11].

Addressing these ecological issues requires a multifaceted approach. Implementing best management practices, such as precision agriculture, can help optimize fertilizer use and reduce runoff. Precision agriculture involves using technology to apply fertilizers more efficiently, based on the specific needs of crops and soil conditions [12]. Additionally, promoting the use of organic fertilizers and soil amendments, such as compost and biochar, can enhance soil health and reduce dependency on synthetic fertilizers [13].

Policy measures are also crucial. Governments can incentivize sustainable farming practices through subsidies and support for research and development in sustainable agriculture technologies. International cooperation is needed to address the transboundary nature of nutrient pollution and to develop global strategies for sustainable fertilizer use [14; 15].

The need for ongoing research is paramount. Current research trends focus on developing enhanced efficiency fertilizers that release nutrients more slowly and in response to plant needs, thereby reducing losses to the environment. Studies are also exploring the potential of nanofertilizers, which use nanoparticles to improve nutrient delivery and uptake by plants [16]. Additionally, research into bioformulations, which combine fertilizers with beneficial microbes, aims to enhance soil health and nutrient availability [17].

Furthermore, establishing long-term fertilization research centres is essential. These centres can provide continuous monitoring and evaluation of fertilizer impacts on soil health, crop productivity, and environmental quality. They can also serve as hubs for developing and testing innovative fertilization strategies and technologies, ensuring that agricultural practices evolve in a sustainable and environmentally friendly manner.

While fertilizers play a vital role in modern agriculture, their ecological impacts are profound and multifaceted. Sustainable management of fertilizer use is essential to mitigate these impacts and ensure the long-term health of both agricultural systems and the broader environment.

The objective of this study was to evaluate the effects of varying nitrogen addition levels on soil ammonium and nitrate pools, as well as on several critical components of nitrogen cycling in soils, including mineralization potential, enzymatic assays of nitrate reductase, and functional microbial groups densities of ammonifiers and denitrifiers.

Materials and methods

Soil samples were taken from topsoil horizon (maximum depth of 20 cm) of agricultural plots managed by the Agricultural Research and Development Station Secuieni (ARDS Secuieni), Neamț County, Romania. This research station has a 49-year experiment with fertilizer additions and crop rotations management (parallel cultures of wheat, corn

and bean). Research area soil type is Chernozem soil with a loamy texture. The treatment scheme involves the application of various nitrogen and phosphorus fertilizer inputs, as shown in Table 1, within plots with areas of approximately 30 m². Nitrogen additions (inorganic forms as ammonium nitrate) were carried out in spring, while phosphorus was added in autumn. The research of the Secuieni station began in the '70s and is a particularly important reference point in the analysis of the long-term impact of fertilizer application within agricultural systems. Sampling was done in October 2020; each sample was composited from 6 subsamples (three within and three between crop rows) and analysed in triplicate.

Table 1 Fertilizer addition scheme managed by ARDS Secuieni

Sample code	N input (kg/ha/year)	P input (kg/ha/year)
V1	0	0
V3	80	0
V5	160	0
V11	0	80
V13	80	80
V15	160	80
V21	0	160
V23	80	160
V25	160	160

Monitored parameters were determined using freshly collected samples to better understand soil nitrogen biogeochemistry. Moisture content was analysed gravimetrically [18] and pH was determined in the lab using a suspension with distilled water with a 1:4 ratio [19]. Soil organic matter content was also done gravimetrically by placing dried samples in crucibles in an oven set with a combustion temperature of 550°C [20]. Available inorganic nitrogen species (ammonium nitrogen and nitrate nitrogen) were extracted using KCl 0.2 M [21] and after filtration the solutions were used in spectrophotometric methods to assess the nitrogen contents, and results were calculated as micrograms/gram dry weight (μg/g.dw). Orthophosphate levels were also analysed colorimetrically using a soil extract with sodium bicarbonate.

Soil potential mineralization rates were assessed using a two-week incubation in anaerobic conditions at 37°C and extraction with KCl 2M was performed at the end [22]. After filtration, the ammonium nitrogen was spectrophotometrically determined. The initial values for this nitrogen species were subtracted and the mineralization potential was expressed as μg N-NH_4^+/g.dw/day).

We assessed the density of two major functional groups: ammonifiers – responsible with decomposition stage of organic matter and denitrifiers which are involved in soil nitrogen regulation since they ultimately release molecular nitrogen

gen (N_2) back into atmosphere [23]. To estimate the density of selected microbial groups, fresh soil samples were first suspended in sterile physiological saline, inoculated in wells containing specific growth medium (peptone water for ammonifiers and Pochon medium for denitrifiers) and incubated for 24 hours [24]. The inoculation used a three replicates scheme per serial dilution – which used a factor of 10. For denitrifiers the starting dilution was 10^{-1}, while for ammonifiers it was 10^{-2} since they are more abundant in the studied soils. After incubation specific reagents were added (Nessler for ammonifiers and Griess I and II for nitrite detection) and the results were numerically converted using McCrady's table [25] and further reported as individuals/g.dw.

Soil enzymatic assays (nitrate reductase) were performed as presented in Abdelmagid and Tabatabai [26]. Samples were added specific substrate (KNO_3). The method required the use of reference samples (samples stored at -20°C) while assay samples were incubated at 25°C and analysed after 24 hours, using nitrite as byproduct of nitrate reductase activity. For this parameter, the low value range required the nanograms scale, with results being reported as ng N-NO_2^-/g.dw/h.

Results and discussions

Soil water content showed a narrow variation interval, with values ranging from 16.26%-17.00% which can be attributed to similar soil structure and texture and therefore a homogenous water capacity retention of the study area. Water content is normal for October (a cooler season in which frequent precipitation can occur in a temperate climate). A similar homogeneity was found for pH values, which ranged between 5.22-5.57, this distribution implying that soils are moderately to strongly acidic since neutral category is between 6.5-7.5 [27].

Soil organic matter, represented by intermediate products of decomposition processes of biological material, depends mainly on the available substrate for this cycling stage. As far as agricultural systems are concerned, the values are lower compared to a natural system dominated by vegetation, as a significant amount of plant material is removed through crop harvesting. Relatively low and extremely similar values are noted for all selected study areas, with values generally of about 5.5%.

A significant variation observed in the analysed parameters was primarily attributed to nitrogen reserves, particularly ammonium nitrogen (Figure 1). This nitrogen species is less soluble compared to nitrate and therefore less susceptible to percolation and it has a buildup tendency in soils [28]. As expected, the accumulation level is strongly correlated with nitrogen input as fertilizer (R^2 value for the correlation between ammonium nitrogen levels and yearly nitrogen input
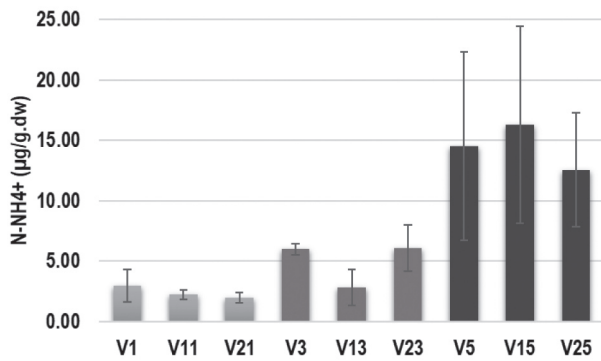
Fig. 1. Soil ammonium nitrogen distribution from Secuieni agricultural complex (October 2020)
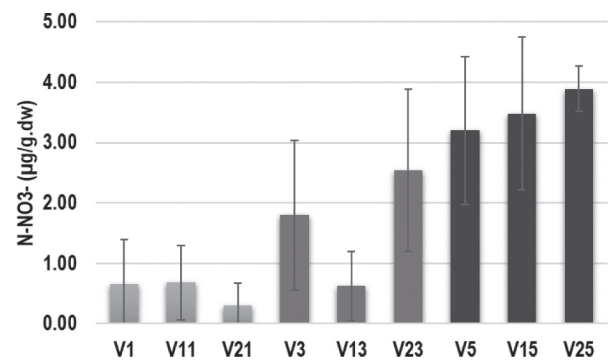

Fig. 2. Soil nitrate nitrogen distribution from Secuieni agricultural complex (October 2020)

of 0 kg, 80 kg and 160 kg is 0.67 – exponential function). For natural systems, ammonium nitrogen is dependent on organic matter content [29], whereas in our study the correlation between ammonium nitrogen and soil organic matter showed a steep decline from 41% in the reference plots to 29% in the intermediate nitrogen addition level (80 kg N/year) to 0.02% in the highest fertiliser input, which further illustrates that ammonium levels are increasingly dependent on nitrogen additions rather than natural cycling drivers.

Similar accumulation trends were observed for phosphorus additions but in this case, no significant difference was reported between the input level, orthophosphate levels reaching a similar plateau for both 80 kg and 160 kg of P per year. This plateau could signal a storage capacity issue, which could pose a risk by transferring excess phosphorus to other ecosystems. This is of special interest since there was little time between fertilization and sampling since phosphorus addition was completed in autumn.

Nitrate levels are significantly lower than the reduced nitrogen species, a situation that can be explained by higher water solubility and losses through percolation, which is one of the key issues in fertilizer management and cultural eutrophication risk [30; 31; 32]. Another contributing factor to lower nitrogen levels in this form is plant assimilation preference for this nitrogen species. This partiality is due *to higher soil mobility* that provides easier root access for plants [33], *energy efficiency* – even if nitrate requires more energy in the absorption stage, it is ultimately easier to metabolize afterwards [34] *synergistic uptake* – nitrate assimilation promotes the concurrent absorption of other necessary elements such as potassium, calcium and magnesium [34] and the *non-volatile* nature of this nitrogen species which makes nitrate a more reliable source of nitrogen compared to ammonium [35]. Accumulation levels across fertilized plots show a strong linear correlation with nitrogen addition (R^2 value is 0.58).

Microbial groups play a crucial role in soil functions and nitrogen cycling, contributing to the overall ecosystems'

health and fertility. A key aspect regarding soil microbiota is the capacity to metabolize organic matter, which can be analysed by estimating soil mineralization potential. Since this function is primarily dependent on substrate (available organic matter), there is little data variation for average values due to similar and low values of soil organic matter (Figure 3). However, point by point analysis suggests that for the highest nitrogen addition there is greater data variability, which could infer that decomposing microbial group is responding to excess nitrogen. More stable values are for the control plots as well as for the intermediate addition level of 80 kg N/year, which seems to be a more tolerated addition level. Nevertheless, mineralization rates are slightly lower (by 5.88%) in fertilized plots compared to reference areas.

A more in-depth analysis of soil microbial compartments was performed by using the results of microbial functional group densities. Ammonifier's densities are below 500 individuals/g dry weight except for plots V11 and V25 (Figure 4). Interestingly, there seem to be more ammonifiers in the fertilized plots which could be due to microbial stimulation induced by added nutrients, signalling a reduced competition. Some studies showed that inorganic fertilizers can sometimes diminish the presence of other microorganisms that compete with this functional group for resources, allowing ammonifiers to proliferate [36; 37; 38].
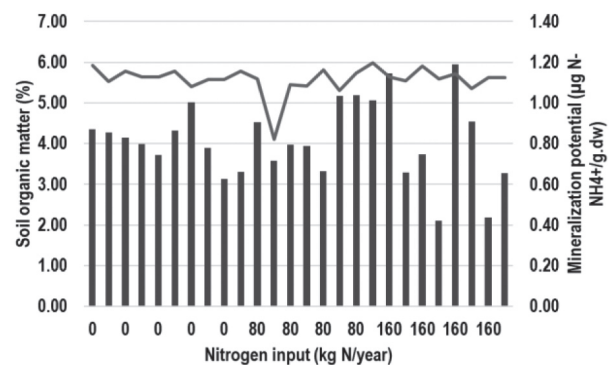

Fig. 3. Distribution of soil organic matter (%) and mineralization potential rates (μg N-NH4+/g.dw/day) from Secuieni agricultural complex (October 2020)

Fig. 4. Soil ammonifiers (ind./g.dw) distribution from Secuieni agricultural complex (October 2020)
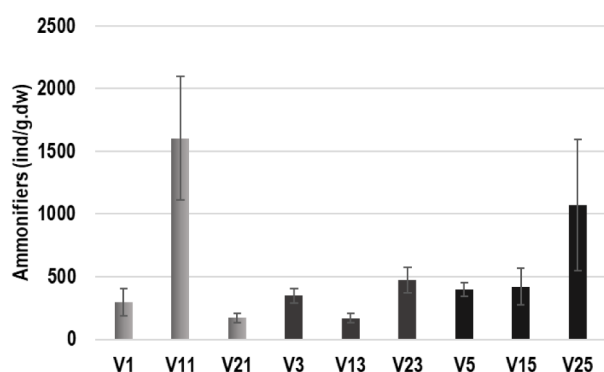

Fig. 6. Soil denitrifiers (ind./g.dw) distribution from Secuieni agricultural complex (October 2020)

Our data shows strong correlations between ammonifying communities and soil ammonium nitrogen for both fertilized plots, whereas there is no correlation for the reference samples between these parameters (Figure 5). Another supporting fact was the correlation between ammonifiers densities and mineralization potential. In this case the trend was descending both for reference samples and highest addition levels, but a very good positive correlation was observed for the samples fertilized with 80 kg N/ha/year, which further suggests that this level of addition is more suitable for soil microbiota health.

Denitrifiers are less abundant than ammonifiers, with ranges five times lower (Figure 6). Only one sampling point (V3) presented an increase in this functional group, but
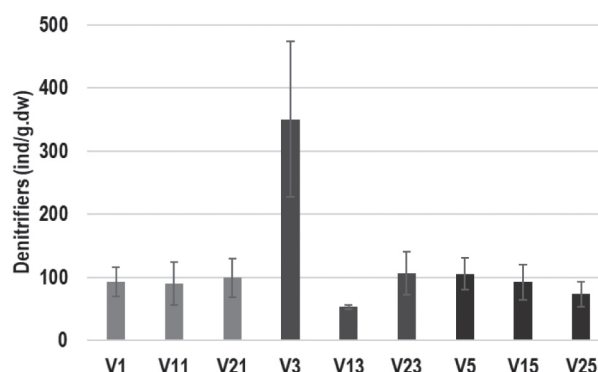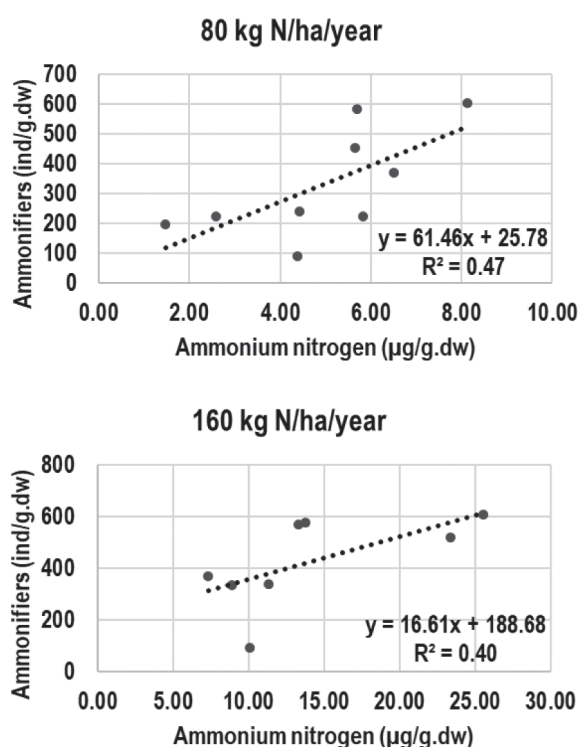

Fig. 5. Correlations for ammonifiers and soil ammonium nitrogen for fertilized plots (top 80 kg N/ha/year; bottom 160 kg N/ha/year from Secuieni agricultural complex (October 2020)

the data regarding nitrate reductase activity does not reflect higher values for this sample. Recent studies proved that inorganic fertilizers could disrupt soil denitrifiers community by reducing both abundance and diversity [39]. A first observation can be made for the fertilized plots that previously shown an accumulation of nitrate, here the densities are generally lower than the reference areas since the primary substrate (nitrate) is more abundant which might indicate a substrate inhibition. Since nitrate is a good substrate for denitrifiers, we also obtained very good correlations between these two parameters. The equations describing this interdependence are logarithmic in nature, suggesting that there is a limiting range of denitrifiers' densities while nitrate levels increase. The degrees of correlation (R^2 values) were: 0.34 for control samples, 0.41 for plots fertilized with 80 kg N/ha/year and 0.32 for those fertilized with 160 kg N/ha/year).

Nitrate reductase activities across samples show a greater value stability for reference samples (Figure 7) and also slight reduction for fertilized plots: control samples have an average value of 29 ng $N-NO_2^-$/g.dw/h, whereas samples from soils fertilized with 80 kg N/ha/year have an average of 25.2 ng $N-NO_2^-$/g.dw/h and those with highest N addition have a mean value of 21.1 ng $N-NO_2^-$/g.dw/h. Though several studies have established that soil enzymatic activity intensifies as a result of fertilization [40], our data suggest a slight decline for this parameter, most likely due to soil pH. It is well established that optimal pH for nitrate reductase activity is between 7.0-8.0 [41]. For instance, one study found that nitrate reduction rates were higher at pH 7.1 compared to pH 5.5, indicating that more neutral or alkaline conditions favour nitrate reductase activity [42]. Another explanation for smaller values of nitrate reductase activity in fertilized plots is the presence of high levels of ammonium, which inhibits nitrate assimilation [43; 44].

Increased nitrate reductase activity can shift the nitrogen cycle towards nitrate reduction rather than denitrification. This shift can reduce the substrate availability for denitrifiers, thereby decreasing their activity and abundance [45].
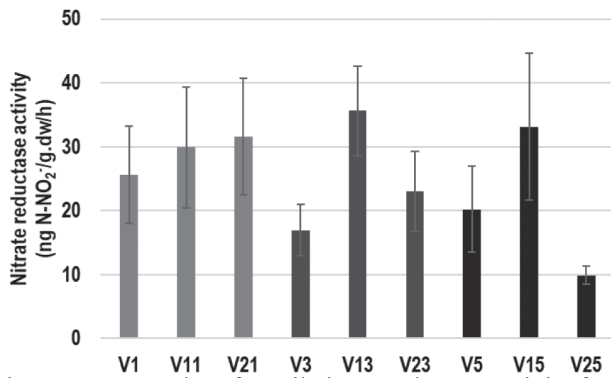
Fig. 7. Average values for soil nitrate reductase activity from Secuieni agricultural complex (October 2020)

Correlations for each replicate samples show a good correspondence between denitrifiers' densities and soil nitrate reductase activity (Figure 8). However, due to lower values from the samples with the highest nitrogen addition, the trend is opposite. These distributions might again suggest that soil microbiota is most disrupted at highest added fertilizer and is more tolerant to the lower nitrogen input.

Conclusions

Inorganic fertilizers, as those used in our research area seem to have a trend of accumulation in soils which is also correlated with input levels. This is especially the case for ammonium with average values for the plots with 80 kg N/ha/year being 4.97 µg $N-NH_4^+$/g.dw and 14.47 µg $N-NH_4^+$/g.dw for the 160 kg N/ha/year addition. Nitrate is more soluble and preferred in biological uptake, so for this nitrogen species soil accumulation levels were lower, averaging 1.66 and 3.52 µg $N-NO_3^-$/g.dw respectively. For control plots there was a good correlation between ammonium and soil organic matter, but the linkage decreased considerably for fertilized soils since the main source in this case was due to fertilizer management and not to natural processes of decomposition.

Nitrogen fertilization induced several changes both to microbial functional groups and to soil processes. Our data shows that soil mineralization potential presented higher data variability, especially for soils under highest nitrogen addition. Ammonifiers' densities seem to be stimulated by added nitrogen, most likely due to suppression of other microbial communities induced by excess nitrogen. Conversely, denitrifying bacteria populations seem to undergo the opposite, a possible explanation being substrate inhibition.

Another parameter that showed variations due to fertilizer addition was soil nitrate reductase activity. Similar to mineralization potential, there is higher data variability, signalling a response to added nitrogen. Average values for nitrate reductase are lower for fertilized soils, the trend being correlated with addition level.
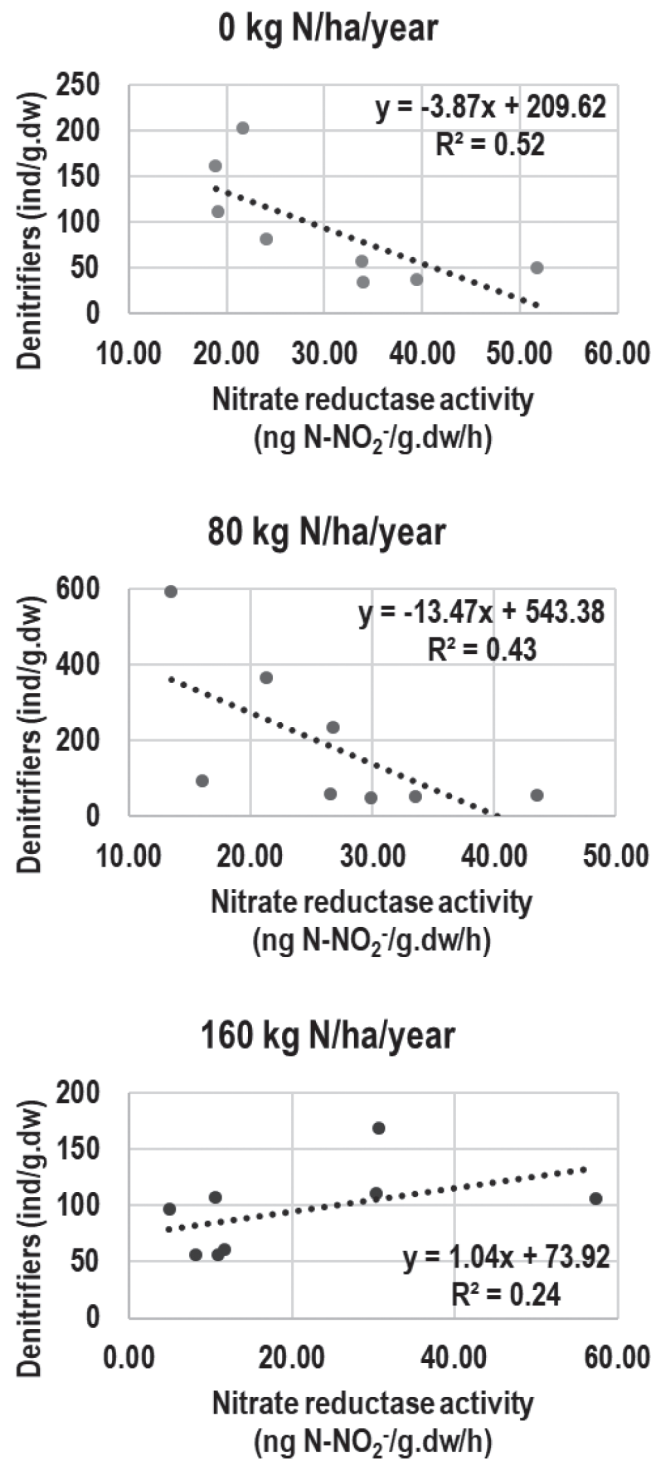

Fig. 8. Correlations for denitrifiers and soil nitrate reductase activities (top 0 kg N/ha/year; middle 80 kg N/ha/year; bottom 160 kg N/ha/year from Secuieni agricultural complex (October 2020)

Our data also suggests that investigated parameters and functions seem to be more resilient to lower levels of N addition (of 80 kg N/ha/year) as compared to values pertaining to nitrogen input of 160 kg N/ha/year.

A very interesting aspect was observed for soil phosphorus levels. Even if the highest addition was double and quite recent to sampling campaign, we found similar soil concen-

trations for fertilized plots, which suggests that a limit was reached regarding soil storage capacity, and this can pose a significant threat by exporting excess phosphorus to other ecosystems.

Long term research studies are crucial in assessing soil health, quality and productivity of agricultural lands. There are still inefficiencies regarding the balance between fertilizer addition amounts and types (inorganic versus organic) and long-term ecological sustainability. More studies are needed to better understand soils' molecular compartments, their responses, and their variable reactions to fertilizer management practices.

Funding

Acknowledgements

Conflicts of interest

The authors declare no conflict of interest.

References

1. Kurdi S, Mahmoud M, Abay KA, Breisinger C. Too much of a good thing? Evidence that fertilizer subsidies lead to overapplication in Egypt. Intl Food Policy Res Inst; 2020 Mar 12.

2. Scavia D, Allan JD, Arend KK, Bartell S, Beletsky D, Bosch NS, Brandt SB, Briland RD, Daloğlu I, DePinto JV, Dolan DM. Assessing and addressing the re-eutrophication of Lake Erie: Central basin hypoxia. Journal of Great Lakes Research. 2014 Jun 1;40(2):226-46. https://doi.org/10.1016/j.jglr.2014.02.004

3. Krasilnikov P, Taboada MA, Amanullah. Fertilizer use, soil health and agricultural sustainability. Agriculture. 2022 Mar 25;12(4):462. https://doi.org/10.3390/agriculture12040462

4. Tyagi J, Ahmad S, Malik M. Nitrogenous fertilizers: Impact on environment sustainability, mitigation strategies, and challenges. International Journal of Environmental Science and Technology. 2022 Nov;19(11):11649-72. https://doi.org/10.1007/s13762-022-04027-9

5. Tian D, Niu S. A global analysis of soil acidification caused by nitrogen addition. Environmental Research Letters. 2015 Feb 20;10(2):024019. DOI 10.1088/1748-9326/10/2/024019

6. Vergé XP, De Kimpe C, Desjardins RL. Agricultural production, greenhouse gas emissions and mitigation potential. Agricultural and forest meteorology. 2007 Feb 12;142(2-4):255-69. https://doi.org/10.1016/j.agrformet.2006.06.011

7. Snyder CS, Bruulsema TW, Jensen TL, Fixen PE. Review of greenhouse gas emissions from crop production systems and fertilizer management effects. Agriculture, Ecosystems & Environment. 2009 Oct 1;133(3-4):247-66. https://doi.org/10.1016/j.agee.2009.04.021

8. Del Grosso SJ, Wirth T, Ogle SM, Parton WJ. Estimating agricultural nitrous oxide emissions. EOS, Transactions American Geophysical Union. 2008 Dec 16;89(51):529-529. https://doi.org/10.1029/2008EO510001

9. Jaiswal B, Agrawal M. Carbon footprints of agriculture sector. In: Carbon Footprints: Case Studies from the Building, Household, and Agricultural Sectors. 2020:81-99. https://doi.org/10.1007/978-981-13-7916-1_4

10. Kanter DR, Chodos O, Nordland O, Rutigliano M, Winiwarter W. Gaps and opportunities in nitrogen pollution policies around the world. Nature Sustainability. 2020 Nov;3(11):956-63. https://doi.org/10.1038/s41893-020-0577-7

11. Kumar V, Kumar R, Singh J, Kumar P. Contaminants in agriculture and environment: health risks and remediation. Agro Environ Media, Publication Cell of AESA, Agriculture and Environmental Science Academy,; 2019 Jun 25.

12. Shafi U, Mumtaz R, García-Nieto J, Hassan SA, Zaidi SA, Iqbal N. Precision agriculture techniques and practices: From considerations to applications. Sensors. 2019 Sep 2;19(17):3796. https://doi.org/10.3390/s19173796

13. Guo XX, Liu HT, Zhang J. The role of biochar in organic waste composting and soil improvement: A review. Waste Management. 2020 Feb 1;102:884-99. https://doi.org/10.1016/j.wasman.2019.12.003

14. Ribaudo M, Delgado J, Hansen L, Livingston M, Mosheim R, Williamson J. Nitrogen in agricultural systems: Implications for conservation policy. USDA-ERS Economic Research Report. 2011 Sep 1(127). http://dx.doi.org/10.2139/ssrn.2115532

15. Kanter DR, Zhang X, Mauzerall DL. Reducing nitrogen pollution while decreasing farmers' costs and increasing fertilizer industry profits. Journal of environmental quality. 2015 Mar;44(2):325-35. https://doi.org/10.2134/jeq2014.04.0173

16. Monreal CM, DeRosa M, Mallubhotla SC, Bindraban PS, Dimkpa C. Nanotechnologies for increasing the crop use efficiency of fertilizer-micronutrients. Biology and fertility of soils. 2016 Apr;52:423-37. https://doi.org/10.1007/s00374-015-1073-5

17. Khan A, Singh AV, Gautam SS, Agarwal A, Punetha A, Upadhayay VK, Kukreti B, Bundela V, Jugran AK, Goel R. Microbial bioformulation: a microbial assisted biostimulating fertilization technique for sustainable agriculture. Frontiers in Plant Science. 2023 Dec 12;14:1270039. https://doi.org/10.3389/fpls.2023.1270039

18. Rasheed MW, Tang J, Sarwar A, Shah S, Saddique N, Khan MU, Imran Khan M, Nawaz S, Shamshiri RR, Aziz M, Sultan M. Soil moisture measuring techniques and factors affecting the moisture dynamics: A comprehensive review. Sustainability, 2002, 14(18), p.11538. https://doi.org/10.3390/su141811538

19. Oman SF, Camões MF, Powell KJ, Rajagopalan R, Spitzer P. Guidelines for potentiometric measurements in suspensions Part B. Guidelines for practical pH measurements in soil suspensions (IUPAC Recommendations 2006). Pure and applied chemistry. 2007, Jan 1;79(1):81-6. https://doi.org/10.1351/pac200779010081

20. Kogut BM, Milanovsky EY, Hamatnurov SA. Methods for determining the organic carbon content in soils (critical review). Бюллетень Почвенного института им. ВВ Докучаева. 2023, (114):5-28. https://doi.org/10.19047/0136-1694-2023-114-5-28

21. Allende-Montalbán R, San-Juan-Heras R, Martín-Lammerding D, del Mar Delgado M, del Mar Albarrán M, Gabriel JL. The soil sample conservation method and its potential impact on ammonium, nitrate and total mineral nitrogen measurements. Geoderma. 2024 Aug 1; 448:116963. https://doi.org/10.1016/j.geoderma.2024.116963

22. Ros GH, Temminghoff EJ, Hoffland E. Nitrogen mineralization: a review and meta-analysis of the predictive value of soil tests. European Journal of Soil Science. 2011, Feb;62(1):162-73. https://doi.org/10.1111/j.1365-2389.2010.01318.x

23. Ren B, Ma X, Li D, Bai L, Li J, Yu J, Meng M, Li H. Nitrogen-cycling microbial communities respond differently to nitrogen addition under two contrasting grassland soil types. Frontiers in Microbiology. Sec. Terrestrial Microbiology 2024 May 30;15:1290248. https://doi.org/10.3389/fmicb.2024.1290248

24. Chauhan A, Jindal T. Microbiological Methods for Water, Soil and Air Analysis in Microbiological Methods for Environment, Food and Pharmaceutical Analysis, Springer Cham 2020, 93-196. https://doi.org/10.1007/978-3-030-52024-3_7

25. Basak S, Shetty PH. Conventional microbial counting and identification techniques. Techniques to Measure Food Safety and Quality: Microbial, Chemical, and Sensory, Springer Cham 2021. 69-89. https://doi.org/10.1007/978-3-030-68636-9_4

26. Abdelmagid HM, Tabatabai MA. Nitrate reductase activity of soils. Soil Biol. Biochem. 1987 19:421–427. doi:10.1016/0038-0717(87)90033-2

27. Oshunsanya OS. Introductory Chapter: Relevance of Soil pH to Agriculture in Soil pH for Nutrient Availability and Crop Performance. IntechOpen; 2019.: http://dx.doi.org/10.5772/intechopen.82551

28. Nieder R., Benbi D.K., Scherer, H.W. Fixation and defixation of ammonium in soils: a review. Biol Fertil Soils. 2011, 47,1–14. https://doi.org/10.1007/s00374-010-0506-4

29. Villarino SH, Talab E, Contisciani L, Videla C, Di Geronimo P, Mastrángelo ME, Georgiou K, Jackson RB, Piñeiro G. A large nitrogen supply from the stable mineral-associated soil organic matter fraction. Biology and Fertility of Soils. 2023 Oct;59(7):833-41. https://doi.org/10.1007/s00374-023-01755-z

30. Bibi S, Saifullah, Naeem A, Dahlawi S. Environmental impacts of nitrogen use in agriculture, nitrate leaching and mitigation strategies. In: Hakeem K, Akhtar J, Sabir M. (eds) Soil Science: Agricultural and Environmental Prospectives Soil science: Agricultural and environmental prospectives, Springer Cham, 2016:131-57. https://doi.org/10.1007/978-3-319-34451-5_6

31. Wang ZH, Li SX. Nitrate N loss by leaching and surface runoff in agricultural land: A global issue (a review). Advances in agronomy. 2019 Jan 1;156:159-217. https://doi.org/10.1016/bs.agron.2019.01.007

32. Fagodiya RK, Kumar A, Kumari S, Medhi K, Shabnam AA. Role of nitrogen and its agricultural management in changing environment. In: Naeem, M., Ansari, A., Gill, S. (eds) Contaminants in Agriculture. Springer, Cham. 2020:247-70. https://doi.org/10.1007/978-3-030-41552-5_12

33. Daryanto S, Wang L, Gilhooly III WP, Jacinthe PA. Nitrogen preference across generations under changing ammonium nitrate ratios. Journal of plant ecology. 2019 Apr;12(2):235-44. https://doi.org/10.1093/jpe/rty014

34. Hachiya T, Sakakibara H. Interactions between nitrate and ammonium in their uptake, allocation, assimilation, and signalling in plants. Journal of Experimental Botany. 2017 May 1; 68(10):2501-12. https://doi.org/10.1093/jxb/erw449

35. Marino Bilbao D, Morán Juez JF. Can Ammonium Stress Be Positive for Plant Performance? Front. Plant Sci., Sec. Plant Physiology Volume 10 - 2019 https://doi.org/10.3389/fpls.2019.01103

36. Fan F, Yang Q, Li Z, Wei D, Cui XA, Liang Y. Impacts of organic and inorganic fertilizers on nitrification in a cold climate soil are linked to the bacterial ammonia oxi-

dizer community. Microbial ecology. 2011 Nov;62:982-90. https://doi.org/10.1007/s00248-011-9897-5

37. Adane A. A Review Study on the Effect Of Selected Organic And Inorganic Fertilizers on Soil Fertility and Crop Productivity. Int. J. Agric. Res. Rev 2023. 11(11) Pp 105-120 DOI: 10.54978/ijarr.2023.

38. Shi TS, Collins SL, Yu K, Peñuelas J, Sardans J, Li H, Ye JS. A global meta-analysis on the effects of organic and inorganic fertilization on grasslands and croplands. Nature Communications. 2024 Apr 22;15(1):3411. https://doi.org/10.1038/s41467-024-47829-w

39. Li Y, Wang M, Li Q, Zhang L, Qin Y, Sun B, Liu H. Changes of Soil Nitrogen Fractions and nirS-Type Denitrifier Microbial Community in Response to N Fertilizer in the Semi-Arid Area of Northeast China. Agronomy. 2023 Aug 24; 13(9): 2212. https://doi.org/10.3390/agronomy13092212

40. Chen T, Cheng R, Xiao W, Shen Y, Wang L, Sun P, Zhang M, Li J. Nitrogen addition enhances soil nitrogen mineralization through an increase in mineralizable organic nitrogen and the abundance of functional genes. Journal of Soil Science and Plant Nutrition. 2024 Mar; 24(1):975-87. https://doi.org/10.1007/s42729-023-01600-0

41. Giles M, Morley N, Baggs EM, Daniell TJ. Soil nitrate reducing processes–drivers, mechanisms for spatial variation, and significance for nitrous oxide production. Frontiers in microbiology. 2012 Dec 18;3:407. https://doi.org/10.3389/fmicb.2012.00407

42. Wang Y, Cao W, Guo J, Zhang M. Effects of Increasing pH on Nitrous Oxide and Dinitrogen Emissions from Denitrification in Sterilized and Unsterilized Forest Soils. Forests. 2022; 13(10):1589. https://doi.org/10.3390/f13101589

43. Rice CW, Tiedje JM. Regulation of nitrate assimilation by ammonium in soils and in isolated soil microorganisms. Soil Biology and Biochemistry. 1989 Jan 1;21(4):597-602. https://doi.org/10.1016/0038-0717(89)90135-1

44. McCarty GW, Bremner JM. Regulation of assimilatory nitrate reductase activity in soil by microbial assimilation of ammonium. Proceedings of the National Academy of Sciences. 1992 Jan 15;89(2):453-6. https://www.jstor.org/stable/2358558

45. Wang Y, Ji H, Wang R, Guo S. Responses of nitrification and denitrification to nitrogen and phosphorus fertilization: does the intrinsic soil fertility matter? Plant and Soil. 2019 Jul 14;440:443-56. https://doi.org/10.1007/s11104-019-04108-8

Original article

Cell adhesion genes expression level in oropharyngeal squamous cell carcinoma and laryngeal squamous cell carcinoma: a preliminary study

MARIAN CONSTANTIN[1,2,*]

[1] Institute of Biology of Romanian Academy, 296 Splaiul Independentei, 060031 Bucharest, Romania

[2] The Research Institute of the University of Bucharest, ICUB, Bucharest, Romania

Abstract

Head and neck cancers (HNCs) are tumors developed in the upper aerodigestive tracts, more than 90% originating in the squamous cells lining the mucosa of the upper airways. There are between 650,000 and 900,000 new cases each year, most of them advanced, resulting in high mortality (five-year survival about 50%). HNCs do not metastasize to distant sites, but often affect local lymph nodes. Their etiology is multifactorial, with smoking, alcohol consumption and HPV infection being the most common. HNCs rapidly enter hypoxia and synthesize angiogenic factors, which contribute to further tumor development and recurrence. Although there is a relatively wide variety of therapeutic strategies, their effectiveness is reduced because of resistance development. Cell adhesion mediated by integrins and the extracellular matrix is an important mechanism of tumor progression. In this study, expression levels of genes involved in cell adhesion were determined in two patients with oropharyngeal squamous cell carcinoma and three patients with laryngeal squamous cell carcinoma. The obtained data showed that there is a differentiation in the expression of genes for collagens (COL15A1, COL18A1, COL4A1, COL4A2 and COL4A3), integrins (ITGA4, ITGAV, ITGB3) and two molecules involved in their interactions (CD44 and MMP2) for the two tumor types, the results obtained need validation on a statistically significant sample.

✉ *Corresponding author: marian Constantin, Institute of Biology of Romanian Academy, 296 Splaiul Independentei, 060031 Bucharest, Romania, email: cvgmarian@gmail.com

Introduction

Although the head region is very complex, encompassing all the organs and bony and muscular structures of the upper airways, the cranial vault, eyes, ears, their appendages, endocrine glands, the cervical spine, cranial and cervical musculature, blood vessels, nerves and the covering integument, the term head and neck cancers refers only to tumors arising in the upper airways [1]. Because the structures of the head and neck are complex, upper airway cancers are highly heterogeneous [2], with more than 90% of their origin in the squamous cells lining the mucosa of the upper airways. Head and neck cancers account for an estimated 650,000 to 900,000 new cases each year [1; 3] and are some of the most common cancers, ranking sixth [3] or seventh [1] worldwide [4; 5]. Head and neck cancers are diagnosed at advanced stages and have a five-year survival of about 50% and high mortality [6]. Head and neck cancers rarely metastasize to distant sites (in less than 10% of cases [7]), but they affect regional lymph nodes with high frequency, greatly complicating the patients' situation [8]. Among the most implicated factors in the etiology of head and neck cancers are: smoking, alcohol consumption, most frequently combined [9-11] and HPV (human papillomavirus) infections [9; 12-19], followed by other factors with variable participation in the occurrence of head and neck cancers: EBV (Epstein-Barr virus) infections [20; 21], gastroesophageal reflux [22], chewing betel quid (Areca nuts) [23], poor oral hygiene [24], oral dysbiosis [25], proinflammatory diet [26; 27], inhalation of air pollutants [8], genetic aberrations [3; 28-31] and epigenetic factors [32].

Therapeutic strategies for head and neck cancers are varied and include cytoreductive surgery, radiotherapy and chemotherapy (when necessary) and, in recent years, innovative therapies such as immunotherapy and targeted therapies, but the results are modest [33]. The low efficacy of treatments may be due to the fact that head and neck tumors rapidly enter hypoxia, synthesizing numerous pro-angiogenic factors that amplify the angiogenic process [34], and to treatment resistance [35]. The association between integrins and components of the extracellular matrix plays an essential role in cell-cell interactions [36]. The extracellular matrix has the structure of a three-dimensional network of fibers, which serves as a physical support and participates in the regulation of cellular processes [37]. The structure of the extracellular matrix in the vicinity of the tumor is remodeled by head and neck cancers, while constantly interacting with the stromal components of the tumor microenvironment [38; 39]. Thus, integrins in the tumor cell membrane support the biosynthesis of extracellular matrix elements, promote the formation of collagen fiber networks, contribute to chemotaxis-driven tumor invasiveness [40] and, by interacting with extracellular matrix elements, integrins A2, A2B, A3, A6, A6, AV and B1 serve to activate PTK2/FAK-PI3K–AKT–mTOR/IKK signaling pathways involved in angiogenesis and evading apoptosis [41]. In the present study we investigated the expression of genes for collagens 15A1, 18A1, 4A1, 4A1, 4A2 and 4A3 and genes for AV and A4 integrins in five patients with head and neck cancers and the relationships between them by constructing a network using String software, available at https://string-db.org/ [42].

Collagens (COLs) are found in the extracellular matrix, being a major component of the tumor microenvironment and participate in tumor fibrosis [43]. They belong to a family of 28 protein types classified into four subfamilies based on the molecular assemblies they form: (i) *fibril-forming collagens*, i.e., collagens I, II, III, V, XI, XXVI, XXVII; (ii) *collagens associated with fibrils with interrupted triple helix*, i.e., collagens IX, XII, XIV, XVI, XIX, XX, XXI, XXII, XXIV, which do not form fibrils but are characteristically associated with the surface of collagen fibrils; (iii) *network-forming collagens*, i.e., collagens IV, VIII, X; and (iv) *membrane-anchored collagens*, i.e., collagens XIII, XVII, XXIII, XXV [44], with collagens I, III and V being produced mainly by cancer-associated fibroblasts (CAFs), and collagen IV mainly by epithelial and endothelial cells, but also some tumors, such as oral squamous cell carcinoma [45], in which COL4A1 appears to promote cell proliferation and migration [46]. Under certain circumstances, tumor cells and tumor microenvironment macrophages (TAMs) can produce significant amounts of collagen [47; 48]. Collagens and elastin, the second most abundant components in the extracellular matrix, form a supramolecular structure resistant to proteolysis, but which is susceptible to matrix metalloproteinases. Proteolysis is facilitated by the binding of MMP2 and MMP9 to collagen and by the activity of remote exosites of the catalytic domain of MMP12 [49].

Integrins (ITGs) are a family of heterodimeric cell adhesion molecules composed of α and β subunits that mediate junctions between cells and between cells and the extracellular matrix [50]. Regulating cell proliferation, survival and migration [51], certain combinations of integrins possess specific roles in carcinogenesis, particularly in metastatic processes and in interactions between tumor cells and the extracellular matrix [52]. Among them, integrin A4 (ITGA4), a receptor for fibronectin [53], promotes cell myogenesis, and the five-membered αV integrins (ITGAV) (αvβ1, αvβ3, αvβ5, αvβ6 and αvβ8) function as receptors for fibronectin, vitronectin and fibrinogen and promote the progression of head and neck squamous cell carcinoma [54].

Patients and methods

Patients and tumor samples. Fragments of tumor tissue and normal-appearing tissue, harvested from the resection border and used as control, preserved in RNA later solution at -20°C were collected from five adult patients with oropharyngeal and laryngeal neoplasms, operated at Ilfov County Emergency Hospital. All procedures carried out were in accordance with the ethical standards of the institutional research committee and the 1964 Declaration of Helsinki and its subsequent amendments, informed consent was obtained from the patients for the processing of the samples, and the study was approved by the ethics committee.

RNA extraction and reverse transcription. Total RNA was extracted with the NucleoSpin RNA II-Total RNA Isolation Kit (ref.740955.50, MACHEREY-NAGEL GmbH & Co. KG, 52355 Düren, Germany) following the protocol in the kit. RNA spectrophotometric analysis was performed on a Perkin-Elmer UV-VIS Lambda 40 spectrophotometer and RNA molecule integrity was analyzed with the Lab on Chip system (AGILENT): kit ul 6000 RNA Nano, on the 2100 bioanalyzer (AGILENT). Reverse transcription reaction was performed with the High-Capacity cDNA Reverse Transcription Kit (cat.no.4368814, APPLIED BIOSYSTEMS, Foster City, CA 94404, USA).

Real-Time PCR. Gene expression analysis was performed in TaqMan Array 96-Well Plates Gene Signature for Human Angiogenesis (92 genes for analysis and 4 housekeeping genes: 18S (for 18S RNA), GAPDH (for glyceraldehyde-3-phosphate dehydrogenase), HPRT1 (for hypoxanthine phosphoribosyltransferase 1) and GUSB (for β-glucuronidase), using TaqMan® Gene Expression Master Mix (2x) (cat. no. 4369016, Amplification reaction was performed on a Real-Time PCR 7500 (Applied Biosystems), and data were analyzed using Data AssistTM v. 3.01 software (Applied Biosys-

tems). The housekeeping genes considered as endogenous controls were 18S and GUSB, which had values closest to 1.

Results

Baseline patient characteristics. Samples were taken from five male patients, aged 53 to 73 years, whose clinical data and anatomopathological diagnosis are shown in Table 1.

Gene expression in head and neck cancers. The expression levels of each gene in the tumor tissue samples from the five patients are shown in Table 2, by comparison with the expression levels in peritumoral tissues with normal histopathological appearance, which have a value of 1. For a gene to be overexpressed, values equal to or greater than 2, i.e. with expression at least double the value in normal tissue, were considered. To form an overview of the grouping of samples and genes with similar expression behavior, the heat map shown in Figure 1 was generated using the Data AssistTM Software v. 3.01 (Applied Biosystems). The distances between samples are calculated in hierarchical clustering based on ΔCT values using Pearson's correlation, and the clustering method is average linkage.

Table 2. Gene expression levels in the five patients, expressing the ratio between the amount of mRNA in the tumor tissue sample and the control sample, Fold Change (RQ).

Gene	P1	P2	P3	P4	P5
CD44	3,55	0,04	5,72	14,19	18,21
COL15A1	0,11	1,02	0,39	0,59	0,66
COL18A1	0,79	0,18	1,64	6,30	7,34
COL4A1	0,72	0,28	0,69	4,36	7,07
COL4A2	0,80	0,76	1,28	8,23	9,49
COL4A3	0,75	17,17	0,17	0,64	0,01
ITGA4	0,79	0,26	35,50	10,63	12,07
ITGAV	2,93	0,45	2,93	6,75	19,81
ITGB3	0,05	1,64	0,55	0,49	4,30
MMP2	0,43	2,49	1,78	0,89	15,35

Table 1. Clinical data and anatomopathological diagnosis of the patients.

| Patients			TNM	Anatomopathological diagnosis	Associated diagnoses	5-year following status
Code	Age	Sex				
P1	55 y	M	T3N2bM1	Well differentiated, keratinized oropharyngeal squamous cell carcinoma; latero-cervical lymph node with metastasis.	Obesity, chronic tonsillitis, weight loss	Deceased
P2	62 y	M	T3N2bM0	Moderately differentiated oropharyngeal squamous cell carcinoma, invasive in the tonsil tissue; no lymph node metastasis.	Type 2 diabetes, obesity, chronic tonsillitis, chronic bronchitis	Relapse
P3	71 y	M	T3N2bM1	Keratinized laryngeal squamous cell carcinoma; latero-cervical lymph node with metastasis.	Chronic tonsillitis, weight loss	Stable
P4	53 y	M	T3N3M1	Moderately to poorly differentiated, nonkeratinized laryngeal squamous cell carcinoma, invasive with necrotic areas; latero-cervical lymph node with metastasis.	Obesity, chronic tonsillitis, chronic sinusitis, gastroesophageal reflux	Deceased
P5	73 y	M	T3N2cM0	Moderately differentiated, invasive laryngeal squamous cell carcinoma; no lymph node metastasis.	Chronic tonsillitis, weight loss	Deceased
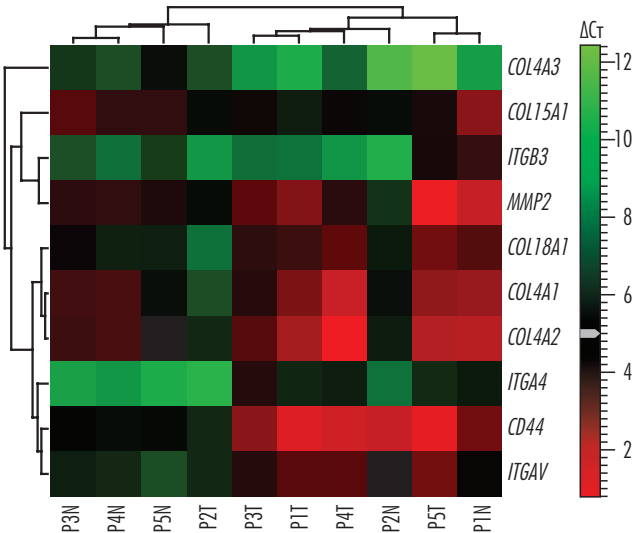
Fig. 1. Heat map displaying gene expression levels.

Gene expression for collagens 15A1, 18A1, 4A1, 4A1, 4A2 and 4A3, AV, A4 and B3 integrins, CD44 and MMP2 is variable, being maintained at low levels in oropharyngeal squamous cell carcinoma, with definite overexpression (values above 2) of *CD44* and *ITGAV* (in one patient) and *COL4A3* and *MMP2*, in the second patient, and at somewhat higher levels in laryngeal squamous cell carcinoma, where *COL15A1* and *COL4A3* are the least expressed genes, all others having expression peaks exceeding 2 in at least one patient (Figure 2). Thus, for the *CD44* gene, one sample of oropharyngeal squamous cell carcinoma and all three samples of laryngeal squamous cell carcinoma were positive; for the *COL15A1* gene all samples were negative, for the *COL18A1*, *COL4A1* and *COL4A2* genes two samples of laryngeal squamous cell carcinoma were positive each; for the *COL4A3* gene, only one sample of oropharyngeal squamous

cell carcinoma was positive; for the *ITGA4* gene all laryngeal squamous cell carcinoma samples were positive, for the *ITGAV* gene one oropharyngeal squamous cell carcinoma sample and all laryngeal squamous cell carcinoma samples were positive, for the *ITGB3* gene one oropharyngeal squamous cell carcinoma sample was positive and for the *MMP2* gene one sample from both groups was positive.

Discussions

In the present study, we aimed to identify the expression levels of genes for collagen and integrin, with two additional genes, *CD44* and *MMP2*, which are not part of these protein families, to observe possible particularities between the two types of cancers. As illustrated in Figure 2, there is a clear differentiation between the two types of tumors, in particular with respect to the overall level of gene expression. Thus, in oropharyngeal squamous cell carcinoma, expression of selected genes appears poorer than in laryngeal squamous cell carcinoma. On the other hand, *COL15A1*, which, according to GeneCards [55], is expressed in a wide variety of tissues, functioning predominantly in basement membrane adhesion complexes to the underlying connective tissue stroma. At the same time, the C-terminal fragment resulting from proteolysis of type XV collagen is restin, a protein with antiangiogenic potential, closely related to endostatin, and reduced *COL15A1* gene expression is probably associated with tumor angiogenesis, a trait that may characterize many head and neck cancers.

The CD44 protein is a cellular receptor involved in cell-cell interactions, cell adhesion and migration, participating in the cell's response to changes in the tumor microenvironment and probably in tumor metastasis [56]. In oropharyn-
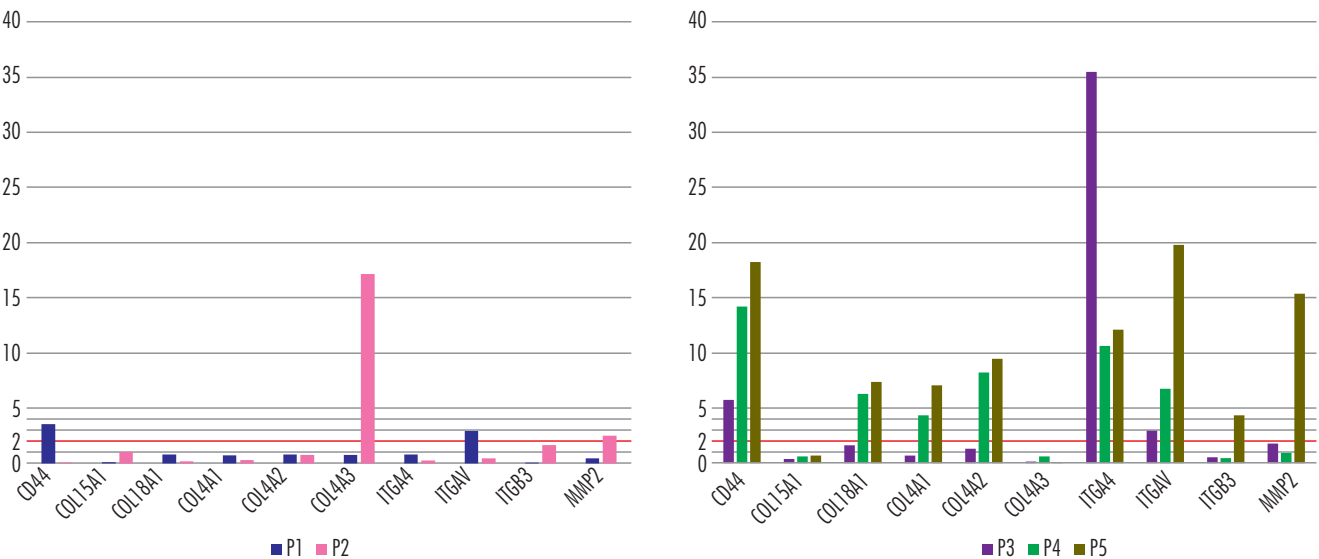

Fig. 2. Gene expression levels in the five patients. On the left, oropharyngeal squamous cell carcinoma cases and on the right, laryngeal squamous cell carcinoma cases. Values of 2 or greater are considered to reflect gene overexpression, and 1 characterizes normal tissue.

geal squamous cell carcinoma, the gene is present in one sample from a patient with keratinized and metastasized cancer, and in laryngeal squamous cell carcinoma in all samples, with the highest level observed in the patient with metastasis, so that no correlation can be made between *CD44* gene expression and metastasis.

Collagen IV is the major component of basement membranes and is composed of three subunits, A1, A2 and A3, the first two subunits being overexpressed in two laryngeal squamous cell carcinoma samples each. Subunit 3 (COL4A3) can be cleaved in the NC1 domain, resulting in an antiangiogenic and antitumor fragment called tumstatin [57], and in head and neck cancers, overexpression of *COL4A3* gene is associated with favorable prognosis [58]. In our cohort, patients 1, 4, and 5 progressed to death, patient 2's tumor, in which the highest *COL4A3* gene expression was reported, relapsed, and patient 3's condition remained stable during the 5-year follow-up period. In this context, the correlation between reduced mRNA levels of *COL4A3* and poor prognosis of patients with oropharyngeal and laryngeal squamous cell carcinoma is confirmed, the exception in patient 2 may be related to the lack of lymph node metastases.

The A1 subunit of collagen XVIII, which can inhibit angiogenesis by binding to heparan sulfate proteoglycans involved in growth factor signaling [59], follows the expression trend of collagen IV A1 and A2 subunits and is overexpressed in patients with laryngeal squamous cell carcinoma who subsequently died.

Integrin A forms heterodimers with integrin B and, anchored in the membrane, interacts with laminins and collagens in the extracellular matrix, establishing the links between the extracellular matrix and the cell, but at the same time participating in the alternative activation of the PI3K–AKT–mTOR signaling pathway, one of the pillars of tumor progression by circumventing apoptosis [41]. In oropharyngeal squamous cell carcinoma, *ITGAV* is overexpressed in one sample, and ITGA4 and ITGB3 are well expressed in laryngeal squamous cell carcinoma samples. Coupled with overexpression of its indirect interactors COL4A1, COL4A2 (via CD44, overexpressed, and SPP1, whose expression was not quantified), overexpression of integrins A4 and AV may indicate activation of the PI3K–AKT–mTOR signaling pathway, unaffected by integrin B3 underexpression.

The expression of the matrix metalloproteinase 2, MMP2, is higher in samples of invasive tumors, but which have not produced lymph node metastases. MMP2 is one of the few enzymes of the MMP family that can be activated at the cell membrane as well as inside or outside the cell. By binding denatured collagens IV and V and elastin and cleaving the extracellular matrix, MMP2 is involved in vascularization, cell migration and metastasis [60].

Further, we present the interaction of selected genes by constructing the protein-protein interaction network using the STRING online database and shown in Figure 3. The variables introduced in the construction of this network were: highest confidence (0.900), to have the certainty of selecting the most likely interactions between the selected proteins, active interaction sources (texmining, experiments, databases, co-expression, neighborhood, gene fusion and co-occurrence), to ensure a bird's eye view of the interactions, and the maximum number of 20 nodes in the first layer added, to ensure the introduction of missing links between the selected proteins, on which occasion CD44 and MMP2 genes were added to the study. Finally, three groups of proteins were differentiated based on functional affinities: Group 1, colored in red in Figure 3, which comprises 25 proteins, mainly integrins (CD44, COL18A1, DMP1, GP6, IBSP, IBSP, ITGA1, ITGA10, ITGA11, ITGA2, ITGA3, ITGA4, ITGA5, ITGAL, ITGAV, ITGB3, ITGB5, ITGB6, ITGB7, ITGB8, MMP2, NANOGP8, SPP1, TNC, TNN and TNR), the light green colored group 2, which comprises 3 members of the large collagen family (COL15A1, COL4A3 and COL4A4), and group 3, with 2 members (COL4A1 and COL4A2). Interactions between proteins in different groups are marked by dashed lines. In the network, most interactions are realized between integrins, transmembrane proteins, which enter the structure of cell-cell and cell-extracellular matrix junctions, and between collagens, which form the largest proportion of the extracellular matrix. The construction of this network made it possible to map the general interactions between the selected genes and to identify the proteins interposed between some of the proteins encoded by the selected genes. Thus, between COL4A1 and COL4A3 or between COL4A2 and COL4A3 is interposed the protein GP6 (platelet glycoprotein VI), a collagen receptor that plays an important role in thrombus formation, blood platelet aggregation [61] and, in some cancers, promotes metastasis, through interaction with cancer cell-derived galectin-3 [62], making it a putative target for anticancer therapies. Between the B3, B5 and A4 integrins and CD44, which interact with type IV collagens, intervenes SPP1 (secreted phosphoprotein 1 gene), present mainly in mineralized matrices. In head and neck squamous cell carcinoma, high SPP1 mRNA levels were correlated with poor overall survival, being a tumor biomarker [63] and may also be targeted in personalized therapies.

Next, to clarify the interactions between the overexpressed genes, a network was constructed for each sample having at least three overexpressed genes (Figure 4), with a confidence level of 0.900, and including only the over-
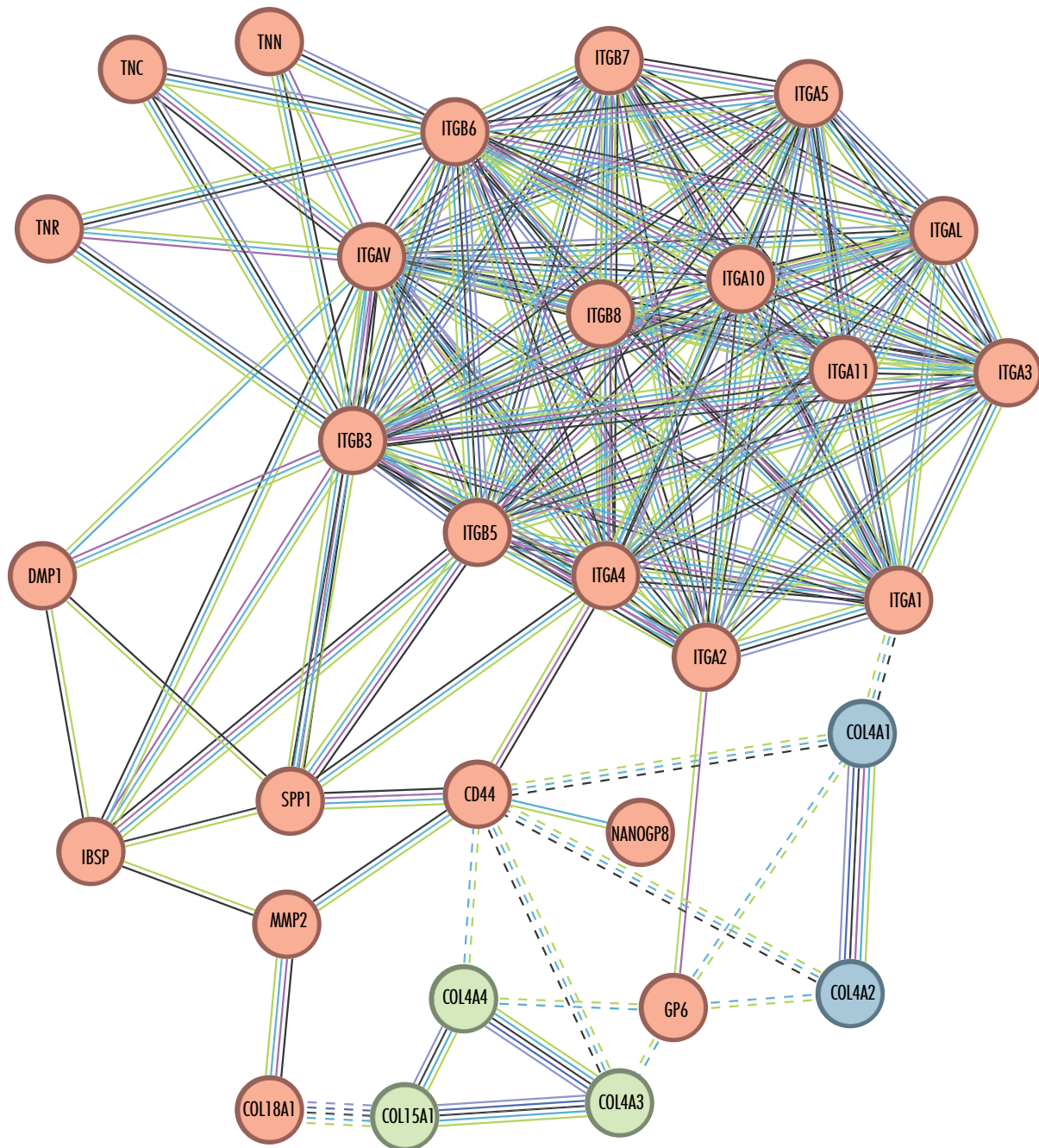
Fig. 3. The network of interactions between selected genes constructed with STRING (https://string-db.org/), with a confidence of 0.900 and including 20 additional interactors, to bind all the selected genes in the network and to identify the linking proteins between them. Using k-means clustering, the genes were grouped into three clusters between which the interactions are highlighted with dashed lines.

expressed genes, without any additional interactors. In the sample from patient 3 (Figure 4A), where CD44, ITGA4 and ITGAV genes are overexpressed, integrin A4 occupies a central place, interacting strongly with integrin AV and less with CD44. Increasing the number of overexpressed genes in the sample from patient 4 to six (CD44, COL18A1, COL4A1, COL4A1, COL4A2, ITGA4 and ITGAV) allowed the realization of a more complex network (Figure 4B), where one pole is occupied by collagens IV (A1 and A2) and the other by integrins AV and A4, linked to the CD44 receptor.

Outside the network is collagen XVIII, which needs MMP2 to be integrated into it. In the sample from patient 5 most of the genes are expressed (CD44, COL18A1, COL4A2, COL4A2, ITGA4, ITGAV, ITGB3 and MMP2), allowing for an increase in the complexity of the interactions between them (Figure 4C). AV, A4 and B3 integrins are clustered in the left pole, with complex interactions between them, and the collagens IV and XVIII are localized on the right side. Interactions between collagen IV A2 and integrins are mediated
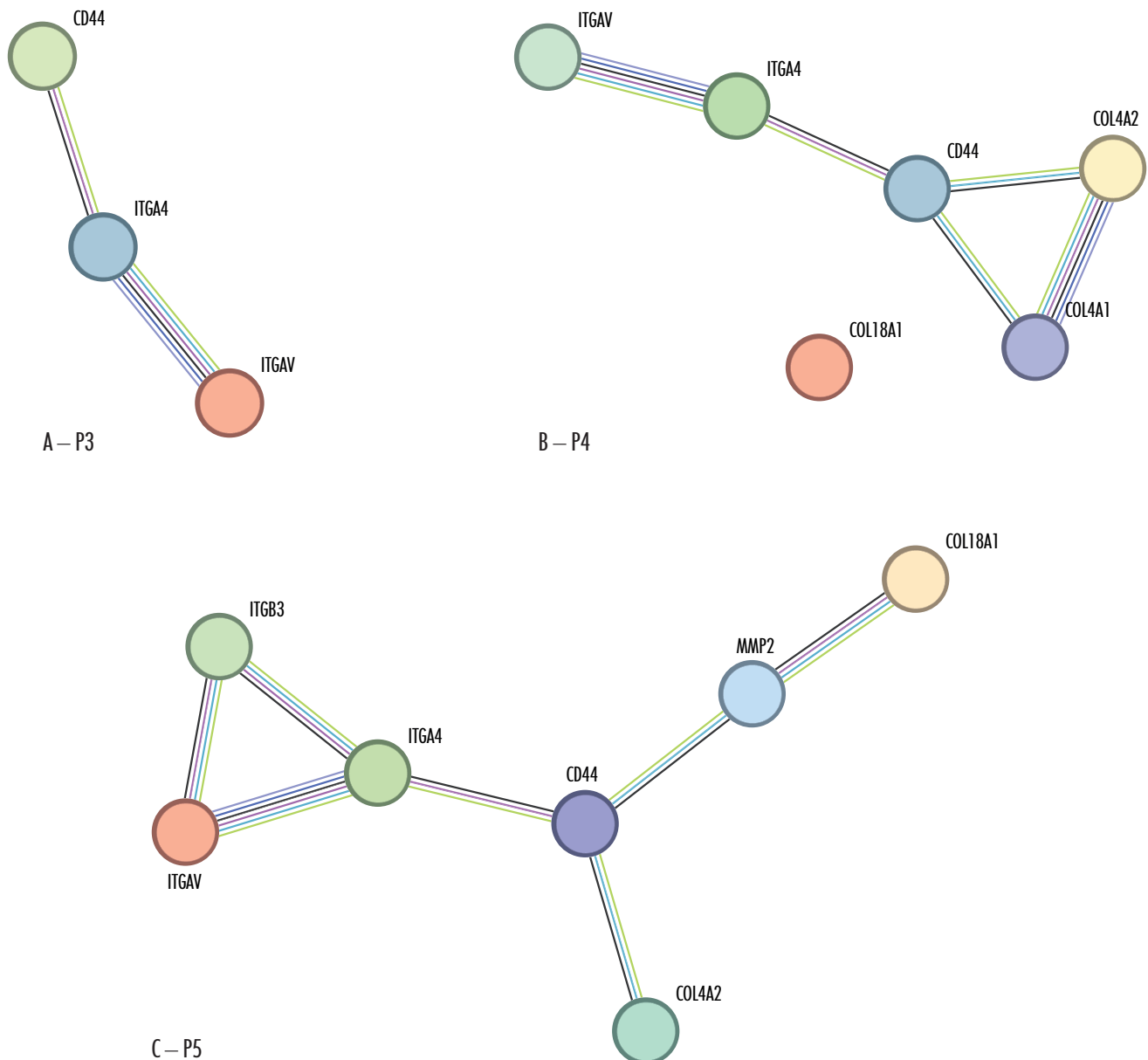
Fig. 4. Protein-protein interaction network constructed with STRING (https://string-db. org/), for samples with at least 3 overexpressed laryngeal squamous cell carcinoma genes, for patients P3 (A), with three proteins (CD44, ITGA4 and ITGAV), P4 (B), with six proteins (CD44, COL18A1, COL4A1, COL4A2, ITGA4 and ITGAV) and P5 (C), with seven proteins (CD44, COL18A1, COL4A2, ITGA4, ITGAV, ITGB3 and MMP2). For the realization of the networks, the confidence level was 0.900.

by CD44, and interactions between collagen XVIII A1 and integrins require two mediators, MMP2 and CD44.

Conclusions and future perspectives

By quantifying the expression levels of CD44, CO-L15A1, COL18A1, COL4A1, COL4A2, COL4A3, ITGAV, ITGA4, ITGB3 and MMP2 genes in the five patients, a differentiation between oropharyngeal squamous cell carcinoma and laryngeal squamous cell carcinoma was observed, in the sense that the second type of cancer causes the overexpression of a higher number of genes, some of them (CD44, ITGA4 and ITGAV) in all three patients analyzed, and

CD44, COL18A1, COL4A1, COL4A2, ITGA4, ITGAV, in patients P4 and P5. After the building of the interaction network using STRING (https://string-db.org/), some proteins, such as COL18A1, were found not to interact directly with any of the proteins in the group, and therefore additional interactors were introduced (e.g. CD44 and MMP9, whose expression levels were quantified, SPP1 and GP6, whose expression levels were not analyzed). Due to the large number and complexity of the interactions between integrins and integrin A1 with the A1 subunit of collagen IV, further studies should increase the number of integrin family members included in the selection of genes analyzed. Integrins

are membrane receptors for extracellular signals that alternatively activate the PI3K–AKT–mTOR signaling pathway. As this pathway is very important for tumor processes, it is necessary to quantify the mRNA expression of some of its members and to establish possible correlations between integrin expression and the expression of these members. Finally, validation of the results and drawing meaningful conclusions in epidemiologic and therapeutic contexts requires an increased number of patients and genes.

Acknowledgements

References

1. Gormley M, Creaney G, Schache A, Ingarfield K, Conway DI. Reviewing the epidemiology of head and neck cancer: definitions, trends and risk factors. Br Dent J. 2022 Nov;233(9):780-786. doi: 10.1038/s41415-022-5166-x. Epub 2022 Nov 11. PMID: 36369568; PMCID: PMC9652141.

2. Iftikhar A, Islam M, Shepherd S, Jones S, Ellis I. What is behind the lifestyle risk factors for head and neck cancer? Front Psychol. 2022 Oct 13;13:960638. doi: 10.3389/fpsyg.2022.960638. PMID: 36312160; PMCID: PMC9608174.

3. Miserocchi G, Spadazzi C, Calpona S, De Rosa F, Usai A, De Vita A, Liverani C, Cocchi C, Vanni S, Calabrese C, Bassi M, De Luca G, Meccariello G, Ibrahim T, Schiavone M, Mercatali L. Precision Medicine in Head and Neck Cancers: Genomic and Preclinical Approaches. J Pers Med. 2022 May 24;12(6):854. doi: 10.3390/jpm12060854. PMID: 35743639; PMCID: PMC9224778.

4. Johnson DE, Burtness B, Leemans CR, Lui VWY, Bauman JE, Grandis JR. Head and neck squamous cell carcinoma. Nat Rev Dis Primers. 2020 Nov 26;6(1):92. doi: 10.1038/s41572-020-00224-3. Erratum in: Nat Rev Dis Primers. 2023 Jan 19;9(1):4. doi: 10.1038/s41572-023-00418-5. PMID: 33243986; PMCID: PMC7944998.

5. Sung H, Ferlay J, Siegel RL, Laversanne M, Soerjomataram I, Jemal A, Bray F. Global Cancer Statistics 2020: GLOBOCAN Estimates of Incidence and Mortality Worldwide for 36 Cancers in 185 Countries. CA Cancer J Clin. 2021 May;71(3):209-249. doi: 10.3322/caac.21660. Epub 2021 Feb 4. PMID: 33538338.

6. Chow LQM. Head and Neck Cancer. N Engl J Med. 2020 Jan 2;382(1):60-72. doi: 10.1056/NEJMra1715715. PMID: 31893516.

7. Constantin M, Cristian RE, Crunteanu I, Tudorache S, Vrancianu CO. Lifestyle features as co-factors in head and neck cancer development. Rom Biotechnol Lett. 2023;28(2):3950-3958. doi: 10.25083/rbl/28.2/3950.3958.

8. Constantin M. Epidemiology, diagnosis, symptoms and TNM classification of head and neck cancers. Rom Biotechnol Lett. 2022; 27(5): 3699-3712 DOI: 10.25083/rbl/27.5/3699.3712.

9. Hashibe M, Boffetta P, Zaridze D, Shangina O, Szeszenia-Dabrowska N, Mates D, Fabiánová E, Rudnai P, Brennan P. Contribution of tobacco and alcohol to the high rates of squamous cell carcinoma of the supraglottis and glottis in Central Europe. Am J Epidemiol. 2007 Apr 1;165(7):814-20. doi: 10.1093/aje/kwk066. Epub 2007 Jan 22. PMID: 17244634.

10. Moyses RA, López RV, Cury PM, Siqueira SA, Curioni OA, Gois Filho JF, Figueiredo DL; Head and Neck Genome Project GENCAPO; Tajara EH, Michaluart P Jr. Significant differences in demographic, clinical, and pathological features in relation to smoking and alcohol consumption among 1,633 head and neck cancer patients. Clinics (Sao Paulo). 2013 Jun;68(6):738-44. doi: 10.6061/clinics/2013(06)03. PMID: 23778492; PMCID: PMC3674275.

11. Chang CP, Siwakoti B, Sapkota A, Gautam DK, Lee YA, Monroe M, Hashibe M. Tobacco smoking, chewing habits, alcohol drinking and the risk of head and neck cancer in Nepal. Int J Cancer. 2020 Aug 1;147(3):866-875. doi: 10.1002/ijc.32823. Epub 2019 Dec 27. PMID: 31837000; PMCID: PMC7906484.

12. Castellsagué X, Alemany L, Quer M, Halec G, Quirós B, Tous S, Clavero O, Alòs L, Biegner T, Szafarowski T, Alejo M, Holzinger D, Cadena E, Claros E, Hall G, Laco J, Poljak M, Benevolo M, Kasamatsu E, Mehanna H, Ndiaye C, Guimerà N, Lloveras B, León X, Ruiz-Cabezas JC, Alvarado-Cabrero I, Kang CS, Oh JK, Garcia-Rojo M, Iljazovic E, Ajayi OF, Duarte F, Nessa A, Tinoco L, Duran-Padilla MA, Pirog EC, Viarheichyk H, Morales H, Costes V, Félix A, Germar MJ, Mena M, Ruacan A, Jain A, Mehrotra R, Goodman MT, Lombardi LE, Ferrera A, Malami S, Albanesi EI, Dabed P, Molina C, López-Revilla R, Mandys V, González ME, Velasco J, Bravo IG, Quint W, Pawlita M, Muñoz N, de Sanjosé S, Xavier Bosch F; ICO International HPV in Head and Neck Cancer Study Group. HPV Involvement in Head and Neck Cancers: Comprehensive Assessment

of Biomarkers in 3680 Patients. J Natl Cancer Inst. 2016 Jan 28;108(6):djv403. doi: 10.1093/jnci/djv403. PMID: 26823521.

13. Aboagye E, Agyemang-Yeboah F, Duduyemi BM, Obirikorang C. Human Papillomavirus Detection in Head and Neck Squamous Cell Carcinomas at a Tertiary Hospital in Sub-Saharan Africa. ScientificWorldJournal. 2019 Apr 2;2019:2561530. doi: 10.1155/2019/2561530. PMID: 31061653; PMCID: PMC6466863.

14. de Sanjosé S, Serrano B, Tous S, Alejo M, Lloveras B, Quirós B, Clavero O, Vidal A, Ferrándiz-Pulido C, Pavón MÁ, Holzinger D, Halec G, Tommasino M, Quint W, Pawlita M, Muñoz N, Bosch FX, Alemany L; RIS HPV TT, VVAP and Head and Neck study groups. Burden of Human Papillomavirus (HPV)-Related Cancers Attributable to HPVs 6/11/16/18/31/33/45/52 and 58. JNCI Cancer Spectr. 2019 Jan 7;2(4):pky045. doi: 10.1093/jncics/pky045. PMID: 31360870; PMCID: PMC6649711.

15. Sabatini ME, Chiocca S. Human papillomavirus as a driver of head and neck cancers. Br J Cancer. 2020 Feb;122(3):306-314. doi: 10.1038/s41416-019-0602-7. Epub 2019 Nov 11. PMID: 31708575; PMCID: PMC7000688.

16. Bulane A, Goedhals D, Seedat RY, Goedhals J, Burt F. Human papillomavirus DNA in head and neck squamous cell carcinomas in the Free State, South Africa. J Med Virol. 2020 Feb;92(2):227-233. doi: 10.1002/jmv.25556. PMID: 31347711.

17. Mahmutović L, Bilajac E, Hromić-Jahjefendić A. Meet the Insidious Players: Review of Viral Infections in Head and Neck Cancer Etiology with an Update on Clinical Trials. Microorganisms. 2021 May 6;9(5):1001. doi: 10.3390/microorganisms9051001. PMID: 34066342; PMCID: PMC8148100.

18. Vani NV, Madhanagopal R, Swaminathan R, Ganesan TS. Dynamics of oral human papillomavirus infection in healthy population and head and neck cancer. Cancer Med. 2023 May;12(10):11731-11745. doi: 10.1002/cam4.5686. Epub 2023 Feb 27. PMID: 36846921; PMCID: PMC10242867.

19. Vani NV, Rama R, Madhanagopal R, Vijayalakshmi R, Swaminathan R. Human Papillomavirus-Attributable Head and Neck Cancers in India-A Systematic Review and Meta-Analysis. JCO Glob Oncol. 2024 Mar;10:e2300464. doi: 10.1200/GO.23.00464. PMID: 38513185; PMCID: PMC10965205.

20. Prabhu SR, Wilson DF. Evidence of epstein-barr virus association with head and neck cancers: a review. J Can Dent Assoc. 2016 Jan;82:g2. PMID: 27548665.

21. Lee LA, Fang TJ, Li HY, Chuang HH, Kang CJ, Chang KP, Liao CT, Chen TC, Huang CG, Yen TC. Effects of Epstein-Barr Virus Infection on the Risk and Prognosis of Primary Laryngeal Squamous Cell Carcinoma: A Hospital-Based Case-Control Study in Taiwan. Cancers (Basel). 2021 Apr 6;13(7):1741. doi: 10.3390/cancers13071741. PMID: 33917480; PMCID: PMC8038767.

22. Eells AC, Mackintosh C, Marks L, Marino MJ. Gastroesophageal reflux disease and head and neck cancers: A systematic review and meta-analysis. Am J Otolaryngol. 2020 Nov-Dec;41(6):102653. doi: 10.1016/j.amjoto.2020.102653. Epub 2020 Aug 5. PMID: 32841763.

23. Sharan RN, Mehrotra R, Choudhury Y, Asotra K. Association of betel nut with carcinogenesis: revisit with a clinical perspective. PLoS One. 2012;7(8):e42759. doi: 10.1371/journal.pone.0042759. Epub 2012 Aug 13. PMID: 22912735; PMCID: PMC3418282.

24. Chang CC, Lee WT, Hsiao JR, Ou CY, Huang CC, Tsai ST, Chen KC, Huang JS, Wong TY, Lai YH, Wu YH, Hsueh WT, Wu SY, Yen CJ, Chang JY, Lin CL, Weng YL, Yang HC, Chen YS, Chang JS. Oral hygiene and the overall survival of head and neck cancer patients. Cancer Med. 2019 Apr;8(4):1854-1864. doi: 10.1002/cam4.2059. Epub 2019 Mar 13. PMID: 30865385; PMCID: PMC6488153.

25. Pandey D, Szczesniak M, Maclean J, Yim HCH, Zhang F, Graham P, El-Omar EM, Wu P. Dysbiosis in Head and Neck Cancer: Determining Optimal Sampling Site for Oral Microbiome Collection. Pathogens. 2022 Dec 16;11(12):1550. doi: 10.3390/pathogens11121550. PMID: 36558884; PMCID: PMC9785010.

26. Argiris A, Karamouzis MV, Raben D, Ferris RL. Head and neck cancer. Lancet. 2008 May 17;371(9625):1695-709. doi: 10.1016/S0140-6736(08)60728-X. PMID: 18486742; PMCID: PMC7720415.

27. Mazul AL, Shivappa N, Hébert JR, Steck SE, Rodriguez-Ormaza N, Weissler M, Olshan AF, Zevallos JP. Proinflammatory diet is associated with increased risk of squamous cell head and neck cancer. Int J Cancer. 2018 Oct 1;143(7):1604-1610. doi: 10.1002/ijc.31555. Epub 2018 Jul 26. PMID: 29696631; PMCID: PMC6203678.

28. Aung KL, Siu LL. Genomically personalized therapy in head and neck cancer. Cancers Head Neck. 2016 Jun 9;1:2. doi: 10.1186/s41199-016-0004-y. PMID: 31093332; PMCID: PMC6457141.

29. Ali J, Sabiha B, Jan HU, Haider SA, Khan AA, Ali SS. Genetic etiology of oral cancer. Oral Oncol. 2017

Jul;70:23-28. doi: 10.1016/j.oraloncology.2017.05.004. Epub 2017 May 17. PMID: 28622887.

30. Huang Y, Zhao J, Mao G, Lee GS, Zhang J, Bi L, Gu L, Chang Z, Valentino J, Li GM. Identification of novel genetic variants predisposing to familial oral squamous cell carcinomas. Cell Discov. 2019 Nov 26;5:57. doi: 10.1038/s41421-019-0126-6. Erratum in: Cell Discov. 2020 Jul 14;6(1):46. doi: 10.1038/s41421-020-00189-3. PMID: 31798960; PMCID: PMC6877579.

31. Farah CS. Molecular landscape of head and neck cancer and implications for therapy. Ann Transl Med. 2021 May;9(10):915. doi: 10.21037/atm-20-6264. PMID: 34164549; PMCID: PMC8184465.

32. Mali SB. Epigenetics: Promising journey so far but ways to go in head neck cancer. Oral Oncol. 2022 Dec;135:106194. doi: 10.1016/j.oraloncology.2022.106194. Epub 2022 Oct 14. PMID: 36252432.

33. Constantin M, Chifiriuc MC, Bleotu C, Vrancianu CO, Cristian R-E, Bertesteanu SV, Grigore R and Bertesteanu G. Molecular pathways and targeted therapies in head and neck cancers pathogenesis. Front. Oncol. 2024;14:1373821. doi: 10.3389/fonc.2024.1373821.

34. Hyytiäinen A, Wahbi W, Väyrynen O, Saarilahti K, Karihtala P, Salo T, Al-Samadi A. Angiogenesis Inhibitors for Head and Neck Squamous Cell Carcinoma Treatment: Is There Still Hope? Front Oncol. 2021 Jun 14;11:683570. doi: 10.3389/fonc.2021.683570. PMID: 34195084; PMCID: PMC8236814.

35. Miserocchi G, Cocchi C, De Vita A, Liverani C, Spadazzi C, Calpona S, Di Menna G, Bassi M, Meccariello G, De Luca G, Campobassi A, Maddalena Tumedei M, Bongiovanni A, Fausti V, Cotelli F, Ibrahim T, Mercatali L. Three-dimensional collagen-based scaffold model to study the microenvironment and drug-resistance mechanisms of oropharyngeal squamous cell carcinomas. Cancer Biol Med. 2021 Mar 27;18(2):502–16. doi: 10.20892/j.issn.2095-3941.2020.0482. Epub ahead of print. PMID: 33772505; PMCID: PMC8185858.

36. Klemm F, Joyce JA. Microenvironmental regulation of therapeutic response in cancer. Trends Cell Biol. 2015 Apr;25(4):198-213. doi: 10.1016/j.tcb.2014.11.006. Epub 2014 Dec 22. PMID: 25540894; PMCID: PMC5424264.

37. Martino MM, Briquez PS, Güç E, Tortelli F, Kilarski WW, Metzger S, Rice JJ, Kuhn GA, Müller R, Swartz MA, Hubbell JA. Growth factors engineered for super-affinity to the extracellular matrix enhance tissue healing. Science. 2014 Feb 21;343(6173):885-8. doi: 10.1126/science.1247663. PMID: 24558160.

38. Junttila MR, de Sauvage FJ. Influence of tumour microenvironment heterogeneity on therapeutic response.

39. Sun Y. Tumor microenvironment and cancer therapy resistance. Cancer Lett. 2016 Sep 28;380(1):205-15. doi: 10.1016/j.canlet.2015.07.044. Epub 2015 Aug 10. PMID: 26272180.

40. Levental KR, Yu H, Kass L, Lakins JN, Egeblad M, Erler JT, Fong SF, Csiszar K, Giaccia A, Weninger W, Yamauchi M, Gasser DL, Weaver VM. Matrix cross-linking forces tumor progression by enhancing integrin signaling. Cell. 2009 Nov 25;139(5):891-906. doi: 10.1016/j.cell.2009.10.027. PMID: 19931152; PMCID: PMC2788004.

41. KEGG Pathways in cancer - Reference pathway. 2020 Sep 12 [cited 2024 Jul 03]. Available from: https://www.genome.jp/pathway/hsa05200

42. STRING: functional protein association networks. Available at https://string-db.org/. Accessed on 03.07.2024.

43. Xu S, Xu H, Wang W, Li S, Li H, Li T, Zhang W, Yu X, Liu L. The role of collagen in cancer: from bench to bedside. J Transl Med. 2019 Sep 14;17(1):309. doi: 10.1186/s12967-019-2058-1. PMID: 31521169; PMCID: PMC6744664.

44. Ricard-Blum S. The collagen family. Cold Spring Harb Perspect Biol. 2011 Jan 1;3(1):a004978. doi: 10.1101/cshperspect.a004978. PMID: 21421911; PMCID: PMC3003457.

45. Hirota J, Yoneda K, Osaki T. Basement membrane type IV collagen in oral squamous cell carcinoma. Head Neck. 1990 Sep-Oct;12(5):400-5. doi: 10.1002/hed.2880120505. PMID: 2211100.

46. Tian X, Sun J, Li C, Zhang K. COL4A1 promotes the proliferation and migration of oral squamous cell carcinoma cells by binding to NID1. Exp Ther Med. 2023 Mar 7;25(4):176. doi: 10.3892/etm.2023.11875. PMID: 37006878; PMCID: PMC10061039.

47. Ohlund D, Lundin C, Ardnor B, Oman M, Naredi P, Sund M. Type IV collagen is a tumour stroma-derived biomarker for pancreas cancer. Br J Cancer. 2009 Jul 7;101(1):91-7. doi: 10.1038/sj.bjc.6605107. Epub 2009 Jun 2. PMID: 19491897; PMCID: PMC2713699.

48. Qiu S, Deng L, Liao X, Nie L, Qi F, Jin K, Tu X, Zheng X, Li J, Liu L, Liu Z, Bao Y, Ai J, Lin T, Yang L, Wei Q. Tumor-associated macrophages promote bladder tumor growth through PI3K/AKT signal induced by collagen. Cancer Sci. 2019 Jul;110(7):2110-2118. doi: 10.1111/cas.14078. Epub 2019 Jun 19. PMID: 31120174; PMCID: PMC6609800.

49. Van Doren SR. Matrix metalloproteinase interactions with collagen and elastin. Matrix Biol. 2015 May-Jul;44-

Nature. 2013 Sep 19;501(7467):346-54. doi: 10.1038/nature12626. PMID: 24048067.

46:224-31. doi: 10.1016/j.matbio.2015.01.005. Epub 2015 Jan 17. PMID: 25599938; PMCID: PMC4466143.

50. Loeser H, Scholz M, Fuchs H, Essakly A, Damanakis AI, Zander T, Büttner R, Schröder W, Bruns C, Quaas A, Gebauer F. Integrin alpha V (ITGAV) expression in esophageal adenocarcinoma is associated with shortened overall-survival. Sci Rep. 2020 Oct 27;10(1):18411. doi: 10.1038/s41598-020-75085-7. PMID: 33110104; PMCID: PMC7591891.

51. Humphries MJ. Integrin structure. Biochem Soc Trans. 2000;28(4):311-39. PMID: 10961914.

52. Lu X, Lu D, Scully M, Kakkar V. The role of integrins in cancer and the development of anti-integrin therapeutic agents for cancer therapy. Perspect Medicin Chem. 2008 Apr 10;2:57-73. PMID: 19787098; PMCID: PMC2746574.

53. Liu G, Yuan C, Ma J, Pan Y, Xu H. Influence of Immune Microenvironment on Diagnosis and Prognosis of Head and Neck Squamous Cell Carcinoma. Front Oncol. 2021 Mar 17;11:604784. doi: 10.3389/fonc.2021.604784. PMID: 33816236; PMCID: PMC8010259.

54. Xu L, Barrett JG, Peng J, Li S, Messadi D, Hu S. ITGAV Promotes the Progression of Head and Neck Squamous Cell Carcinoma. Curr Oncol. 2024 Mar 1;31(3):1311-1322. doi: 10.3390/curroncol31030099. PMID: 38534932; PMCID: PMC10969037.

55. COL15A1 Gene - Collagen Type XV Alpha 1 Chain. 2024 Apr 02 [cited 2024 Jul 05]. Available from: https://www.genecards.org/cgi-bin/carddisp.pl?gene=COL15A1.

56. CD44 Gene - CD44 Molecule (IN Blood Group). 2024 Apr 02 [cited 2024 Jul 05]. Available from: https://www.genecards.org/cgi-bin/carddisp.pl?gene=CD44.

57. COL4A3 Gene - Collagen Type IV Alpha 3 Chain. 2024 Apr 02 [cited 2024 Jul 05]. Available from: https://www.genecards.org/cgi-bin/carddisp.pl?gene=COL4A3.

58. Yang X, Wu Q, Wu F, Zhong Y. Differential expression of COL4A3 and collagen in upward and downward progressing types of nasopharyngeal carcinoma. Oncol Lett. 2021 Mar;21(3):223. doi: 10.3892/ol.2021.12484. Epub 2021 Jan 21. PMID: 33613712; PMCID: PMC7859474.

59. COL18A1 Gene - Collagen Type XVIII Alpha 1 Chain. 2024 Apr 02 [cited 2024 Jul 05]. Available from: https://www.genecards.org/cgi-bin/carddisp.pl?gene=COL18A1.

60. MMP2 Gene - Matrix Metallopeptidase 2. 2024 Apr 03 [cited 2024 Jul 05]. Available from: https://www.genecards.org/cgi-bin/carddisp.pl?gene=MMP2.

61. GP6 Gene - Glycoprotein VI Platelet. 2024 Apr 03 [cited 2024 Jul 05]. Available from: https://www.genecards.org/cgi-bin/carddisp.pl?gene=GP6.

62. Mammadova-Bach E, Gil-Pulido J, Sarukhanyan E, Burkard P, Shityakov S, Schonhart C, Stegner D, Remer K, Nurden P, Nurden AT, Dandekar T, Nehez L, Dank M, Braun A, Mezzano D, Abrams SI, Nieswandt B. Platelet glycoprotein VI promotes metastasis through interaction with cancer cell-derived galectin-3. Blood. 2020 Apr 2;135(14):1146-1160. doi: 10.1182/blood.2019002649. PMID: 32040544.

63. Cai X, Zhang H, Li T. The role of SPP1 as a prognostic biomarker and therapeutic target in head and neck squamous cell carcinoma. Int J Oral Maxillofac Surg. 2022 Jun;51(6):732-741. doi: 10.1016/j.ijom.2021.07.022. Epub 2021 Sep 4. PMID: 34489157.